Università degli Studi di Salerno

Dipartimento di Ingegneria dell'Informazione, Ingegneria Elettrica e Matematica applicata

Dottorato di Ricerca in Ingegneria dell'Informazione
XII Ciclo – Nuova Serie

TESI DI DOTTORATO

Bidirectional Metering Advancements and Applications to Demand Response Resource Management

CANDIDATO: **MARCO LANDI**

TUTOR: **PROF. ANTONIO PIETROSANTO**
PROF. GEORGE GROSS

COORDINATORE: **PROF. ANGELO MARCELLI**

Anno Accademico 2012 – 2013

To my Family

And

To my dear Pinchpessa

I would like to express my heartfelt gratitude to Prof. Pietrosanto for having granted me the opportunity to pursue my Ph.D. in his research group. I simply cannot thank him enough for his patient guidance and support.
I owe a debt of gratitude and my special thanks to Prof. Gross, for having welcomed me at UIUC and constantly pushing me to do my best.
I wish to thank Prof. Liguori for her precious advice and help not limited only to research work.
A three-year work is never a journey undertaken alone. Therefore, I wish to thank all the people in the measurement research groups of UniSa, UniCas and SUN that honored me with their friendship and assistance.
No acknowledgements can be complete without thanks to my parents and family. I owe to my family everything I am and could not have accomplished anything without their support.

Finally, I would like to thank the Italian Measurement Group (G.M.E.E.) for contributing in supporting my research.

Contents

List of Figures

List of Tables

Acronyms

AEV	=	All Electric Vehicle
AMI	=	Advanced Metering Infrastructure
AMR	=	Automated Meter Reading
BV	=	Battery Vehicle
CAES	=	Compressed Air Energy Storage
DER	=	Distributed Energy Resource
DG	=	Distributed Generation
DoD	=	Depth of Discharge
DR	=	Demand Response
DRR	=	Demand Response Resource
EIS	=	Electrochemical Impedance Spectroscopy
ERE	=	Electric Range Extender
ES	=	Energy Storage
ESS	=	Energy Storage System
EV	=	Electric Vehicle
HEV	=	Hybrid Electric Vehicle
ICE	=	Internal Combustion Engine
OCV	=	Open Circuit Voltage
PHEV	=	Plug-in Hybrid Electric Vehicle
PHS	=	Pumped Hydro Storage
PQ	=	Power Quality
SG	=	Smart Grid
SoC	=	State of Charge
SoH	=	State of Health
V2G	=	Vehicle-to-Grid

Introduction

The power grid is currently undergoing a major transformation, which will reshape it completely. Driven by the increasing prices of energy and raising demand, by the need to effectively integrate new types of sources and loads and to deliver electricity more efficiently, a smarter grid, which relies heavily on ICT, measurements and automatic control technology, is being developed. One of the fundamental goals is to empower customers with new and advanced services and applications, elevating them to active users of the power grid.

This thesis work focuses on devices and measurement and management techniques for Demand Response Resources (DRRs). Demand Response (DR) refers to the intentional modification of electricity usage by end-use customers during system imbalances or in response to market prices. While initially developed to ensure reliability during peak load hours, currently DR provide a wide array of services that bring significant advantages in economic, environmental and system stability terms. Peak shaving, absorption of excess generation and load shifting allow for a better utilization of the available resources and reduce the need for expensive and polluting peaking reserves, while frequency up/down regulation services improve system reliability. Deeply connected to DRRs are storage technologies: in fact, these can provide the same services and be managed in the same way, incurring also in fewer limitations. Therefore, this work includes techniques targeted to storage technologies, with specific reference to battery storage.

An effective integration of DRRs and battery storage into the power grid requires a metering and communication network, which allows for real-time monitoring of the state of the grid and of the available resources. In addition, models and operational tools are needed to manage the grid, integrating such resources. Goal of the thesis work is answering to these needs with the development of suitable measurement techniques and management algorithms and the realization of a low-cost device for the implementation of those methodologies. The realized device, based on an ARM microcontroller, implements a smart

meter to be installed in customers' premises, which acts as hub for all energy consumptions and allows the realization of DR programs. In addition, it can be embedded onboard battery storage systems for online monitoring purposes.

The thesis is structured in four Chapters, organized as follows.

Chapter 1 provides a description of the goals of a smart grid implementation and the technical challenges involved. The benefits and limitations of new grid resources, such as DRRs and storage systems, are analyzed. Moreover, the role of measurement systems and devices, as well as the issues these systems have to face in a smart grid environment, are introduced.

Smart meters represent a key driver for the transition to a smart grid, allowing for monitoring the state of the grid and actively involving customers. In Chapter 2, smart metering research and industrial efforts are introduced and the requirements for a smart meter and the related metering infrastructure are described. The proposed implementation for a low-cost real-time bidirectional smart meter is realized. The advanced measurement solutions that allow the meter to exhibit good measurement performances are described in detail. The meter can interact with other meters, acting as a central hub for all energy consumptions. For a smart meter to bring significant advantages to the power grid, it must be supported by an AMI, which acts as the interface between users and grid stakeholders, providing the system operators with measured data and providing users with pricing data and information regarding their own consumptions. Therefore, an AMI prototype is proposed. The presence of actuators on the smart meter and the implementation of a load management strategy in the AMI management unit allows for the realization of load curtailments in response to energy price signals, therefore attaining the deployment of DR programs.

For an effective integration of batteries into grid planning and operations, the degradation they are subjected to while cycled must be taken into account. In Chapter 3, advanced battery monitoring techniques are introduced. Two lightweight measurement techniques for estimating battery state of health, based on a fuzzy logic and on a neural network approach, are described. Moreover, a fast technique to estimate the values of the parameters of the equivalent-circuit battery

model is described. The value of the parameters influences not only the electrical behavior, but can also be used to estimate battery health. These measurement techniques can be implemented on a measurement device embedded in the battery, thus attaining online monitoring. In addition, a system-level battery degradation model that relates battery energy throughput to capacity decay, taking into account also the impact of depth of discharge, temperature and discharge current, is proposed.

In Chapter 4, an application of the developed battery measurement techniques and degradation model to the management of fleets of electric vehicles in a V2G framework, is presented. A management strategy, which explicitly takes into account battery degradation during the allocation of ancillary services provision among the vehicles, is proposed. This strategy results in extended battery lifetime and, under the assumption that the service provider is responsible also of the acquisition and maintenance of batteries, in the maximization of aggregator's assets.

Chapter 1

Measurements and metering needs for Demand Response Resources in a Smart Grid setting

The power grid is evolving into a smart system, capable of integrating all types of sources and loads, able to react autonomously to variations in grid conditions and to favor active customer participation. This evolutionary step poses numerous technical challenges. There is the need to develop and implement metering, communication and command infrastructures for timely grid monitoring and control. Common standards to guarantee interoperability among grid devices from different manufacturers are still lacking. In addition, the data that these devices and technologies provide must be effectively utilized: there is still lack of robust life cycle and operational models for new grid devices and applications. Among the new smart grid applications, Demand Response (DR) represents a viable and cost-effective way of improving system reliability, of attaining a more efficient energy utilization and of maximizing consumers' utility.

In the smart grid context, the role of measurement techniques and devices is a prominent one: automatic control of the electrical system is not realizable without an accurate picture of the state of the grid itself.

With particular focus on DR, and the resources that are involved into DR programs, in this Chapter the goals and technical issues in the realization of a smart grid, and the measurement needs and challenges are introduced.

1.1 The Smart Grid

1.1.1 The need for evolution of the power grid

The term *grid* has traditionally indicated an electric system capable of performing electricity generation, transmission, distribution and control [1.1-1.2]. The power grid is then the system that allows the transformation of energy sources into electricity and its delivery to the customers. Principal objective is to meet the electrical energy needs of the customers at the "least cost" with an acceptable degree of safety, reliability and quality. Differently than in other systems and businesses, electric utilities are bound to respect an *obligation to serve* all present and future customers, that is meeting the load at each instant of time. Moreover, such obligation must be met taking into account the salient characteristics of electricity: inability to store large amounts of energy and the *just-in-time* nature of electricity production and consumption. No other service/commodity has such stringent requirements and consequently reliability is a most fundamental property of electricity service [1.2].

The power grid has always been built, until now, with a vertical approach, following a producer-customer paradigm: few power plants produce the energy required by a multitude of customers, often located far away from the "production sites". Centralizing the production of energy accounts for better economies of scale, therefore reducing costs. The shortcomings of this paradigm, however, are emerging and calling for improvements of the power grid.

A grid architecture as the one just described is essentially *unidirectional*, with utilities and grid operators that have no real-time information from the termination points of the grid. Therefore, the system must be oversized to be able to withstand the foreseeable worst conditions in terms of network operations, i.e. a demand peak. The downsides of such an approach become evident in case of a disservice: in some areas, the utility is aware of an outage only when it receives customer calls for assistance. Moreover, the continuous rise in demand of electric power, combined with reduced investments into electric power infrastructure, is compromising the safety margins, decreasing system stability. If for the generation and transmission sides of the grid

some kind of monitoring and control system like SCADA (Supervisory Control And Data Acquisition) have been put in place, utility companies have still no control over the distribution network, which represents the most critical part of the power grid since nearly 90% of power outages and disturbances are originated there. The chance to control the power grid remotely gives the opportunity to react to changes in the demand without the need to oversize the grid infrastructure and power plants.

The economic aspect of existing grid operations represents another shortcoming to be taken into account. At the moment, spinning reserves and auxiliary generators are used to face sudden demand peaks: such generators are characterized by high costs and impact heavily on electricity prices during peak hours. Moreover, the inherent inefficiencies of the grid determine rising losses in the transmission and distribution network [1.1],[1.3-1.4].

As fossil fuels get depleted and generally more expensive, renewable energy will play a fundamental role in power generation. However, resorting to resources like wind and solar implies having to deal with their natural fluctuation. Therefore the adaptability of the power grid and its ability to accommodate generators characterized by non-predictable generation patterns becomes an issue.

The introduction of electric vehicles poses another challenge to the power grid. Without the chance to intervene directly on the loads, electric vehicles represent a mere additional demand, which is forecasted to increase over time and become so relevant that the existing power grid may not be able to sustain it.

Finally, reaching a more environmentally sustainable electricity generation represent an additional challenge. The whole system, from generation to distribution, should attain a better efficiency and a reduction of greenhouse gases and air pollutant emissions.

The reported issues highlight the need for vast improvements of the power grid, realizing a smarter system capable to dynamically change and adapt to fluctuations of sources and loads, therefore being able to guarantee stability and reliability in grid operations. In literature, such a system is generally referred to as the *Smart Grid*.

1.1.2 The concept of Smart Grid

There is no unique definition for the *Smart Grid*. The European Technology Platform [1.5] defines it as:

> *‹‹ A Smart Grid is an electricity network that can intelligently integrate the actions of all users connected to it – generators, consumers and those who do both – in order to efficiently deliver sustainable, economic and secure electricity supplies››.*

According to the U.S. Department of Energy [1.6]:

> *‹‹ A Smart Grid uses digital technology to improve reliability, security and efficiency (both economic and energetic) of the electric system, from large generation through the delivery systems to electricity customers and a growing number of distributed generation and storage resources››.*

Surely, the Smart Grid represents the evolution of the existing grid and makes extensive use of power systems, IT and communication technologies to effectively and efficiently deliver electricity to all the users of the grid. Two are the concepts around which the idea of a smart grid revolves: the pervasive use of computer-based remote control and automation, and the bidirectional flow of both energy and information.

Up to now the energy flew in only one direction, from the power plants to the customers: therefore, these constitute mere “end users”, loads, strictly dependent from the centralized generation plants to fulfill their electricity needs. Nonetheless, the increasing diffusion of renewable resources based generators is allowing for the creation of small size power plants that connect to the grid at the distribution level. Moreover, small scale generators may be installed directly by individual users in their premises: in this context they become not simply passive consumers, but active actors on the power grid. The producer and consumer roles are not fixed anymore, but can be considered dynamic: the same power user can act as a buyer of energy, but can also produce locally his own electricity and be willing to sell to the other users of the grid the amount that exceeds his needs.

The same situation may arise with the diffusion of electric vehicles and their usage, while connected to the grid for charging, as distributed energy reserve. In this way, electric vehicles may act as provider of

ancillary services to the power grid: this paradigm goes under the name of Vehicle-to-Grid.

For this scenario to be effective, the power grid must allow bidirectional power flows: particularly, referring to the distribution side of the grid, becomes crucial the chance of interaction between multiple users.

Naturally, this evolution of the grid needs to be sided by bidirectional information flows: i.e. the power users willing to feed the grid with their own produced electricity need to be informed of the prices they can sell their energy at, and need to receive clearance by the system operator, which is actively monitoring the state of the grid, to input such electricity into the grid. Renewable energy resources, given the variability of their primary sources, need to negotiate their access to the grid, and to communicate energy generation availability or need for compensation by other backup sources and generators.

The future grid must be equipped with and adequate metering and communication infrastructure. The meters, to be installed in customer premises, at transmission network nodes, in the distribution network and at production sites, are essential to gather a real-time picture of the state of the power grid. Sensors, transducers, signal acquisition and processing devices then represent the real world interface for the information and communication infrastructure, which is the backbone of a smart grid. Advanced metering infrastructure have been the object of research and investments in recent years: Automatic Meter Reading (AMR) constitutes the first attempt at monitoring all the parts of the grid.

Moreover, having real time data allows for taking proper countermeasures when an unforeseen event occurs or when the situation on the grid changes: for example it is possible to increase the generators' output when the load is foreseen to increase, or it is possible to allow the injection of electricity into the grid from renewable resources when they become available, or to deliver electricity through other paths when a transmission line is overloaded. Naturally, such a system requires bidirectional communication: the utility company not only may read data from the users (i.e. consumptions or usage statistics), but can directly interact with them, sending load commands or price signals. This is the principle on which architectures such as the

Advanced Metering Infrastructure (AMI) are based upon. The chance to send command or price signals to devices connected to the grid constitutes the basis for the applicability of load shaping programs, thus attaining proper Demand Response.

The additional step brought about with the *Smart Grid* is having a pervasive control and management algorithms that can take actions on the grid automatically, without the need for human intervention. The power grid becomes then an intelligent system, self-managed and capable of auto-healing and automatically integrate its different parts in the most effective and efficient way [1.3]. Note that the concept of *efficiency* and *optimality* in this case depend on the goals set in designing the management algorithms: it may mean ensuring the highest revenues to all the stakeholders of the grid, or minimizing the environmental impact, or also to exploit renewables as much as possible, or to minimize electricity consumptions.

Another important aspect to consider is the modification of topology of the electrical network. Up to now, the grid has been mainly a vertical system; however, the diffusion of small scale generators determines the presence of distributed electricity sources, connected to the grid at the same level as the loads. Therefore, the electrical network is transforming into a more horizontal and less hierarchical system: the electricity locally produced can supply the customers in the neighborhood, reducing the energy to be transferred from the central power plants. This not only may alleviate transmission-related issues, but can avoid or at least make less impactful phenomena like domino failures: users connected to a local grid may auto-sustain themselves with the locally produced electricity, being, at least for a limited period, independent from the main grid. This behavior, known as *islanding*, can bring about a complete reshape of the grid topology: it can be organized as an aggregation of local grids (the so-called *microgrids*) [1.1],[1.4].

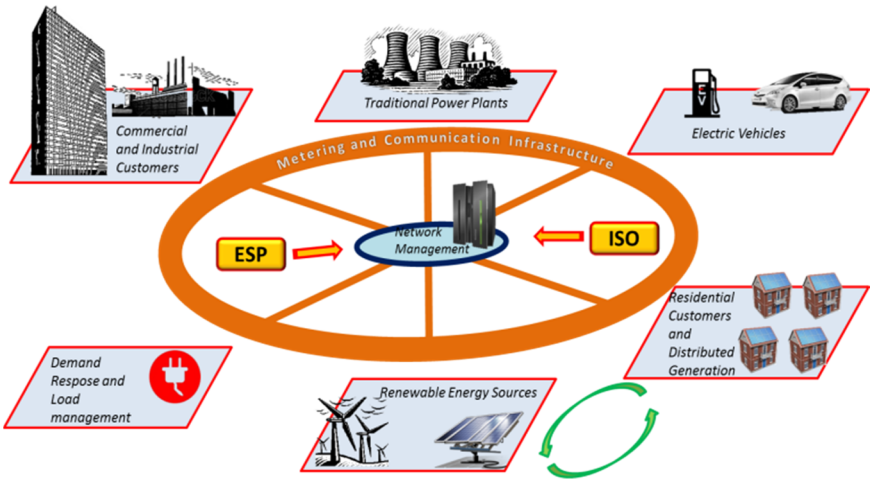

Figure 1.1 – Integration of all grid actors in a smart grid

In conclusion, the main goals and benefits related to the implementation of a *Smart Grid* can be summarized in:

- The ability to accommodate all generation and device options
- Pervasive system automation: ability to respond to system disturbances, auto-healing capabilities, optimization of all grid assets
- Ability to monitor the characteristic electric quantities and the power quality, taking actions to ensure the best possible quality
- Decreasing oil consumptions by reducing the need for inefficient generation during peak periods
- Active customer participation and the opportunity of enabling new grid services and functions

Table 1.1 – Comparison between today's grid and the Smart Grid

Preferred characteristics	Today's Grid	Smart Grid
Active Customer participation	-Customers are uninformed and do not participate	-Informed, involved customers -Demand Response programs -Distributed Energy Resources
Accommodation of all generation and storage options	-Dominated by central generation -Obstacles for full exploitation of distributed generation	-Many distributed energy resources -Focus on integration of renewable sources
New products, services and markets	-Limited, poorly integrated wholesale markets -Limited opportunities for consumers	-Mature, well-integrated wholesale market -Growth of new electricity markets with customer participation
Power quality	-Focus on outages -Slow response to power quality issues	-Power quality is a priority, with a variety of quality/price options -Rapid resolutions or grid-related issues
Optimization of assets and efficient operation	-Little integration of operational data with asset management	-Grid is continuously and thoroughly monitored -The grid becomes proactive, flexible and capable of adapting to varying grid conditions
Self-healing	-Responds to prevent further damage –Focus on protecting assets following a fault	-Automatically detects and responds to problems -Focus on prevention, minimizing impacts on grid stakeholders
Resiliency against cyber-attacks and natural disasters	-Vulnerable to attacks and natural disasters -Slow response	-Resilient to cyber-attacks and natural disasters -Rapid restoration capabilities

1.1.3 Technical challenges

Renewable energy systems, such as solar, wind, geothermal and hydropower, have the potential to make a substantial contribution to power supplies. Their effective integration onto the grid, one of the requirements a smart grid must satisfy, involves dealing with the

intrinsic variable nature of their output in order to optimize the operation of the entire system. Therefore, even existing power plants will need to be operated differently. System-level flexibility may be attained also resorting to storage and demand response programs. However, there is still the lack of proper modeling tools for operations and planning, as well as policy and regulation, that may provide insight on an integrated management and interaction of all energy resources [1.1],[1.4],[1.7].

Distributed Generation (DG), Demand Response Resources (DRRs) and Energy Storage Systems (ESSs), also onboard electric vehicles, can improve grid flexibility and enable a cleaner, more reliable and efficient power generation and delivery system. DG and ESSs, collectively referred as Distributed Energy Resources (DERs), and DRRs can also help in relieving transmission congestion and in favoring the penetration of renewable resources. As for DERs, there is still a lack of coordination, with units operated on local autonomous basis, and of metering infrastructures and models that can provide grid stakeholder with sufficient visibility on DERs operations, and their impacts on the grid. DRRs are increasingly looked at, not only for peak shaving, but as part of distribution operations, capable of increasing grid efficiency and reliability and of providing ancillary services (i.e., regulation). However, a metering, communication and command infrastructure, for real-time information on the status of the grid and DRRs control, is still missing [1.4],[1.7-1.9].

As seen, a smart grid requires bidirectional energy and information exchange. Therefore, all the electrical infrastructure, in particular the distribution grid where most of the distributed generation resources will be located, need to be modified: i.e. safety devices and measures must be altered considering that electricity may be fed into a section of the network from both ways, power converters must be redesigned as 4-quadrant systems, instead of two-quadrant ones [1.1],[1.4].

A pervasive sensing and communication network must be put in place: sensing devices that monitor the status of the grid at each level are needed; at the same time such devices must be able to communicate to the independent system operator the status of the electrical network. Therefore suitable communication protocols must be developed. In fact, they should allow real-time communication and should be interoperable

across different devices produced by different manufacturers, so that a single element of the infrastructure may be substituted with an alternative one without any hindrance in functionality. Massive amount of data need to be collected and properly utilized. In fact, renewable resources, ESSs, DG, DRRs add complexity to the grid and require grid operators to be able to respond to fast dynamic changes to maintain system stability and security. Therefore, comprehensive grid models and system operator tools must be developed and must be able to fully utilize the vast amounts of data being generated by the new technologies and devices being deployed [1.4],[1.7-1.9].

One aspect to emphasize is the security of data communication: since the monitoring infrastructure collects and transmits sensible information about all the users (i.e. statistics of consumption of a single user, personal data needed for billing and accounting), encryption techniques must be adopted to guarantee that the communication channel is secure. Moreover, being the electrical network a fundamental asset, in the scenario in which all the management is done relying on ICT technologies, protecting the information infrastructure from unwanted intrusions becomes a top priority. Hence, cyber-security is one of the key issues in the development of a smart grid scenario. In the security issues is included also the tampering and fraud detection: a system that has auto-healing and self-management capabilities in the eventuality of a manumission need to be able to locate it and restore the normal operating conditions [1.7-1.10].

With the deployment of networked sensors and development of advanced metering infrastructures, the amount of available data is enormous. Mining, analyzing, and managing the data can deliver meaningful and actionable information for model inference and state-based control. Data analytics can help inform planners, operators, and business units regarding the value and use of grid resources, in addition to supporting autonomous control of operations. On this account, proper decision tools and advanced control methodologies for operators to facilitate automated responses to optimize the system and allow distributed decision-making must be developed. Devices in the sensing and communication network must be able to receive commands, integrating or interfacing with actuation devices that allow to intervene on the grid. Different attempts have been made at realizing such and

architecture, first with SCADA (only for generation and transmission) and AMI. However, what makes the Smart Grid a leap forward is the provision of adaptive management algorithms, which realize full automatic operation and control [1.7].

The evolution of the grid into a smart system involves new technologies, devices and applications that need to be backed by robust operational and business models. In fact, it is still not completely understood the marketability and return on investment (ROI) for some of the new grid applications. There is the need for performance metrics to build cost-benefit and life cycle models for the new grid devices and applications: such models can drive the investments and allow to develop new businesses. The transformation of passive customers into active users on the grid requires open access to the energy market, and allows for mutual interaction – not only from a technical point of view, but also in terms of business relations – between all grid stakeholders. An example is represented by the idea of Virtual Power Plants (VPPs): users, not necessarily close one to another, can sell the energy they produce on the market, acting together as if they are a single power plant [1.1],[1.7].

Electric power industry regulatory framework and business models are still geared toward the old grid, and regulatory incentives for reliability, efficiency and renewables are fragmented. There is the need for standardization of protocols, methods, algorithms and certification of the multitude of metering devices on the grid. Another issue is the lack of policy coordination among entities and regulatory bodies that may influence grid development: a system so interconnected requires certain and shared policies, which instead often rely on the decisions of single local or state government. On this regard, given the heavy reliance of smart grid technology on grid measurement data, it must be won the resistance of some communities to smart metering devices installation [1.7-1.9].

1.2 Demand Response

Demand Response (DR), with its ability to improve grid flexibility and help for a more efficient and effective power delivery, represents

an integral part of a smart grid. The U.S. Department of Energy (DOE) defines DR [1.11] as:

> *‹‹Changes in electric use by demand-side resources from their normal consumption patterns in response to changes in the price of electricity, or to incentive payments designed to induce lower electricity use at times of high wholesale market prices or when system reliability is jeopardized. ››*

DR includes all intentional modifications to consumption patterns of electricity of end-use customers that are intended to alter the timing, level of instantaneous demand, or the total electricity consumption. By promoting interaction and responsiveness of the customers, DR brings about short-term economic benefits for both customers and utilities. In addition, since the overall system reliability results improved and the peak demand reduced, DR helps in reducing overall plants and capital cost investments, and postpones the need for electricity network upgrades.

Since 1970s, utilities have implemented some kind of Demand Side Management (DSM) program, referring with it to any activity that influences the loads on the customer side of the meter. DSM refers only to energy and load-shape modifying activities undertaken in response to utility-administered programs. It does not refer to energy and load-shape changes arising from the normal operation of the marketplace or from government-mandated energy-efficiency standards.

DR entails active participation of customers, in the form of their electricity loads, in balancing electricity supply and demand around the clock with side-by-side competition with supply-side resources. In addition, DR is achieved also through the application of a variety of resource types, including storage and dispatchable loads. Demand Response Resources (DRRs) curtail their loads in response to an economic signal. In fact, although many DR program exist, reduction or shifting of loads is attained either by means of dynamic electricity pricing rates or by means of incentive payments: this last is the case of both programs that involve direct load control and the market-based ones, which involves customers bidding on the market their load reductions [1.12].

Customers participating in DR programs can alter their electricity demand in three different ways:

- reducing their electricity consumptions through load curtailment strategies;
- moving energy consumptions to a different time period;
- using locally generated or stored energy, thus reducing their dependence from the main grid.

DRRs help to balance the supply and demand, allowing to attain various load-shape objectives, such as peak clipping, load shifting, valley filling, and in general ensuring load flexibility. In addition, DRRs have an important role in helping in ancillary service provision.

Demand response resources can offer a wide range of potential benefits, among which [1.13-1.15]:

- Consumers attain bill savings and incentive payments, maximizing their utility; moreover, they become more aware of their own consumptions.
- System operators have a more flexible mean to meet contingencies.
- From the point of view of the generation system, not only load flexibility entails having to resort less to peaking units and can defer network expansions, but can be an important option for mitigating the problems caused by variability of the output of renewable energy sources.

Naturally, there are some limitations and drawbacks connected to use of DRRs: among these, the intrinsic limited potential for DRR implementation, reduced economic advantages when energy recovery in lower-load hours is considered, and potential unintended consequences such as the increase in electricity prices for loads not participating in curtailment provision.

To realize active customer participation, and allow the implementation of DR programs, a bidirectional metering infrastructure is required. With the diffusion of smart meters, customers not only have a clearer picture of their consumptions, but are provided with direct access to energy markets (or, for DR implementations, to load curtailment providers). Through smart meters and an Advanced Metering Infrastructure (AMI) connected to controllable electronic devices, energy management functions can be attained: especially in residential applications, to be accepted by customers, implementation

of DR programs need to be as transparent as possible, enabling users to easily adjust their own energy use [1.7].

A final remark revolves around storage technologies: in a way, DR constitutes a particular case of grid storage. Up to now, given high costs of grid storage, research focus has been on how to effectively integrate and optimize DRRs and Energy Storage (ES), minimizing total costs. However, the services ES and DRRs can provide are essentially the same, with storage devices limited only by the storage capacity (on the other hand, DRRs, involving curtailments that should not hinder customer services, are intrinsically limited to a maximum potential). Therefore the same strategies, enabling devices and infrastructures are applicable in both cases.

1.3 Measurements and metering requirements for SG and DRR management

1.3.1 General and open issues

In order to deploy the advanced applications that constitute integral part of a smart grid, measurement devices, metering infrastructures and communication technologies play a fundamental role. Integration of renewable sources, effective use of distributed generation, implementation of DR programs, all require having specific knowledge about each resource and the ability to make such data available to system operators, utilities and all grid stakeholders. The more the grid moves away from a centralized structure, the more there is the need to coordinate multiple independent players, deeper is the needed knowledge of the state of all parts of the grid [1.1], [1.4], [1.7-1.9].

The first and foremost issue regarding metering requirements for a smart grid is that some of the new grid applications such as DERs and DRRs, still lack of uniform characteristic metrics to evaluate their performance and impact on the grid. A common protocol framework to evaluate, measure and verify aspects such as Energy Efficiency or DR is still missing, with current methodologies varying widely across proposers, markets, organizations and regulatory bodies. Therefore,

there is still lack of agreement on the core system measurements that are needed to the future power system. In some cases, like power measurements in non-sinusoidal conditions (detailed further on), the definition of the measurands have been developed for grid conditions not satisfied anymore, and there is still lack of unanimous agreement on the new definitions to adopt, among several proposed.

A smart grid must be designed for real-time adaptability to changing grid conditions. Therefore, real-time measurements are needed: sensors, data acquisition devices and meters must be able to collect timely measurements, and to make the data available to all grid users. On this account, the diffusion of smart meters and Automated Metering Infrastructures (AMIs) is a key step for the realization of advanced grid applications. However, apart from winning resistance of customers to install smart meters and "opt-out" from utilities' programs for their installation, the devices should be low-cost ones and, possibly, "plug&play". There is the need to develop new wide band voltage and current sensors, which can provide accurate and reliable measurements even under electric absorption/generation in presence of power electronic devices (DC/AC and AC/DC converters, co-generation small plants, etc.) characterized by strongly deformed waveforms.

Through an AMI, for wholesale market participation, visibility of users' consumptions and availability of locally produced/stored energy, as well as availability for load curtailments, need to be provided to grid operators, aggregators, and all other market participants. To implement concepts such as energy efficiency, especially in residential and commercial applications, metering devices need to be able to aggregate all customer-sided energy consumptions and energy availability, and to give visibility of such information not only to grid operators, but also to customers themselves. In fact, informing them about their own consumptions represents the first step in turning passive customers into active grid users.

Effective grid operation depends on the ability of fusing data coming from the vast multitude of sensing devices throughout the grid and integrate them into comprehensive grid models and operational tools.

Up to now, AMI architectures have been developed by different companies - being them utilities, telecom companies or grid service providers – and often employ proprietary technology and protocols. For

an effective interaction of all grid actors interoperability of all grid devices must be guaranteed. Therefore, common standards for grid communications need to be developed and adopted. On this account, several research projects, such as the OPEN meter project, have focused on interoperability as one of the key drivers to truly realize the pervasive sensing and communication network required for smart grid operation.

Finally, another topic related to measurements for the grid is the synchronization between grid metering devices. For a picture of the status of the grid to be significant, acquisition devices need to adopt the same time reference. At the moment, solutions like the phasor measurement units, which allow to monitor the state of the grid, adopt the GPS signal as time reference. There is the need for resilient high-resolution time resources to complement and extend GPS.

1.3.2 Metering needs and requirements

The transformation of passive customers into active users, able to provide services to the grid and sell their energy or capacity availability on the market requires devices able to perform bidirectional measurements. In addition, real-time awareness of a smart grid needs for such measurements not only to be acquired in real-time, but also to convey them to grid operators. Moreover, throughout the grid monitoring infrastructure, smart devices can use such data to intervene on the system, realizing distributed control schemes. All this requires for devices to be able to communicate with each other, both to send data and receive commands.

Meters should be the means by which customers are made aware and can analyze their own consumptions, so to be able to act proactively on the grid. Therefore, one of the metering requirements is to provide users with informative instruments to take actions in the field of energy efficiency, distributed generation, demand response, energy storage.

Among the goals of the described evolution of the power grid is to provide to all grid users better power quality. In fact, due to the diffusion of nonlinear loads and switching power supplies, the voltage and current waveform that can actually be measured on the power grid are far from their ideal sinusoidal form. Phenomena like harmonic and

inter-harmonic distortion, dips and swells, sags and sages must be taken into account. The challenge is particularly complex, since under this conditions it must be defined not only how to perform the measurements, but also what to measure. Moreover, while the definitions of active and reactive power in sinusoidal conditions are clear and there is unanimous agreement on the physical significance of such terms, when moving to non-sinusoidal signals there are several different interpretations in literature. In the presence of distorted current and voltage waveforms the classical metrics used for the evaluation of the active and reactive power and energy lose their usefulness because there is a lack of unique definition of the measurand. The standard IEEE 1459 [1.16] tries to address this topic, but still there is no unanimous agreement on the metrics (or their correction factors) which need to be adopted. The disagreement naturally propagates to the factors that need to be considered while testing the metering devices: there are different standards applicable to active and reactive power measurement devices such as EN 62052-11, CEI EN 62053-21, CEI EN 62053-23, CEI EN 50160, and IEC EN 61000-3-2 [1.17-1.21]. Several kind of disturbances can be considered (underlining once again that this is not a topic definitely assessed in literature): deviations from fundamental frequency, supply voltage fluctuations, light flicker, voltage dips and interruptions, overvoltages, dissymmetry, voltage and current harmonics and interharmonics.

In the following paragraphs, an analysis of power quality and power measurement metrics is provided.

1.3.2.1 Power quality

The increasing diffusion of non-linear loads, such as switching power supplies, determines a relevant distortion of the waveforms on the power grid. In fact, such loads represent a source of current harmonics and inter-harmonics: as their concentration increases, the interaction with other devices installed in the same environment increases too, determining a bigger influence on the electricity distribution system. The current harmonics and inter-harmonics interact with the distribution system impedance, causing as a consequence even

deformations in voltage waveforms. The distorted waveforms can be the cause of a wide array of problems, ranging from over-heating in distribution transformers and in electric motors, to malfunctions in electronic equipment. Given the implications, and being electricity a service and a product, as such the supplier must meet some degree of quality in the power supply. The Power Quality (PQ), in its most general form, represent the evaluation and the analysis of the distortion in voltage and current waveforms, with respect to their nominal values, on the power grid, with the aim of containing their negative side effects.

The reference standards for power quality are CEI EN 50160 and IEC 61000-4-30 [1.20-1.21]. Certainly, the most relevant form of low power quality is represented by outages: being the continuity of service the fundamental type of service to provide customers, it has the priority

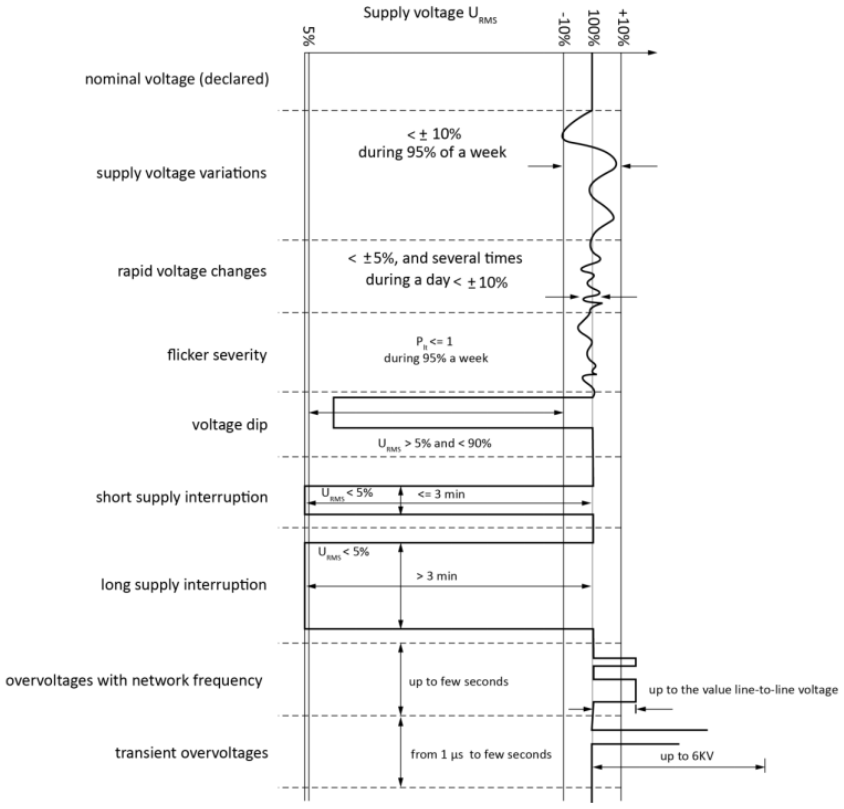

Figure 1.2 – EN50160 requirements in graphical form

against every other factor that may deteriorate the quality of the supply. Mainly eight different phenomena that deteriorate power quality may be listed:

- *Alteration of RMS value*
- *Short-duration alterations (interruption/voltage sags/voltage swells)*
- *Long-duration alterations (extended interruption/over-voltages/ under-voltages)*
- *Supply voltage unbalance*
- *Harmonic distortion*
- *Inter-harmonic distortion*
- *Voltage fluctuations (flicker)*
- *Transient disturbances*

In addition to these, fluctuation of the fundamental frequency is to be taken into consideration. In fact, the frequency of the fundamental keeps steady if there is exact parity between generation and demand. However, even in case power balance condition is met exactly, random increase or decrease in loads disrupts the balance. Frequency variations are extremely important, since many users are extremely sensible to such phenomenon. The CEI EN 50160 sets as a PQ requirement for the fundamental frequency to be contained in the ±1% around the nominal value for 95% of the time.

1.3.2.2 Power metrics

When considering the computation of instantaneous power in case harmonics and inter-harmonics are present in the current and voltage waveforms, their multiple interactions give rise to several products, not representative of the energy exchange, but whose correct interpretation would be needed for a correct management of the electrical system.

While the definitions of active and reactive power in sinusoidal conditions are clear and there is unanimous agreement on the physical significance of such terms, the interpretation of the additional terms present in non-sinusoidal conditions is still object of much debate in literature. Several authors have proposed different definitions for electrical power quantities in non-sinusoidal conditions, trying to extend to this domain the properties that active, apparent or reactive power have in the sinusoidal domain. In general, different schools of

thought resort to different approaches regarding the measurement algorithms (identified as *metrics*) to compute the electrical power quantities of interest. The main ones are:

i. *Theories in the frequency domain*
ii. *Theories in the time domain*
iii. *Theories at instantaneous values*

The *theories in the frequency domain* apply to periodic waveforms and are based on the decomposition of the signals with the Fourier series. These approaches originate from *Budeanu*'s theory [1.22]. While preserving the same definition for apparent power, a kind of superposition of effect is considered, adopting in non-sinusoidal conditions the same definitions for active and reactive power defined in sinusoidal conditions. However, they do not include all the power terms. The same inconsistency is obtained considering the apparent power. To make up for the inconsistencies Budeanu resorts to an additional power term, the *distortion power*. Other theories following the same school of thought, such as the ones by *Shepherd and Zakikhani* [1.23] or *Sharon* [1.24], arise from criticism and corrections to Budeanu's theory.

The *theories in the time domain* arise from the current-splitting principle and are born from the one developed by *Fryze* [1.25]. In fact, current is divided into two terms, one of the same shape of the voltage waveform and an orthogonal component, accounting for the difference total current and the first term. This approach preserves the definition of apparent power. The active power is instead relative only to the first current term, with the non-active power obtained from the apparent and active ones. Basically the foundation of Fryze's theory is considering non-active all the power components that cannot be considered active. The theories of *Kusters and Moore* [1.26], *Page* [1.27], *Czarnescki* [1.28], extend Fryze's approach, decomposing the non-active current and relate its components to physical properties of the considered load.

The *theories at instantaneous values* rely on power definitions that include time-dependent terms, instead of constant quantities like RMS and average values. Such approaches, like the ones from *Ferrero and Superti-Furga* [1.29], are becoming increasingly diffused thanks to

developments in power electronics and control techniques, which enable them to be applied in active systems for harmonic compensation.

With the scientific debate still open, up to now the only standard regarding the power measurements in sinusoidal and non-sinusoidal conditions is the IEEE 1459-2010 [1.16]. It partly adopts some definitions from the theories introduced in the previous paragraphs and partly introducing new ones. The aim of the standard, even if not reaching univocal definitions, is to provide a mean to analyze the electrical supply and to help the design and use of instrumentation for power measurements.

1.3.3 Measurements for storage and battery management

Storage systems will play a fundamental role in ensuring grid flexibility and reliability. In particular, batteries represent an attractive solution to propel many of the new grid applications (i.e., penetration of renewable sources, development of a grid topology organized in *microgrids*), and, with their costs decreasing, they will become more and more diffused. However, there is the need for models and tools that allow an estimation of their useful life: only then storage systems can be fully encompassed them into grid investments planning.

Batteries are complex systems and, although complicated but accurate model that describe their behavior exist, to be effectively integrated into the grid simpler system-level models, which capture only the parameters required for the specific applications the batteries are used for, are needed.

Battery measurements involve their electrical behavior, requiring in this case monitoring quantities such as output voltage, current, power output. One of the key parameters that is needed to effectively utilize batteries is the state of charge, which represents the energy stored into the battery, and therefore its availability: there exist techniques that allow to obtain such value as an indirect measurement starting from electrical quantities.

Since a battery tends to degrade with usage, lowering the amount of energy it can hold, all battery operational parameters need to be weighted versus battery degradation, by using aging models.

Chapter 2

Design, realization and testing of a real-time bidirectional smart meter

In the Smart Grid (SG) arena, measurement systems play a primary role no longer related only to energy billing but also to the online monitoring of the network. As the source of the data for the functioning of the network, these measurement systems constitute a fundamental element of the "smart" architecture. Typically, we refer to the metering system as the "smart meter". The smart meters are required to perform accurate and real-time bidirectional power and energy measurements. Indeed, the Directive 2006/32/EC states the customers must be billed for their actual consumption: such specification may only be met through reliance upon real-time metering devices that monitor the actual state of the network. Moreover, the possibility for a user to act both as a customer and as an energy supplier poses the need for bidirectional metering devices.

The smart meter must perform also another essential task to achieve higher energy efficiency: it should help the customers in building up better awareness regarding their consumptions and, eventually, ease up their path to a better energy utilization.

In this Chapter we introduce the implementation of a low-cost real-time bidirectional smart meter, designed to guarantee good measurement performances in sinusoidal and non-sinusoidal conditions, and able to interact with other meters (such as gas and heat meters) acting as a hub for all energy consumptions. We then present our proposal for the metering infrastructure, which includes the meter and provides both customers and system operators with visibility of all energy consumptions. In addition we describe a load management policy, implemented on the management unit of the metering infrastructure, that makes use of the actuators embedded on the meter to administer load curtailments in response to energy price signals.

2.1 Electricity meters to face new challenges

2.1.1 Evolution of electricity meters

Electricity meters are devices used to measure the quantity of electricity supplied to a customer, essentially to be used for billing and to calculate transmission and distribution costs for grid operators. The most common type of meter is the accumulation one: it integrates the power absorption over a period of time, generally coinciding with the billing period. Then the reading of the measurements is carried out manually by an operator. More recently, meters that record energy usage over shorter intervals have been adopted: they allow for better customer profiling and therefore to design tariffs that reflect demand, and for the customers to better understand their consumptions.

However, it must be noted that manual reading of customers' consumptions represents a relevant cost for utility companies. For this reason, systems that allow for users' consumptions reading and correct billing without the need of a human operator have been of great interest in research and industry fields. Consequently, several Automatic Meter Reading (AMR) programs have been developed: in this case digital measurement data is obtained and transmitted to the utility company via a one-way communication network.

Although AMR allows for a better monitoring of the distribution network, it results still limited in the services it can provide to customers and utilities.

As an evolution of the metering devices and architecture, a two-way communication infrastructure has been introduced. The so called Advanced Metering Infrastructure (AMI), and the meters interfacing with it, can bring significant advantages to all the stakeholders of the power grid (see Table 2.1). First of all, the customers may be directly informed about their consumptions, leading in the long run to better electricity utilization and, ultimately, to energy savings. In addition, the customer service is improved and suppliers can apply variable pricing schemes. Finally, demand response resource management and distribution control can be attained.

Table 2.1 – Advantages of smart metering

	Energy suppliers and network operators benefits	Customer benefits	Overall benefits
Short-term	Lower metering costs and more accurate readings	Improved information determines energy savings	Better customer service
	Easier detection of frauds and theft	More frequent and accurate billing	Variable pricing schemes
	Reducing peak demand via Demand Response	Integration with home area automation	Better energy utilization through better management of DR and DG
Long-term	Better planning of generation, network, and maintenance	Enablement to sell ancillary services to the grid (DR, DG, V2G)	Easier integration of new technologies such as EVs
	Support real time system operation		

The idea of a smart grid is in direct continuity with the automation brought about with the AMI, extending its advantages (see Figure 2.1). In fact, relying on the metering and communication infrastructure, the "smart" evolution of the power grid consists in developing new applications, favoring the interactions of new and old actors on the grid,

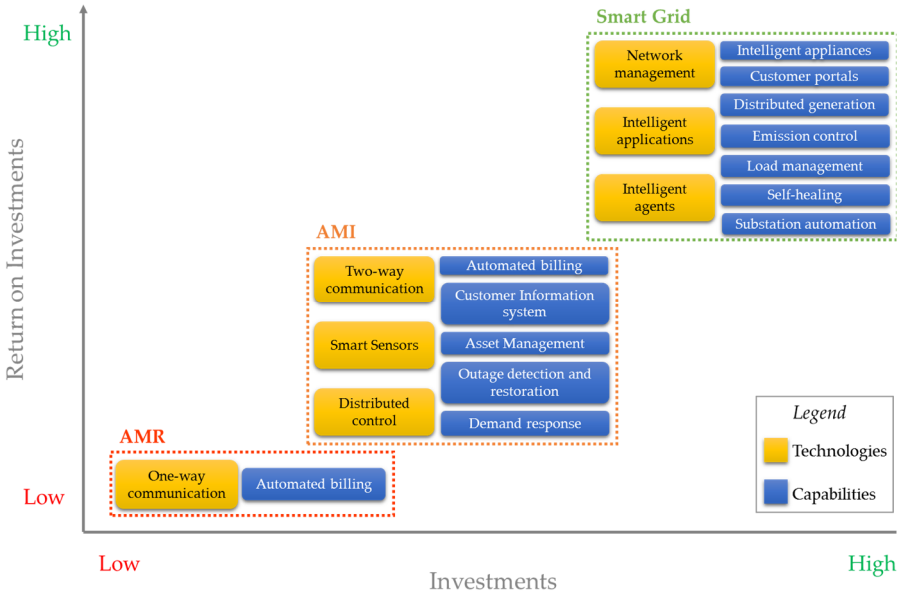

Figure 2.1 – Comparison of Return on Investments vs. Investments between AMR, AMI and Smart Grid

and in providing new and innovative services to the customers. The SG fully encompasses the capability for two-way communication of the network, supporting advanced grid applications such as load management, distribution automation, power quality monitoring, negotiations and bidding on the open energy market.

2.1.2 Current smart meter developments

The metering infrastructure represents a key enabler for the realization of the vision of a smart grid. Thus, devices to measure electricity consumptions and provide advanced features compatible with new grid applications are the object of much research and regulatory effort, investments, and multiple research projects.

Due to the regulatory push by EU, many Member States have implemented, or are about to implement, some legal framework for the installation of smart meters, as shown in Figure 2.2. In some of them electronic meters have already been installed diffusively, even in the absence of specific legal requirements [2.1].

Reports assess that, as of 2011, 45 million of smart meters have already been installed in the EU [2.2] and forecasts are for 180 to 240 million installations by 2020, with customer penetration of about 70% [2.2-2.4] (see Figure 2.3). Significant investments have already been

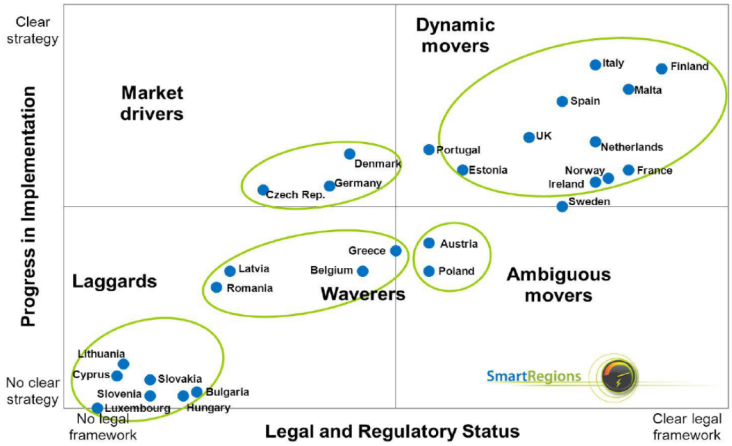

Figure 2.2 – Progress in Implementation vs. Legal and Regulatory Status

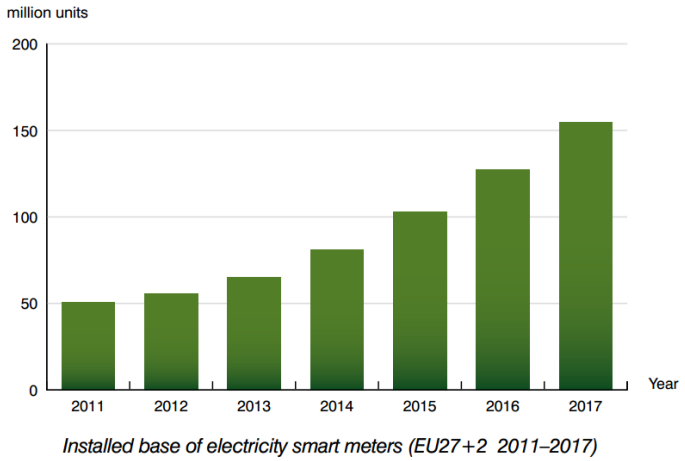

Figure 2.3 – Installed base of electricity smart meters [2.4]

mobilized and a few countries have already proceeded to full smart metering rollout. A conservative estimate is that at least € 5 billion have been spent to date on smart metering pilot projects and roll-outs. Considering the Member States that, at this date, have already committed themselves to, or shown strong interest in, a full smart metering rollout, we can estimate that the total investment in smart metering will be at least € 30 billion by 2020.

The several research projects currently in place in the EU Member States, highlight that three communication infrastructure options are typically available for smart metering purposes: communication via the electricity grid (Power Line Carrier, PLC), communication via telephone lines and the cable infrastructure (ADSL, TV distribution cable) and wireless communication (mobile telephony, Radio Frequency - RF). The choice of a particular communication option strongly depends on the local conditions. However, according to available information, the most widespread communication option is the combined use of PLC for the connection of the smart meter with the concentrator in a secondary substation and the use of GSM/GPRS for the concentrator/management system connection [1.4],[2.2]. On this regard, it is worth citing the OPEN meter project [2.5-2.7], which aims at providing a set of widely accepted open standards to guarantee interoperability of systems and devices to be adopted in the Automated Metering Infrastructure.

Germany and Italy have proven to be two of the most active European countries in the development and adoption of automated metering infrastructures. Interoperability and coordination are the main drivers in the German E-Energy framework. It encompasses six different and complementary projects related to the implementation of a smart ICT-based power grid, integrating all the actors of the future grid. The Smart Watts project [2.8-2.9] aims at realizing active customer participation in a demand response framework: the smart meters are needed to provide near-time consumptions data, used to adjust energy prices dynamically and offer economic incentives for customers to shift their consumptions to off-peak (cheaper) periods. Similar approach is followed by the MeRegio project [2.8],[2.10], aiming at in-house appliances optimization according to energy price signals for better energy use and energy savings.

With a budget of over €2 billion, Italy accounts for almost half of the total spending related to smart meters projects in the EU. The great majority of this budget is however attributable to only one project, the *Telegestore* project by generation and distribution operator ENEL, which consisted in the national roll-out of smart meters in Italy [2.2].

From the several projects in place on the topic, a common trait emerged: the main barriers to the adoption of smart metering technologies and infrastructures in Europe are policy-related, social or regulatory, rather than technical. They range from lack of interoperability standards to regulatory uncertainty regarding roles and responsibilities in the new smart grid applications, from consumer resistance against new technologies and habits to limited repeatability of pilot projects due to different local policies. To overcome such problems and reach coordination throughout the Union, projects like the Meter-ON were born, aiming to provide any grid stakeholder with clear recommendations on how to tackle the technical barriers and the regulatory obstacles endangering the uptake of smart metering technologies and solutions in Europe [2.11].

Great is the thrust towards the adoption of smart grid and smart metering technologies also in North America. In the U.S. 38 million of smart meters are currently installed, and the Federal Energy Regulatory Commission (FERC) forecasts they will be 65 million by 2015. From the point of view of providing better customer services, industry is

working to favor interoperability and clearer information to customers: with this aim, the Green Button Initiative focuses on the adoption of a common and standardized format for energy data coming from smart meters and AMR meters. Efforts to standardize the format of energy usage information and protect customer privacy have fostered the rapid development of new applications to further engage and inform customers.

The diffused adoption of smart meters helps also in managing a now aging power grid, allowing for quicker identification of outages and potential problems on the grid. However it must be pointed out that there is not uniformity in regulations over all the States, leading in some cases to local regulations hindering the realization of an all-automated metering infrastructure (it is the case of "opt-out" programs, which leave to individual customers the opportunity to forgo advanced meter installations) [2.12]. Nonetheless, fueled by industry-led adoption projects, penetration of smart meters and AMI is growing, as shown in Figure 2.4.

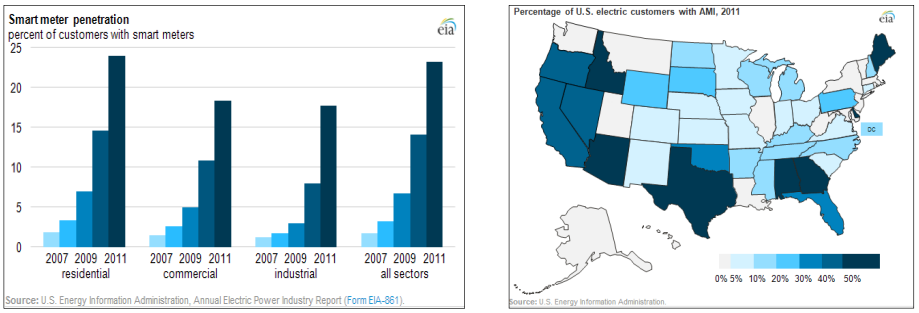

Figure 2.4 – Smart meter penetration in the U.S.

2.1.2.1 OPEN meter project

The main objective of the OPEN meter project is to specify a comprehensive set of open and public standards for AMI, supporting electricity, gas, water and heat metering, based on the agreement of all the relevant stakeholders in this area, and taking into account the real conditions of the utility networks so as to allow for full implementation. The Scope of the project is to address knowledge gaps for the adoption of open-standards for smart multi-metering equipment and all relevant

aspects – regulatory environments, smart metering functions, communication media, protocols, and data formats – are considered within the project. The result of the project is a set of draft standards, based on already existing and accepted standards wherever possible. These standards include the IEC 61334 series PLC standards, the IEC 62056 DLMS/COSEM standards for electricity metering, the EN 13757 series of standards for utility metering other than electricity using M-Bus and other media. These existing standards will be complemented with new standards, based on innovative solutions developed within the project, to form the new body of AMI / smart metering standards. The resulting draft standards will be fed into the European and International standardization process.

The project is strongly coordinated with the smart metering standardization mandate given by the European Commission to the European Standardization Organizations, CEN, CENELEC and ETSI. The OPEN-meter project should remove a perceived barrier to the wide scale adoption of smart metering in Europe, by ensuring that the requirements for smart metering can be met by products and systems based on open, international standards to ensure interoperability, and that are accepted and supported by the widest possible circle of stakeholders. The OPEN meter project is financed by the European Commission within the Seventh Framework Programme, Area 7/1: Smart Energy Networks / Interactive distribution energy networks.

2.1.3 Industrial products

2.1.3.1 Networked Energy Services (NES) smart grid system from Echelon

The Networked Energy Services (NES) [2.13] is a software-driven smart grid solution what incorporates smart meters, grid connectors and concentrators, and system software (see Figure 2.5). The meters are deployed in a meshed network and communicate with each other and with the concentrator via Power Line Communication (PLC). Communication with the utility's management system is based on an IP connection. Optional modules allow connection over ZigBee.

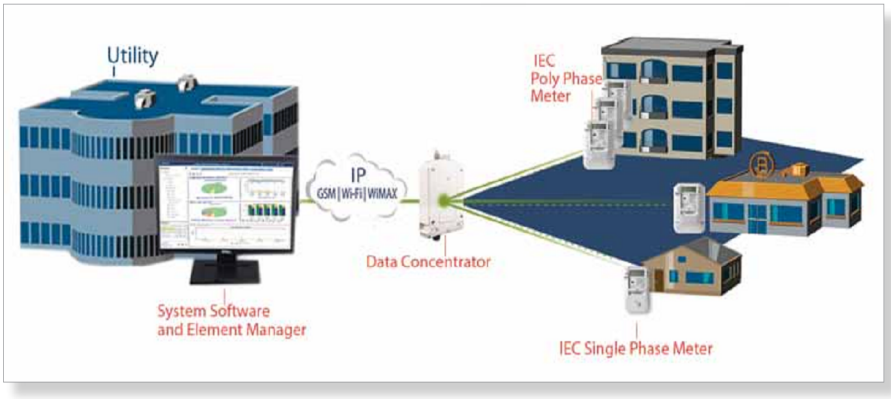

Figure 2.5 – A graphical representation of NES from Echelon

The main component of NES smart grid systems is the IEC Single Phase Smart Meter, designed for residential and small commercial energy consumers. Each meter provides a set of different energy services when operating within the NES system. Some of these services are: automated two-way meter reading, power quality measurements and analysis, remote electronic disconnect and local physical reconnect, distribution system asset optimization, outage detection and restoration management, blackout detection, real-time direct load control, load profiling, billing for time-of-use, prepay, and optional max demand, display of energy consumptions and relevant energy usage parameters.

The main metrological characteristics are reported in the following:

- Active: Class 1 certified to IEC 62053-21, Class B certified to EN 50470-3 (MID)
- Reactive: Class 2 certified to IEC 62053-23
- Operating temperature: -40˚ to +70˚ C
- Voltage:
    - 220V to 240V phase-to-neutral, range -20% to +15% (MTR 1000 Series)
    - 230V phase-to-neutral, range -20% to +20% (MTR 0600 Series)
- Frequency: 50Hz +5%
- Service type: 1-phase, 2-wire

2.1.3.2 The Grid IQ AMI P2MP Solution from GE digital energy

The Grid IQ AMI P2MP Solution [2.14], represented in Figure 2.6, is a metering and communication infrastructure, which makes use of a Point-to-Multipoint or RF "Star" architecture. The Smart Meter SGM1100 adopts PLC communications with the DLMS/COSEM protocol to interact with the Access Point. The Access Point is designed for indoor or outdoor operation and can be easily deployed on buildings, utility poles or communication towers enabling low cost pervasive coverage in the most challenging environments. The Smart Meter Operating System (SMOS) provides visibility to data retrieved from network management services. SMOS also provides the back-office integration functions that deliver data from across the network to core operational systems, such as Outage Management Systems and other applications. SMOS supports various industry standard interfaces and protocols.

The Smart Meter allows time-of-use billing measures, multiple load profile recording and multi energy recording; in addition monitors power quality parameters and stores statistical and historical load data with up to 1 minute resolution. Finally, it allows for remote firmware update.

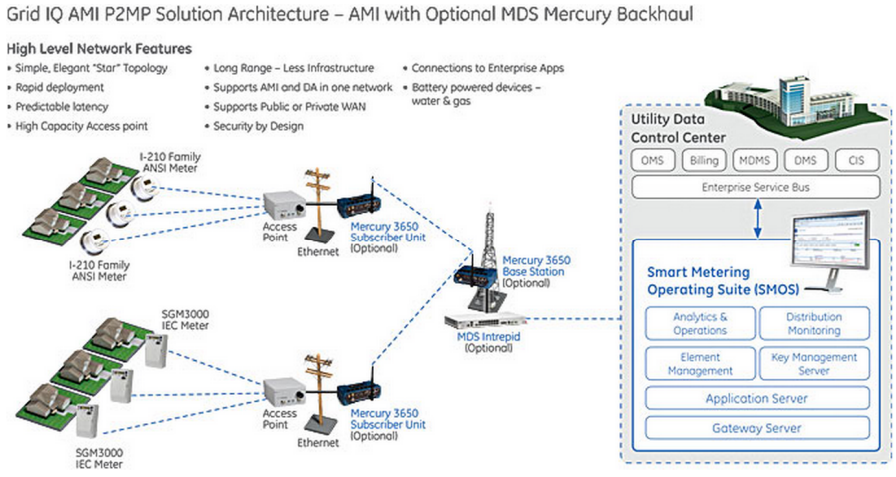

Figure 2.6 – A graphical representation of "The Grid IQ AMI P2MP Solution" from GE digital energy

From a metrological point of view, the meter main characteristics are:

- Active: Class B certified to EN 50470-3 (MID)
- Reactive: Class 2 certified to IEC 62053-23
- Operating temperature: -25˚ to +70˚ C
- Nominal voltage: 230 V ±20%
- Configuration: Single phase single element direct connect

2.1.3.3 Other products

Some other industrial manufacturers, such as Texas Instruments, Accent, etc., provide Integrated Circuits, System-On-Chips, Printed Circuit Boards, etc. for the development of Smart Metering solutions [2.15-2.16]. They can be used by manufacturers of smart metering solutions to produce industrial implementations.

2.2 Mathematical formulation for power quality indices and power metrics

One of the main requirements in designing a measurement device and, specifically, a power meter is the definition of the quantities that must be measured. Some of these are well defined in literature and standards, while for some others there are no unanimous definitions. For this reason, before designing the measurement device, it is important to provide the mathematical formulations of the quantities of interest. With the purpose of designing a device that exhibits good measurement performances even in non-sinusoidal conditions, we resort to metrics for power measurements specifically developed under the assumption of non-sinusoidal waveforms and we consider the computation of power quality indices. To better explain the algorithms and signal processing techniques implemented in the device, in this paragraph, the mathematical definitions of the main power measurements approaches and power quality indices are provided.

2.2.1 Power quality indices

As seen in paragraph 1.3.2.1, power quality (PQ) represents the evaluation and the analysis of the distortion in voltage and current waveforms. As such, some metrics that allow to quantify waveform deformation, and that allow standards to set PQ requirements, are needed. The main indices which allow to evaluate the power quality are reported below:

The ***Root Mean Square*** **(RMS) value** for a continuous signal $f(t)$, over an interval $[T_1, T_2]$ integer multiple of the signal period is given by:

$$RMS = \sqrt{\frac{1}{T_2 - T_1}\int_{T_1}^{T_2} [f(t)]^2 \, dt}$$

The ***Root Mean Square*** **(RMS) value** for a sequence of N discrete samples $\{x_1, x_2, ..., x_N\}$ becomes:

$$RMS = \sqrt{\frac{1}{N}\sum_{i=1}^{N} x_i^2}$$

Current harmonic distortion (ITHD):

$$ITHD = \frac{\sqrt{\sum_{h=2}^{\infty} I_h^2}}{I_1} \cdot 100 \quad (\%)$$

Where I_1 represents the current at the fundamental frequency and I_h is the *h-th* current harmonic.

Voltage harmonic distortion (VTHD):

$$VTHD = \frac{\sqrt{\sum_{h=2}^{\infty} V_h^2}}{V_1} \cdot 100 \quad (\%)$$

Where V_1 represents the voltage at the fundamental frequency and V_h is the *h-th* voltage harmonic.

Short-term flicker severity (P_{ST}):

P_{ST} is calculated over a period of ten minutes according to a standardized formula which takes into account the response of the human eye and brain. Given d_{max} the maximum relative voltage change, and F the shape factor associated with the voltage change, P_{ST} is computed as follows:

$$t_f = 2.3(F d_{\max})^{3.2} \quad \rightarrow \quad P_{ST} = \left(\sum t_f / T_p\right)^{1/3.2}$$

with T_p the observation period. The value of P_{ST} shall not be greater than1.

Long-term flicker severity (P_{LT}):

P_{LT} is calculated from a sequence of 12 P_{ST} values over a twelve hour interval, according to the following formula

$$P_{LT} = \sqrt[3]{\sum_{i=1}^{N} \frac{P_{STi}^3}{12}}$$

The value of P_{LT} shall not be greater than 0.65.

2.2.2 Power metrics

In paragraph 1.3.2.2, we introduced the different theories and approaches regarding power metrics. In the following, we provide the mathematical formulation for *Budeanu*'s [1.22] and *Fryze*'s [1.25] approaches, and an overview of the formulations introduced in the IEEE 1459-2010 standard [1.16].

In sinusoidal conditions, the instantaneous power $p(t)$, which is the product of voltage and current waveforms, is composed of a constant term (the active power) plus a time-dependent term. If $v(t)$ and $i(t)$ represent voltage and current waveforms

$$v(t) = \sqrt{2}\cos(\omega_1 t) \tag{2.1}$$

$$i(t) = \sqrt{2}\cos(\omega_1 t - \varphi) \tag{2.2}$$

The instantaneous power $p(t)$ is given by:

$$p(t) = v(t)i(t) = VI[\cos(\varphi) + \cos(2\omega_1 t - \varphi)] \tag{2.3}$$

$$\begin{aligned} p(t) &= VI\cos(\varphi)[1 + \cos(2\omega_1 t)] + VI\sin(\varphi)\sin(2\omega_1 t) = \\ &= P[1 + \cos(2\omega_1 t)] + Q\sin(2\omega_1 t) \end{aligned} \tag{2.4}$$

P represents the active power, a unidirectional component that is responsible for the energy exchange. Reactive power Q accounts for power fluctuations in AC circuits which do not result into net transfer

of energy. Active and reactive power can be related via the apparent power S:

$$S = VI = \sqrt{P^2 + Q^2} \tag{2.5}$$

The situation, however, changes when harmonics and inter-harmonics are present in the current and voltage waveforms. In fact, considering an example with both voltage and current waveforms with an additional harmonic, we obtain:

$$v_d(t) = \sqrt{2}V_1\cos(\omega_1 t) + \sqrt{2}V_2\cos(\omega_2 t) \tag{2.6}$$

$$i_d(t) = \sqrt{2}I_1\cos(\omega_1 t - \varphi_1) + \sqrt{2}I_2\cos(\omega_2 t - \varphi_2) \tag{2.7}$$

In this case the instantaneous power $p(t)$ is given by:

$$\begin{aligned} p_d(t) = v_d(t)\, i_d(t) = {} & [V_1 I_1 \cos(\varphi_1) + V_2 I_2 \cos(\varphi_2)] + \\ & + [V_1 I_1 \cos(2\omega_1 t - \varphi_1) + V_2 I_2 \cos(2\omega_2 t - \varphi_2)] + \\ & + \{V_1 I_2 \cos[(\omega_1 - \omega_2)t + \varphi_2] + V_1 I_2 \cos[(\omega_1 + \omega_2)t - \varphi_2] + \\ & + V_2 I_1 \cos[(\omega_2 - \omega_1)t + \varphi_1] + V_2 I_1 \cos[(\omega_1 + \omega_2)t - \varphi_1]\} \end{aligned} \tag{2.8}$$

The multiple interactions of voltage and current waveforms determine additional terms, which are not representative of an energy exchange. It is on the definition and physical interpretation or these terms that the power metrics theories differ from each other.

Budeanu's approach belongs to the *theories in the frequency domain* and is based on the decomposition of the signals with the Fourier series. In this case, the definition of apparent power is preserved, and for active and reactive power the same definitions as in sinusoidal conditions are employed. Their expressions are:

Active power:

$$P = \sum_{n \in N} V_n I_n \cos(\varphi_n) \tag{2.9}$$

Reactive power:

$$Q_B = \sum_{n \in N} V_n I_n \sin(\varphi_n) \tag{2.10}$$

As it is clear comparing these expressions to Equation (2.8), they do not include all the power terms. The same inconsistency is obtained considering the apparent power: in fact, it can be proven that $S^2 > P^2 + Q_B^2$. To make up for the inconsistencies, Budeanu has to introduce an additional power term, the *distortion power*, defined as:

$$D_B = \sqrt{S^2 - P^2 - Q_B^2} \tag{2.11}$$

Fryze's theory, instead, operates in the time domain and stems from the current-splitting principle.

Considering a system with an applied voltage $v(t)$ and a current $i(t)$ flowing into it, having the same periodicity, the current can be divided into two terms:

$$i(t) = i_a(t) + i_r(t) \tag{2.12}$$

Where

$$i_a(t) = \frac{\frac{1}{T}\int_0^T vi\,dt}{\frac{1}{T}\int_0^T v^2\,dt} v(t) = \frac{P}{V^2} v(t) \tag{2.13}$$

The $i_a(t)$ is called *active current*, and has the same shape of the voltage waveform. The second current term $i_r(t)$, orthogonal to $i_a(t)$, is the *non-active* current, representing the difference between total and active current:

$$i_r(t) = i(t) - i_a(t) \tag{2.14}$$

This approach preserves the definition of apparent power S. The active power P is dependent only on the current component $i_a(t)$, and the non-active power N is obtained from the apparent and active ones:

$$P = \frac{1}{T}\int_0^T vi\,dt = \frac{1}{T}\int_0^T vi_a\,dt \tag{2.15}$$

$$N = \sqrt{S^2 - P^2} \tag{2.16}$$

Therefore, in Fryze's approach, all power components that cannot be considered active are included in the non-active power term.

Basically the foundation of Fryze's theory is considering non-active all the power components that cannot be considered active.

Finally, we report the formulations introduced by the IEEE 1459 standard: it still doesn't solve the scientific debate providing definitions unanimously accepted, but provides a reference for the design and use of instrumentation for power measurements.

The standard does not specify method of analysis for the waveforms, recurring implicitly to the FFT. The fundamental idea expressed in the IEEE 1459 is the decomposition of voltages and currents into a component representing the signal at the fundamental frequency and another component including all the harmonics and inter-harmonics (considered harmful for the electrical system). In the following the most relevant formulations introduced in the standard are reported.

Voltage:

$$V^2 = V_1^2 + V_H^2 = V_1^2 + \sum_{h \neq 1} V_h^2$$

Current:

$$I^2 = I_1^2 + I_H^2 = I_1^2 + \sum_{h \neq 1} I_h^2$$

Active power:

$$P = \frac{1}{T}\int_0^T p(t)\,dt = P_1 + P_H$$

Apparent power:

$$S^2 = (VI)^2 = (V_1 I_1)^2 + (V_H I_1)^2 + (V_1 I_H)^2 + (V_H I_H)^2$$

Fundamental apparent power:

$$(V_1 I_1)^2 = S_1^2 = P_1^2 + Q_1^2 = (V_1 I_1 \cos\varphi_1)^2 + (V_1 I_1 \sin\varphi_1)^2$$

Non-fundamental apparent power:

$$S_N^2 = (V_H I_1)^2 + (V_1 I_H)^2 + (V_H I_H)^2 = S^2 - S_1^2$$

Non-active power:

$$N = \sqrt{S^2 - P^2}$$

2.3 The realized measurement device

As seen in paragraph 2.1.3, commercial AMI and smart grid management solutions are available on the market. Designed as integrated systems, they often adopt proprietary protocols, data structure or formats: this vertical approach is intended for the products to be sold and customized for the individual utility, thus not favoring

interoperability. In addition, most of the commercial solutions are characterized by class B performance (according to the EN 50470-3).

In this thesis work, a prototype design and realization of a smart meter and the related metering infrastructure is proposed. The meter is based on an ARM microcontroller, which guarantees a low-cost realization. Nonetheless, the measurement performances allow for classification of the meter in class C (according to MID and OIML-R46). With the adoption of innovative power measurement techniques, the ability for bidirectional real-time accurate measurements, in sinusoidal and non-sinusoidal conditions, is attained. Moreover, the presence of proportional and binary actuators on the smart meter allows the deployment of demand response programs. To this aim, a management strategy, implemented on the AMI control center, which allows the prioritization of loads and favors active user participation is developed.

Allowing the connection with other meters (such as hot water and gas meters), the realized smart meter poses as measurement and communication hub for all energy consumptions, which are presented clearly to the user through a web interface.

In the following paragraphs a detailed description of the proposed AMI, the smart meter and related sensing devices and advanced power measurement techniques, the management unit and the implemented load management strategy is provided.

2.3.1 The Advanced Metering Infrastructure (AMI)

The smart meter needs a supportive communication infrastructure to deliver all the benefits associated with its adoption. Therefore, the design of a meter requires the broader challenge of integrating it into an existing infrastructure, or designing and implementing a new one.

The second approach is the one followed here: a network scheme for an AMI is proposed, with the smart meter being not only the measurement device, but also the interface for connecting customers to all the other actors of the grid. In particular, the system was designed with the goal of being able not only to convey measurement data to a management center, but also to allow the reception of price signals from the market and of Demand Response (DR) command signals, enabling

remote load management for the customers who agreed to participate in DR programs.

In addition, the smart meter is thought and realized as a central hub for monitoring all kind of energy consumptions: it can be connected to smart gas and hot water meters, collecting their measurements and acting as a gateway towards a management center.

The proposed AMI (see Figure 2.7) is composed of three main parts: the Remote Measuring Units (RMUs), the Peripheral Measurement Units (PMUs) and a Management Unit (MU) [2.17]. The RMUs are the actual sensing devices: they execute measurements regarding electrical energy, gas and hot water consumptions and, using a data bus, can transmit such data to a PMU. A Peripheral Measurement Unit has the task of collecting measurements from the RMUs, perform data processing if required (for example, regarding electricity consumption, usage statistics related to a specific customer can be computed or power quality metrics may be elaborated) and send the information to the MU.

In fact, the PMUs act like gateways between RMUs and the Management Unit. Moreover, oftentimes it is not important to send upstream the complete measurement data, but some aggregated synthetic data may suffice: in this case the PMUs have also the task of computing synthetic information starting from the measurement data

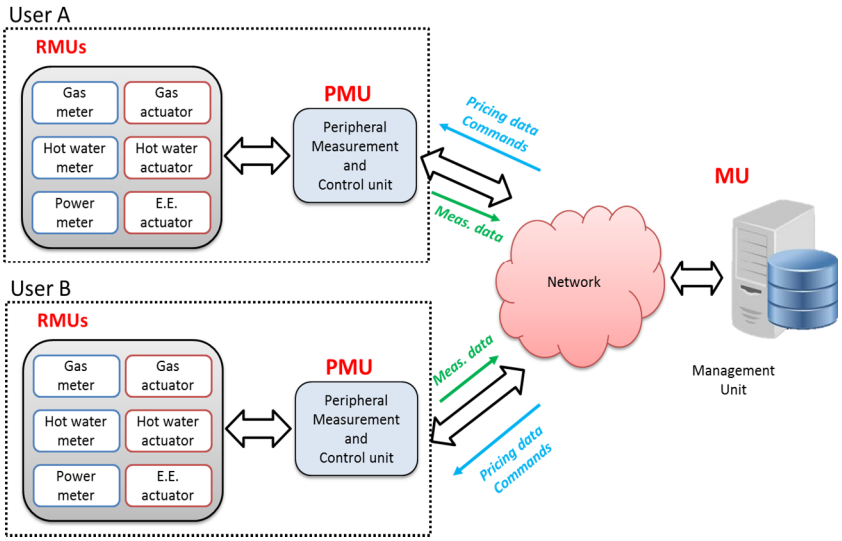

Figure 2.7 – A graphical representation of the proposed AMI architecture

from the RMUs. It is, for example, the case of power quality measurements indexes: if power outages occur, of course the management unit and the system operator should be notified as soon as it happens; however, if there are only sags or swells, which do not hinder the service continuity but must be monitored since degrade the quality of the supply, a synthetic measure (i.e. the number of sags during the day) is more indicative.

This network can also be made of several PMU levels; typical examples of application where the network can be sectioned in different branches are: university campuses, great enterprises and hospitals with different departments connected to different lines.

The MU represents the interface of the AMI with the System Operator (SO): it communicates data regarding loads and consumption statistics relative to an aggregation of customers. Therefore provides the SO with relevant information for managing the grid. Moreover, it provides to the users an informative picture of their own consumptions, allowing them to analyze not only current energy usage, but also to compare it to historical data. In addition to that, as stated before, the system is designed with the ability to manage DR programs. Thus, the MU is also the interface with the open energy market: it can receive information regarding line congestion and availability of energy; it also receives market prices and, according to the received data, can put in place a strategy to administer load curtailments to customers who agreed to participate in DR programs. In the actual implementation of the prototypes, instead of prices in the open market or incentives, prices of a Time of Use (TOU) tariff have been considered.

The commands are then conveyed, through the PMUs, to the RMUs. From a functional point of view, the realization of load curtailments procedures needs the presence of actuators, which have to be integrated in the scheme now depicted. In particular, they are placed at the same level as the RMUs, requiring the communication bus (to the PMU) to be bidirectional, thus communicating upwards the measurements results and receiving the actuation commands.

The MU can also provide support for Distributed Generation (DG), allowing each user to sell his energy on the market. In an ideal configuration, the MU may provide the cheaper solution to the user and at the same time allow the SO to cut down absorption peaks.

In designing a metering architecture as described in the previous paragraph different requirements have been held into account relatively to the different components:

- The RMU must have basic signal processing capabilities for computing i.e. RMS values, active and non-active power, and to adapt the data to a format compatible with the communication protocol. The RMU embeds wideband transducers, which satisfy requirements set by the standards for power quality analysis. The communication is entrusted to the communication module of the meter, which interacts with the data bus. The bus may rely on different mediums and different standards, depending on the environment and on the convenience.
- Actuators for reducing electrical, gas and hot water flows are placed at the same level as RMUs, so they should have suitable communication modules too in order to receive commands by MU through the PMUs.
- The Peripheral Measurement and control Unit is an embedded system based on microcontroller. It acquires data sent by the RMUs and integrates this information into a "synthetic energy consumption figure" to be sent to the MU. To this aim the PMU has to be able to compute statistics regarding the user and, i.e. relatively to the electrical energy, to extract Power Quality indices, which will be sent to the MU. The PMU also works as a gateway for the DR commands, issued by the MU and directed to the actuators, which are at the same level as the RMUs.
- The MU is implemented on a conventional workstation and must be able both to interact with the System Operator and to take action in the field of DR. The MU is equipped with a web interface, where customers can check their consumptions and energy bill.
- The DR commands are determined through a management and optimization algorithm that takes into account prices of electricity and a threshold price set by the customer. The prototype system regards only electricity consumptions, but correspondent strategies may be put in place also for gas and hot water consumptions.

2.3.2 The smart meter

The realized smart meter prototype is based on an ARM Cortex M3 microcontroller and integrates both the functions of a RMU and of a PMU. The goal in designing the meter was to realize a low cost (about 30 €/unit) real-time metering device, capable of bidirectional energy measurement and communication, which works as the central hub for all energy consumptions. In the following, the specifications and the realizations are described, referring to the electricity meter. The assumption is that gas and hot water meters perform independently their own measurements, with the proposed smart meter acting only as gateway for the data they provide.

2.3.2.1 Specifications to meet

The first and main purpose of a smart meter is obtaining accurate and timely bidirectional electric energy measurements. In particular, it must be pointed out that the meter has to perform its measurements on distorted voltage and current waveforms, therefore it has to resort to advanced measurement techniques and power metrics. In fact, traditional measurement techniques are limited in the sense that they have been developed referring to sinusoidal conditions, while the real waveform measureable on the power grid are far from sinusoidal. The traditional metrics for the computation of active and reactive power and energy lose their meaning, since there is not a univocal definition of the measurand. Therefore, both the hardware (sensors, A/D converters, architecture of the microcontroller) and the software implemented on the controller need to be designed for the application of advanced power measurement techniques and to perform power quality measurements.

Being part of a more complex infrastructure, the smart meter must be equipped with communication devices that allow it to send its data to a Management Unit and, at the same time, receive information and commands. Moreover, it must be able to interface with the meters in charge of hot water and gas consumption measurements.

Naturally, the ability to receive commands is based on the assumption that the meter has onboard proper actuators that can translate digital command signals into actions in the grid. In particular,

to cover all possible applications scenario, two different kind of actuators are considered in the following: proportional, which can regulate their output in the continuous domain, and binary, which can only be set to on or off position.

The realized prototype is designed to be applicable in three-phase systems and is composed of three mono-phase units. Thus, in the following only the single mono-phase unit is described.

2.3.2.2 Meter architecture

From a functional point of view, the meter consists of the following blocks: i) metering unit that tracks the energy usage of the customer and processes the billing, ii) communication unit that enables two way digital communication with the energy company iii) actuation unit that connects and disconnects the loads.

From a physical point of view, each meter consists of: i) transduction section composed by voltage and current sensors and level adapters, ii) processing section that acquires the output of the sensors, processes the acquired samples and stores the results in a memorization unit, iii) displaying device, iv) communication front-end.

The voltage and current transducers are connected to the microcontroller ADCs, which perform the acquisition of the electrical quantities. The proportional actuator is managed via the DAC, while digital I/O ports are used to exchange data with the gas and hot water meter, and to command the binary actuators.

For the prototype realization, CAN interface is used for communication. However, from a software point of view, the communication front-end is handled by a “virtual port”, which can make use of all the interfaces and communication devices provided by the STM32F103RE microcontroller. For example, it can be used with the RS232C connection or used to drive WiFi or Bluetooth modules for wireless communication. The configuration is depicted in Figure 2.8.

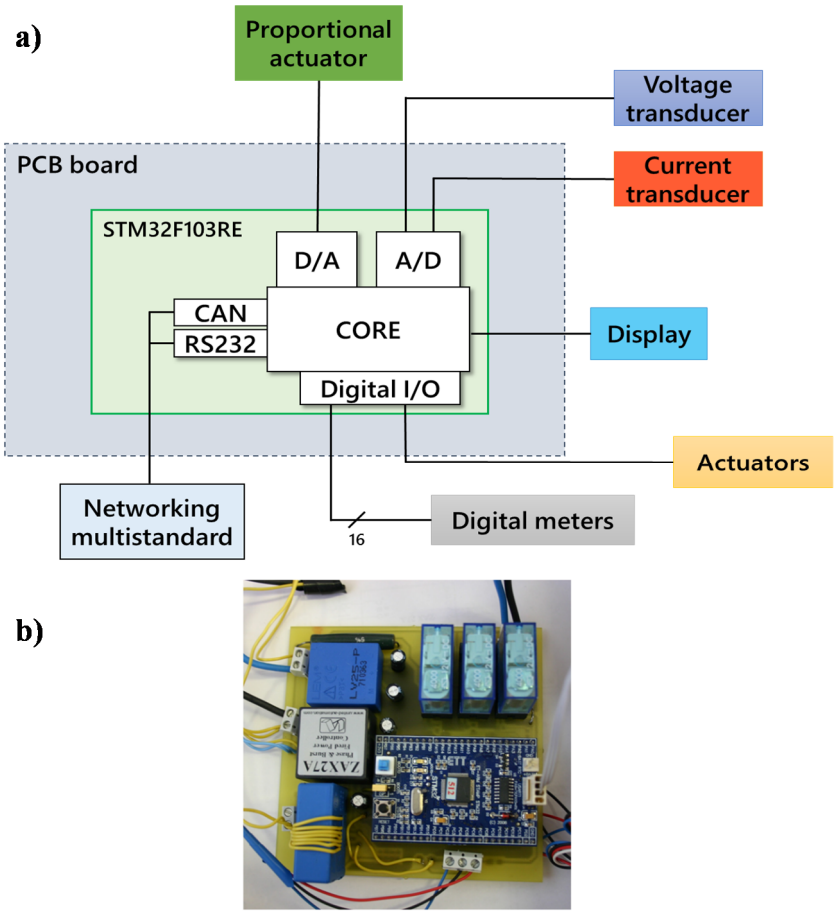

Figure 2.8 – Implemented smart meter: system architecture (a) and photo of the prototype (b)

The microcontroller, while ensuring that the real time specification is met, has to manage both the operations relative to the real time signal acquisition (the signal from the voltage and current transducers represents an input to the onboard ADCs) and the execution of power measurements metrics. Ideally, the first of these operations is carried out by the RMU while the PMU covers for the second one: implementing both function on the same microcontroller poses a stricter requirement on the processing time. Being the RMU directly connected to the microcontroller, no particular communication protocol has been implemented.

The MU is implemented on a conventional workstation; the connection to the PMU represented by the microcontroller is realized through Wi-Fi, using a serial port as output for the STM32F103 and a serial to Wi-Fi external converter. A simple Wi-Fi receiver can be used on the personal computer.

Through the use of a gateway (in the prototype system the gateway is represented by a router) a network the MU and the meter use to communicate is set up. Many different meters may interact with the same network, interfacing with the MU. It must also be noted that not necessarily the network is a "local" one: with the gateway providing an open address, the MU can reach the network of the meters remotely.

2.3.2.3 The transducing sensing devices

Measurements on voltage power networks involve issues not faced in measurements applied to other types of systems. First of all, they require precise means for scaling currents and voltages down to usable metering levels. For most practical purposes, this role has been adequately fulfilled by magnetic core instrument transformers, i.e. Voltage Transformers (VT) and Current Transformers (CT). Another requirement regards their linearity over a wide frequency range, so to be able to analyse the whole spectrum of voltage and current waveforms. In accordance with the IEC 61000-4-30 [1.21], the bandwidth of the sensing system should be at least of 2.5 kHz, so to ensure the possibility to analyse up to the 50^{th} harmonic of the voltage waveform. However, instrument transformers currently available for measuring harmonics are characterized with a parasitic capacitance that causes resonance problems. In addition, the transformers have a nonlinear magnetization characteristic: this property causes the transformer core to saturate in some cases and to inject harmonics of its own into the measurements. Moreover, the inductive and capacitive effects they exhibit strongly limit their dynamic performance. Typically, commercial instrument transformers are usable in the narrow 50-400 Hz frequency range. Obviously, those limits make VT and CT unusable for the analyses of high frequency harmonic and of low frequency inter harmonic components. Therefore, new type of voltage

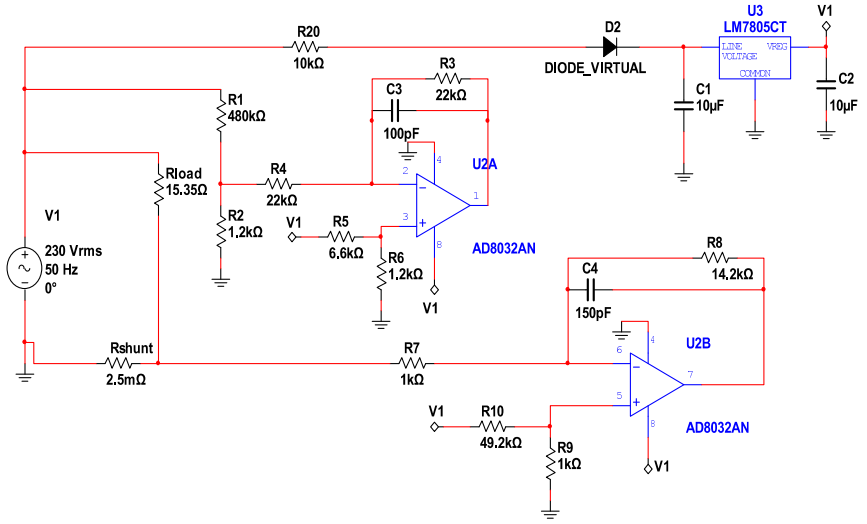

Figure 2.9 – Circuit diagram of the CVCT

and current transducers were developed to make the smart meter able to measure power quality disturbances in a wide frequency range [2.18].

Voltage and current sensing section consists in a prototype of a Combined Voltage and Current Transducer (CVCT) [2.19-2.20]. The block scheme is shown in Figure 2.9 and a photo is in Figure 2.10. As it can be seen it is made of simple electrical and electronic components and thus represents a low-cost solution. The two sections of the CVCT are powered from the input voltage waveform: a simple half-wave rectifier and a linear regulator obtain a 5 V_{DC} single supply from 230 V_{AC}. Voltage transducer is a high impedance resistive divider with a differential operational amplifier, current transducer is a low-resistance resistive shunt with a differential operational amplifier. Input voltage is in the range $[-460\sqrt{2}, 460\sqrt{2}]$ V, which corresponds to a root mean square (rms) value equal to 460 V_{RMS}, in order to make the meter able to measure power quality parameters such as voltage swells. Current input is in the range $[-30\sqrt{2}, 30\sqrt{2}]$ A, which corresponds to a

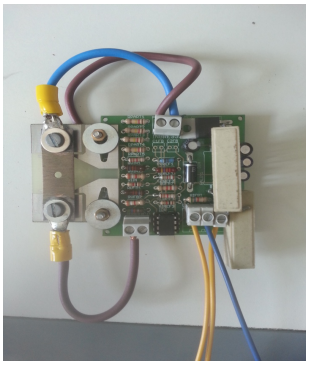

Figure 2.10 – A photo of the realized CVCT

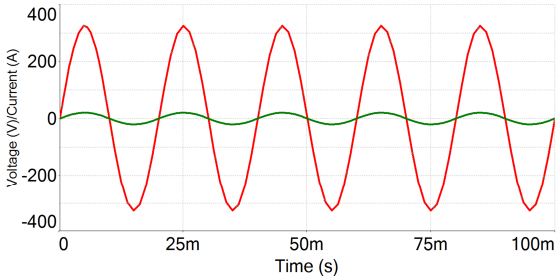

Figure 2.11 – Voltage (red) and current (green) at the input of CVCT

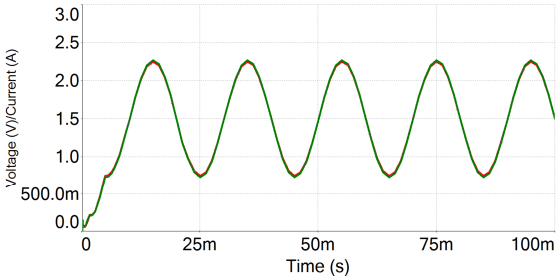

Figure 2.12 – Voltage (red) and current (green) outputs of CVCT with inputs of Figure 2.11

rms value equal to 30 A_{RMS}. Both the outputs are in the range [0,3] V, in order to be suitable for microcontroller analog inputs; with inputs equal to zero the outputs correspond to 1.5 V_{DC}. The realized CVCT has been simulated in Multisim environment. Figure 2.11 and Figure 2.12 show, respectively, inputs (230 V_{RMS} and 15 A_{RMS}) and outputs of the CVCT.

From Figure 2.12 it can be seen that: 1) outputs are inverted with respect to inputs, 2) the signal becomes stationary after a small transient due to stabilization of supply voltage by linear regulator, 3) mean values are 1.5 V for both outputs. In Figure 2.13 magnitude and phases of the outputs, from the AC analysis simulation, are shown: it can be seen that in the range of interest for power quality analysis, i.e. until 10 kHz, frequency bandwidth of the CVCT is suitable for power quality analysis applications. The ratio error of the developed transducer is of the order of 0.1% up to 10 kHz.

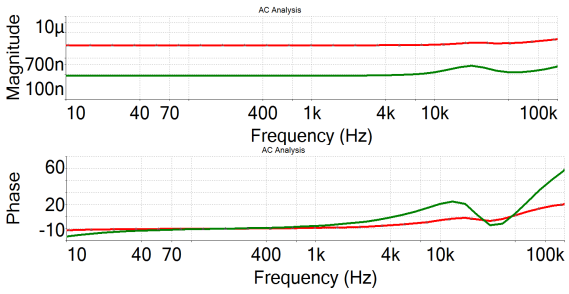

Figure 2.13 – AC analysis of the realized CVCT: magnitudes and phases of the outputs

2.3.2.4 Microcontroller characteristics

In the prototype system, the Electrical Energy RMU and the PMU have been condensed into a single device based on a STM32F103RE microcontroller [2.21]. It constitutes a good compromise between cost, computational capabilities and available peripherals.

In fact, the cost of the device should be kept as low as possible to favor adoption by industries and customers. Moreover, relevant characteristics of the chosen microcontroller architecture make it ideal for power and energy monitoring applications.

The STM32F103RE is based on an ARM Cortex M3 32 bit RISC core, capable of operating up to 72 MHz, with characteristic performance of up to 1.25 DMIPS/MHz. Moreover, it implements a 3-stages execution pipeline (see Figure 2.14), so that each clock cycle three different instructions are executed.

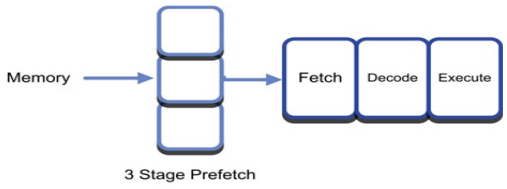

Figure 2.14 – ARM core 3-stages execution pipeline

The Nested Vector Interrupt Controller (NVIC) provides a flexible and efficient way to manage interrupt handling, allowing for the prioritization of interrupt sources: once defined the priorities, the NVIC manages nested interrupts automatically, without any software intervention. NVIC structure and interrupt handling are represented in Figure 2.15.

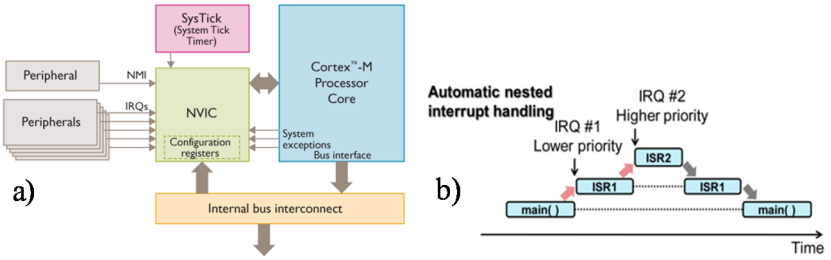

Figure 2.15 – NVIC architecture (a) and interrupt handling (b)

Applied to the smart meter, automatic management of nested interrupts means that the meter is more easily programmed while, at the same time, still being able to respond to service requests according to their priority. For example, it is the case of requests of data or application of commands from the management unit, or receiving data from gas and hot water meter.

The microcontroller is equipped with three 12 bit ADC, with minimum conversion time as low as 1μs, two of which can be synchronized and programmed for simultaneous acquisition. With reference to power measurements, this means that voltage and current can be measured simultaneously, allowing for the computation of the instantaneous power without having to compensate for delays between acquisitions of the two waveforms (see Figure 2.16).

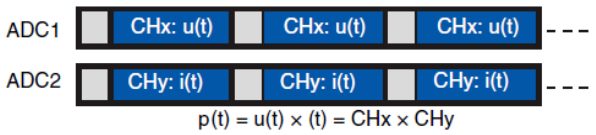

Figure 2.16 – Application of simultaneous acquisition from ADC1 and ADC2 to power measurements

Moreover, the acquisition and the communication with I/O peripherals can be managed through the onboard DMA, without any CPU actions. The DMA also provides hardware support for circular buffer management, particularly of interest in real-time monitoring applications, which require continuous acquisition.

The presence of general purpose and advanced timer, and more important their ability to trigger the signal acquisition from the ADCs, is another notable feature, allowing for tuning the acquisition frequency so to be in synchronous conditions with the fundamental frequency of the signal.

The STM32F103 is also equipped with a 12 bit DAC, a wide array of digital I/Os and several communication interfaces (among which RS232, SPI, I2C, CAN), which allow for an easy interconnection with other components and devices.

Finally, the ARM Cortex Microcontroller Software Interface Standard (CMSIS) embedded in the Cortex core enables consistent and simple software interfaces to the processor for interface peripherals, real-time operating systems, and middleware, simplifying software re-

use. That ensures that the smart meter can be upgraded with relative ease with a more powerful microcontroller, given the same pin layout, preserving the firmware.

2.3.2.5 Actuators

The prototype meter is equipped with two different kind of actuators: a proportional one and three binary actuators.

For the proportional one, a BTA16-800BRG TRIAC and the respective control module ZAX27A have been considered. With this solution, electric loads of up to 400 V and 16 A can be powered.

The binary actuators are essentially latching relays, specifically the Omron G2R. They act like on/off switch for the loads connected to them. The presence of three latching relays allows for sectioning the circuit the meter has to monitor into three branches, each of whom can be powered separately.

2.3.2.6 Firmware implementation

The firmware has been programmed using the Keil µVision IDE: this allows to write the code using C programming language. Moreover, the same IDE can be used to debug the software. To download the firmware on the microcontroller, the device was connected via JTAG port and ICE and operated directly from programming and debug environment.

The microcontroller decodes the digital signal coming from the hot water and gas meters, and manages the data acquisition, via its internal ADCs, from voltage and current transducers.

The firmware manages the data acquisition, with a sampling frequency of 10 kHz. The implemented software adopts on line data processing to obtain the desired quantities. For this aim, an accurate synchronization is essential because most parameters depend on the actual fundamental frequency, so frequency deviation from nominal value need to be continuously monitored. To be able to track alterations in the signal fundamental frequency of the signal and maintain synchronous sampling, a timer, set accordingly to the measured

fundamental frequency, triggers the acquisition by the ADCs. The whole procedure is better described in the following paragraph.

The processing section is able to calculate the following parameters: i) voltage and current rms values, ii) active power (P) and power factor (PF), iii) energy consumption, iv) power consumption profile, v) frequency, vi) voltage and current Total Harmonic Distortion (THDV and THDI) and vii) voltage dip events. Moreover usage statistics relative to electricity consumption are computed. In particular the number of interruptions during the 24 hours, the daily and monthly maximum and minimum request, and the average demand over the 24 hours and the month are considered.

For gas and hot water, difference of temperature (for the latter) and volume (for both of them) are the monitored parameters.

The measured data is then sent to a concentrator (role performed in this case by the PMU) and then conveyed to the MU. On the MU a database is implemented to store the received data.

The smart meter can also receive commands regarding the binary and proportional actuators. Moreover the MU can execute queries and force a measurement data transfer from the meter.

2.3.2.7 Power measurement issues and adopted solutions

The proposed smart meter can be included in a modern class of meters called static meters. They are based on the analog to digital conversion of voltage and current signals and their numeric processing. By means of suitable metrics, applied on voltage and current signals, the quantities of interest (i.e. power, energy, etc…) are retrieved.

The voltage and current RMS values are computed using Eulero's Equations (2.17)-(2.18). In particular, the values are computed for every 200 ms long window, and sent to the concentrator, as mean values, every 5 s or at user's request.

Considering N the ratio between the sampling time and the length of the window, the relations (2.17)-(2.19) calculate voltage and current RMS values and the active power:

$$V_{RMS}^2 = \frac{1}{N}\sum_{k=0}^{N-1} v_k^2 \tag{2.17}$$

$$I_{RMS}^2 = \frac{1}{N}\sum_{k=0}^{N-1} i_k^2 \tag{2.18}$$

$$P = \frac{1}{N}\sum_{k=0}^{N-1} v_k\, i_k \tag{2.19}$$

An on-line algorithm is adopted, leading to (2.20)-(2.22):

$$V_{RMS}^2(k) = V_{RMS}^2(k-1) + \frac{v_k^2 - v_{k-N+1}^2}{N} \tag{2.20}$$

$$I_{RMS}^2(k) = I_{RMS}^2(k-1) + \frac{i_k^2 - i_{k-N+1}^2}{N} \tag{2.21}$$

$$P(k) = P(k-1) + \frac{v_k i_k - v_{k-N+1} i_{k-N+1}}{N} \tag{2.22}$$

With Δt the sampling time, the energy evaluated at the *k-th* step is:

$$E(k) = E(k-1) + P(k)\Delta t \tag{2.23}$$

The Power Factor is calculated with (2.24):

$$PF(K) = \frac{P(k)}{S(k)} = \frac{P(k)}{I_{RMS}(k) V_{RMS}(k)} \tag{2.24}$$

where P, I_{RMS}, V_{RMS}, S e PF are the values of $P(k)$, $I_{RMS}(k)$, $V_{RMS}(k)$, $S(k)$ e $PF(k)$ after the starting transient.

As seen, the presence of non-sinusoidal signals on the grid demands for definitions, and associated algorithms to compute quantities of interest, different from the ones usable in sinusoidal conditions. Once having voltage and current samples, whatever of the metrics previously seen can be implemented. Of course, the choice impacts on the processing power required for the computation and, strongly related to it, the time needed for the algorithms to run.

In the realized smart meter, both Fryze's and Budeanu's metrics are implemented Equations (2.9)-(2.16). The default one, however, is Fryze metric, as for Equations (2.12)-(2.16). The choice was determined by the fact that, operating in the time-domain, it does not require the computation of the DFT and, more importantly, the identification and separation of the frequency components (as seen, for

example, in Budeanu's algorithm). Therefore, the software is less resource hungry and the time to devote to power metrics computation shortens considerably. In addition, it represents the most conservative approach, since every distortion term is included in the non-active power. Fryze's metric represents also the preferred mathematical expression recommended for the instrumentation design.

As stated in the system specifications, the meter must perform bidirectional power measurements. After applying the chosen power measurement algorithm, still there is no information on the sign of non-active power: an ancillary method is used to overcome this limitation. In the following, a 50 Hz system is assumed in describing the method adopted; nonetheless, the algorithms, with opportune modifications, retain their validity even in case signals with a 60 Hz fundamental are considered. First of all, in determining the signs of the power terms, only the current and voltage waveform at the fundamental frequency have been considered. In particular, depending on the phase angle between voltage and current, the direction of the power flow can be obtained. Using the Goertzel algorithm [2.22], fixing the fundamental frequency, voltage and current are transposed into the frequency domain. The algorithm is implemented in the form of an IIR filter that computes a single-bin DFT output. With N number of samples and $x(n)$ the input signal, the filter output is defined by:

$$y_m(n) = \sum_{r=0}^{N-1} x(r)\, e^{j2\pi m\,(n-r)/N} = \sum_{r=0}^{N-1} x(r) W_N^{-m(n-r)} \tag{2.25}$$

and can be computed in a recursive way as

$$y_m(n) = W_N^{-m}\; y(n-1) + x(n) \tag{2.26}$$

where $y_m(-1) = 0$. The DFT output frequency coefficient $X(m)$ equals the output of the difference Equation (2.26) at the time index $n = N$.

$$X(m) = y_m(N) \tag{2.27}$$

In our case, *N=2000.* The output of the filter, specialized for voltage and current signals at the fundamental frequency (m), can be written as:

$$V(m) = \mathrm{Re}_V + j\,\mathrm{Im}_V = V_0\, e^{j\alpha} \tag{2.28}$$

$$I(m) = \mathrm{Re}_I + j\,\mathrm{Im}_I = I_0\, e^{j\beta} \tag{2.29}$$

$$V(m) = V_0 [\cos(\alpha) + j\sin(\alpha)] \quad (2.30)$$

$$I(m) = I_0 [\cos(\beta) + j\sin(\beta)] \quad (2.31)$$

So it follows:

$$\mathrm{Re}_V \mathrm{Re}_I + \mathrm{Im}_V \mathrm{Im}_I = V_0 I_0 \cos(\alpha - \beta) = V_0 I_0 \cos(\varphi) \quad (2.32)$$

$$\mathrm{Re}_V \mathrm{Im}_I - \mathrm{Im}_V \mathrm{Re}_I = V_0 I_0 \sin(\alpha - \beta) = V_0 I_0 \sin(\varphi) \quad (2.33)$$

The outputs of the Goertzel algorithm can be directly used to retrieve the sign, as shown in Figure 2.17. The capability to determine the sign of both active and non-active power allows for bidirectional measurements.

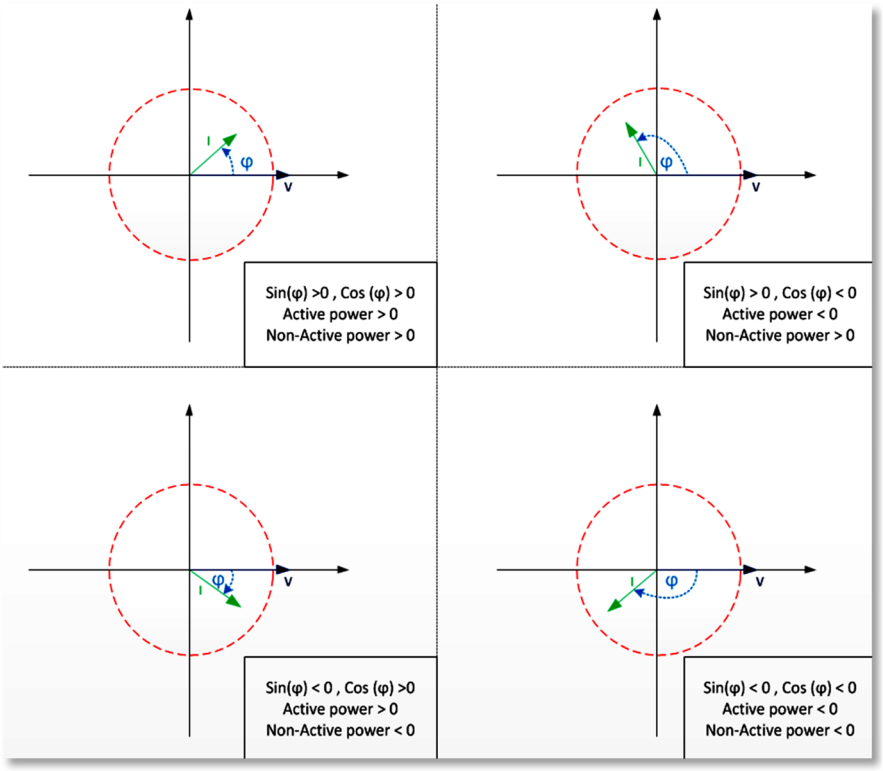

Figure 2.17 – 4-quadrant graphical representation of power flow directions

Since the quantities of interest strongly rely on the fundamental frequency, the meter should also be able to follow the fundamental frequency variations, preserving its performance even in case such frequency increases or decreases. To this end, each observation period the frequency of the fundamental is calculated and the sampling time is adjusted every 5 seconds, using the timer 1 of the microcontroller, programming the sampling rate to adapt to the measured fundamental and guarantee synchronous sampling. Executing the Goertzel algorithm for a set of five frequencies {40, 45, 50, 55, 60} [Hz], centered around the nominal value of the fundamental, five points in the frequency domain can be obtained. An interpolation and analysis algorithm is then executed [2.23] to search for the maximum of the obtained lobe and find the desired frequency value (see Figure 2.18).

In fact, once obtained the array containing the amplitudes of the five spectral lines Φ[m], and found the maximum of the vector at the index value ρ, is possible to determine the parameters needed for the interpolation. The first required parameter is ε, defined as:

$$\varepsilon = \begin{cases} 1 & if \quad \Phi[\rho+1] \geq \Phi[\rho-1] \\ -1 & if \quad \Phi[\rho+1] \leq \Phi[\rho-1] \end{cases} \tag{2.34}$$

With the use of ε, the other two parameters required by the implemented method can be obtained:

$$\alpha = \frac{\Phi[\rho+\varepsilon]}{\Phi[\rho]} \tag{2.35}$$

$$\delta = \varepsilon \frac{\alpha}{\alpha+1} \tag{2.36}$$

Finally, the desired frequency value γ can be obtained with the equation

$$\gamma = \Omega + (\rho+\delta)\Delta f \tag{2.37}$$

With, for the case at hand, Ω corresponds to 40 Hz and Δf is the frequency resolution, corresponding to 5 Hz.

Being the acquisition from the ADCs triggered by an internal programmable timer, it is possible to obtain a synchronous sampling modifying the programmed interval between two trigger events

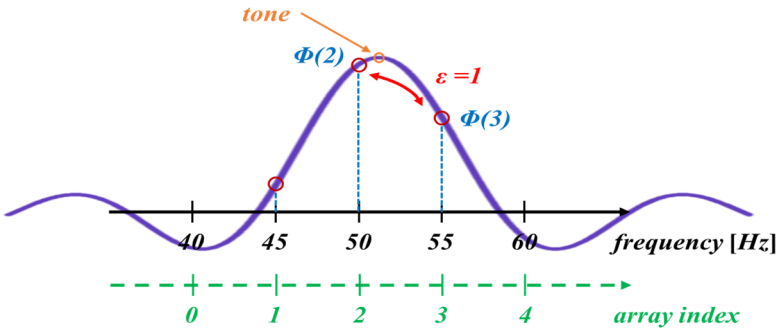

Figure 2.18 – Graphical representation of the interpolation algorithm used to retrieve the exact frequency of the fundamental

accordingly to the previously determined frequency of the fundamental. The procedure is illustrated in Figure 2.19. The acquisition is such that each period of the signal 200 samples are acquired: the sampling frequency, adjusted to the determined fundamental frequency of the signal to comply to the requirement of synchronous sampling, is computed as the fixed number of samples per period multiplied by the

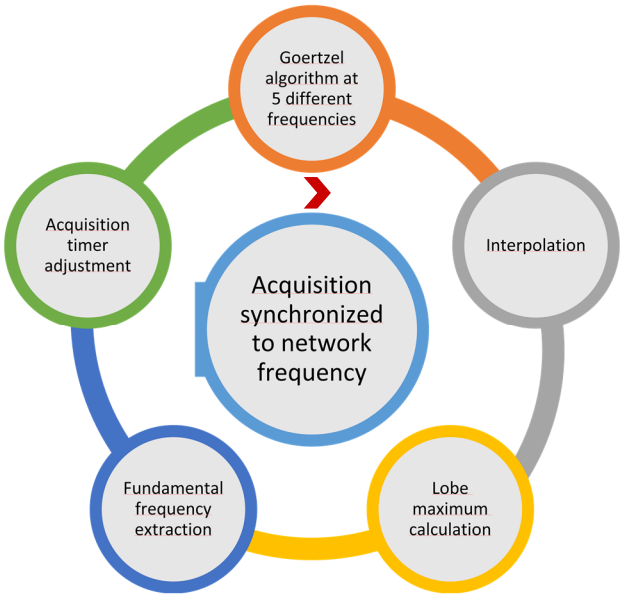

Figure 2.19 – Implemented procedure to ensure synchronous sampling

newfound fundamental frequency. The algorithm used to determine the sign is based on the Goertzel algorithm at the fundamental frequency: it is updated at each observation period (5s) with the correct frequency. Compared to the widespread hardware PLL-based solution, the software lock on the fundamental frequency helps in keeping low the cost of the device, while not sacrificing performance.

2.3.2.8 Code description and explanation

Clock configuration

System clock is set to the maximum frequency allowed by the STM32F103, which is 72 MHz. For the peripheral buses APB1 and APB2 the clock is set to 36 MHz and 72 MHz respectively.

ADC configuration

The ADCs depend on the APB2 bus. Through the use of the related prescaler, their clock is set to 12 MHz: with a configuration of the sampling time of 1.5 cycles, the total conversion time is as low as 1.17 μs.

The base acquisition frequency is 10 kHz, and is modified accordingly with the measured frequency, as explained in the previous paragraph.

ADC1 and ADC 2 are used to measure voltage and current respectively. Their acquisition is synchronized: they are both set with the same conversion time, and the start of conversion of ADC1 also triggers the start of the second one. Having synchronized measurements is particularly important when determining the instantaneous power: according to its definition, instantaneous power is determined by the product of voltage and current *at the same instant*. In fact, in case of a delay in the current samples with respect to the voltage ones, a phase error would be determined: if known, some sort of compensation should be implemented; in case it is not systematic, it would determine erroneous measurements.

DAC and GPIO configuration

The DAC is used to drive the proportional actuator according to the commands received from the MU. The DAC output is automatically

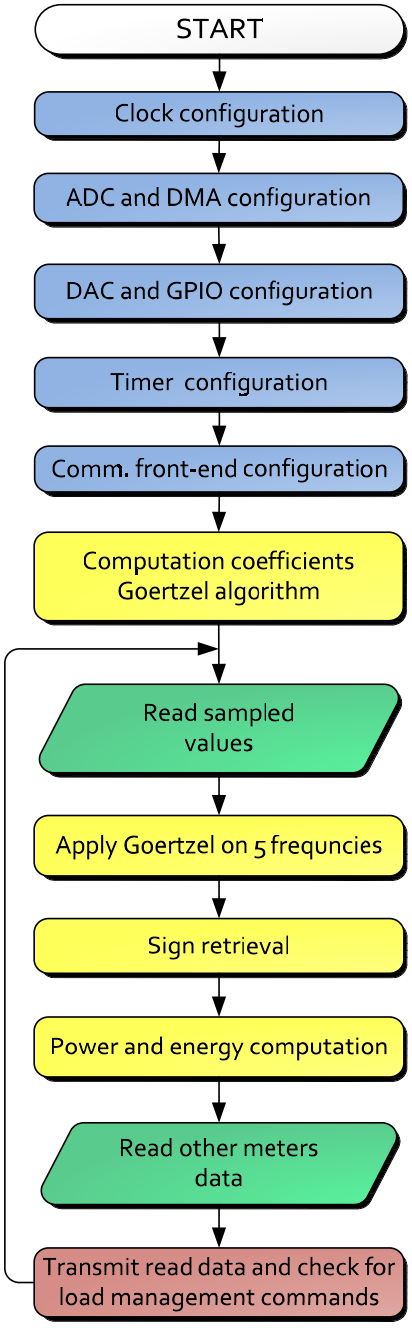

Figure 2.20 – Block diagram of the implemented firmware

connected to the GPIO port pin A4.

GPIO A3 and A6 pin are used as inputs for the ADC1 and ADC2 respectively. The latching relays used to section different branches of the circuit are commanded with the output ports A0, A1, A5.

Timer configuration

The TIM1 is used to trigger the acquisition from the ADCs: the algorithm to identify the fundamental frequency is used to determine the content of the ARR timer register, which is the value the timer (configured as a counter) has to reach to generate the trigger event for the ADCs. The timer makes use of the internal clock, set to 72 MHz.

Communication front-end configuration

The communication is handled through a "virtual port", which can be set to use – by means of the microcontroller peripherals libraries – any of the communication interfaces available on the microcontroller (SPI, I2C, RS232, CAN).

The USART (Universal Synchronous Asynchronous Receiver Transmitter) is the serial port used to communicate

with the MU: in fact, through the use of a serial to WiFi converter, the Meter is connected to the same wireless network where the MU is situated.

The serial port is configured for functioning at 115000 baud, with 8-bit words, a start and stop bit and no parity. At the end of each cycle, the measurement data is transmitted and, in case any load management command is received, proper actuators settings are applied.

Goertzel algorithm to identify fundamental frequency

To prevent measurements errors deriving from fluctuation in the fundamental frequency of the acquired signals, the precedently described algorithm to identify the correct frequency is implemented.

The Goertzel algorithm allows for the computation of real and imaginary part of a specific spectrum line of the Fourier transform of a signal. Applying it to the previously indicated five frequencies, which include the limits regulatory bodies have fixed for the fundamental frequency on the grid (the system is thought for a 50 Hz grid, but can be easily modified for the application to 60 Hz networks), the magnitude of the frequency components in the neighborhood of the actual fundamental frequency can be retrieved. The evaluation of current and voltage at fundamental frequency allows for the computation of ITHD and VTHD. In the following, the C-like code relative to the Goertzel algorithm is reported.

```
/* k50, k55, k60, k45, k40
     normalized frequencies*/


ReCoeff50= 2* cos( 2*Pi * k50);
ImCoeff50= 1* sin( 2* Pi * k50);

ReCoeff40= 2 * cos( 2*Pi *
k40);
ImCoeff40= 1 * sin( 2*Pi * k40);

ReCoeff60= 2* cos( 2*Pi * k60);
ImCoeff60= 1* sin( 2*Pi * k60);

ReCoeff45= 2* cos( 2*Pi * k45);
ImCoeff45= 1* sin( 2* Pi * k45);

ReCoeff55= 2 * cos( 2* Pi *
k55);
ImCoeff55 = 1* sin( 2*Pi * k55);
```

```
//all parameters initialized to zero
//v(n) is the voltage sample
//code executed in a N-cycles loop

par40  = v(n) + ReCoeff40 *a1 -
b1;
b1 = a1;  a1 =  par40;

par45  = v(n)+ ReCoeff45 *a2 - b2;
b2 = a2;  a2 =  par45;

par50  = v(n) + ReCoeff50 *a3 -
b3;
b3 = a3;  a3 =  par50;

par55  = v(n) + ReCoeff55 *a4 -
b4;
b4 = a4;  a4 =  par55;

par60  = v (n) + ReCoeff60 * a5 -
b5;
b5 = a5;  a5 =  par60;
```

```
RePart40 = 0.5*ReCoeff40* a1 - b1;
ImPart40 = ImCoeff40 * a1;
Ampl40=sqrt(RePart40^2+ImPart40^2);

RePart45 = 0.5*ReCoeff45* a2 – b2;
ImPart45 = ImCoeff45 * a2;
Ampl45=sqrt(RePart45^2+ImPart45^2);

RePart50 = 0.5*ReCoeff50* a3 – b3;
ImPart50 = ImCoeff50 * a3;
Ampl50=sqrt(RePart50^2+ImPart50^2);

RePart55 = 0.5*ReCoeff55* a4 – b4;
ImPart55 = ImCoeff55 * a4;
Ampl55=sqrt(RePart55^2+ImPart55^2);

RePart60 = 0.5*ReCoeff60* a5 – b5;
ImPart60 = ImCoeff60 * a5;
Ampl60=sqrt(RePart60^2+ImPart60^2);
```

To retrieve the actual fundamental frequency of the signal, included in the boundaries defined by the analyzed frequencies, a part of the Interpolated FFT (IFFT) described in [2.23] is implemented.

```
//ricerca del max
MaxIndex = 0;
maxAM=amplitudes[0];

for( jj=1 ; jj<5 ; jj++ )
{
        if( amplitudes[jj]>maxAM )
        {       maxAM=amplitudes[jj];
                MaxIndex=jj;
        }
}

if (MaxIndex==0)
        frequency=40;
else if (MaxIndex==4)
        frequency=60;
else
{
        if( amplitudes[MaxIndex+1]>=amplitudes[MaxIndex-1] )
                eps= 1;
        else
                eps=-1;

        alpha=amplitudes[MaxIndex+eps]/amplitudes[MaxIndex];
        delta_i=eps*(alpha/(1+alpha));
        frequency=40+(MaxIndex+delta_i)*deltaF;
}
```

The retrieved frequency is then used to set up the timer that triggers the following acquisition.

Sign retrieval

As described in Equations (2.28)-(2.33), once having the real and imaginary part of the Fourier transform of voltage and current at the frequency component of interest, is possible to retrieve the sign of the power. To this account, the Goertzel algorithm is applied to the frequency identified as fundamental with the algorithm reported in the previous paragraph. The C-language code segment for the algorithm is reported below.

```
//N-> Number of samples
//k-> Normalized frequency
ReCoeff = 2.0*cos(2.0*pi*k/N);
ImCoeff = sin(2.0*pi*k/N);
a = 0.0;
b = 0.0;
for (n=0; n<N; n++)
  {          PartOut= x(n) + ReCoeff*a - b;
             b = a;
             a = PartOut;
  }
ResRe = 0.5*ReCoeff*a - b;
ResIm = ImCoeff*a;
```

```
ResRe_V =0.5*ReCoeff_V*a_V – b_V;
ResIm_V = ImCoeff_V*a_V;
ResRe_I = 0.5*ReCoeff_I*a_I – b_I;
ResIm_I = ImCoeff_I*a_I;

segnoSin = ResIm_V * ResRe_I - ResIm_I * ResRe_V;
segnoCos = ResRe_V * ResRe_I + ResIm_I * ResIm_V;
Angolo  = 180.0/Pi*atan2( segnoSin, segnoCos);
```

The retrieved sign is then applied to the power measurement.

Power and Energy computation

To compute active and non-active power Fryze's metric is adopted as default. Energy is obtained, each 200 ms, by scaling Equation (2.22) with the length of the observation period. It must be noted that, since the STM32F103 executes calculations over integer values, a scale factor is considered to convert the sampled values to integer and to convert back the results of the computation.

Measurement data transmission and application of load management commands

At the end of each acquisition cycle, the smart meter sends the data to the MU, reads any load curtailment commands and executes them.

2.3.3 Communication protocol

The communication is managed independently of the specific interface and communication protocol, through the use of a "virtualized communication interface". For the prototype implementation, the smart meter network adopts the CAN protocol [2.24]. In fact, it constitutes a reliable low-level communication interface that guarantees: i) low-cost implementation, ii) noise immunity, iii) easy configuration, iv) multicast network. The CAN protocol, standardized in ISO 11898-1 [2.25], was specifically designed to operate seamlessly even in presence of high electromagnetic disturbances thanks to the adoption of

transmission signals with a balanced difference of potential. The bit rate can be up to 1 Mbit/s in shorter than 40-meter nets. Slower speeds allow for communication over greater distances (125 kbit/s to 500 m) as in the considered case. A priority based bus arbitration allows to transfer first messages with higher priorities: if the bus is idle, any node may begin to transmit; however, if two or more nodes begin to send messages at the same time, the message with the higher id (which has more dominant bits, i.e., zeroes) will overwrite other nodes lower id's, so that eventually (after this arbitration on the id) only the dominant message remains and it is received by all nodes. Messages with numerically smaller values of id have higher priority and they are transmitted first. The CAN communication is implemented by the STM32F103RE.

2.3.4 Management unit

The Management Unit is constituted, in the prototype system, by a workstation. The measurement data the PMUs sends through the network connection (again, in the prototype system such connection is realized by means of WiFi) is archived on a MySQL-managed database on the MU. To access such database, and to control the devices connected to the MU, a web-server with the relative user interface was implemented.

The monitoring and configuration panel is realized via a web interface: an approach that allows the user to remotely check his consumptions or to modify his supply agreement.

The presence of actuators on the prototype board allows for the realization of Demand Response programs. The load curtailments, in this case, can be managed automatically, if proper management policies and algorithms have been implemented on the MU; moreover, through the web-interface the user can log-in and directly intervene on his loads both from local or via remote access via http protocol.

The MU needs to communicate with the System Operator, to whom it provides measured data and statistics: the data can be used to have a picture of the state of the grid, but can also be made available to other grid actors to formulate advanced customer-oriented tariffs and services.

Figure 2.21 – Management Unit web interface

Web interface

For the purpose of testing the prototype AMI system, the meter was connected to the MU via WiFi. Moreover, the workstation implementing the management unit was equipped with an open IP address, so to be reachable from devices external to the local network including the measurement and management devices.

The PC posing as MU was designed to act also as a web server, providing an interface (Figure 2.21) to access the locally stored database. The PHP-based webpage allows to access all the connected meters and, for each meter, shows power consumption readings, energy and hot water and gas consumptions. Moreover relevant information regarding load management is shown: three button indicate the state of the relays (ON or OFF) and can be used to manually disconnect or re-connect the loads attached to the relative branch of the grid monitored by the selected meter; a graph reports the prices of electric energy, as provided by the SO. In the prototype system, the prices of energy are the key parameters for managing load management: in fact, it has been assumed that the user or an energy manager (in case of a complex network) can set a threshold, which the system uses for determining the load curtailments, that is directly bounded to the prices of electricity.

Therefore, communication with the SO represents a key point. In the implemented prototype infrastructure, data from the system operator has been obtained and inserted in the MU manually; of course,

a suitable communication protocol should be found in agreement with the SO and adopted for any real-world implementation of the system.

2.3.5 Load management implementation

2.3.5.1 The adopted strategy

In general, Demand Response techniques can help reducing the need for new power plants by displacing some loads from peak hours. In our system, a strategy for automatic load management based on user-defined cost threshold has been implemented. Considering a number of N users, each of them having M different branches to which loads are connected, the total absorbed power at the instant t is given by the sum of the power for all the branches:

$$P_{TOT}(t) = \sum_{i=1}^{N} \sum_{j=1}^{M} P_{ij}(t) \tag{2.38}$$

Assuming that each branch is equipped with a switch that can turn off the associated branch or can power it up again, and that the state of the branch is represented by the binary variable σ_{ij} (σ_{ij}=1 if the branch ij is powered up and σ_{ij}=0 if the corresponding switch is open) then the Equation (2.38) becomes:

$$P_{TOT}(t) = \sum_{i=1}^{N} \sum_{j=1}^{M} \sigma_{ij} P_{ij}(t) \tag{2.39}$$

As said before, the goal of the system is to implement automatic load management. Introducing a power threshold Λ, the problem configures as a nonlinear optimization:

$$\min[\Psi(\bar{\sigma}, t)] \tag{2.40}$$

Where the cost function is:

$$\Psi(\bar{\sigma}, t) = \Lambda - P_{TOT}(t) = \Lambda - \sum_{i=1}^{N} \sum_{j=1}^{M} \sigma_{ij} P_{ij}(t) \tag{2.41}$$

and $\bar{\sigma}$ represent the matrix containing the binary of the different branches, which represent the decision variables. If the absorbed power tend to be greater than the threshold, one or more branches will be disconnected (the corresponding decision variable is set to 0); similarly, when the threshold increases, more branches can be powered up again, until Ψ is minimized. The optimization configures as a constrained problem: in fact, being Λ the power value not to be overcome, it must be guaranteed that:

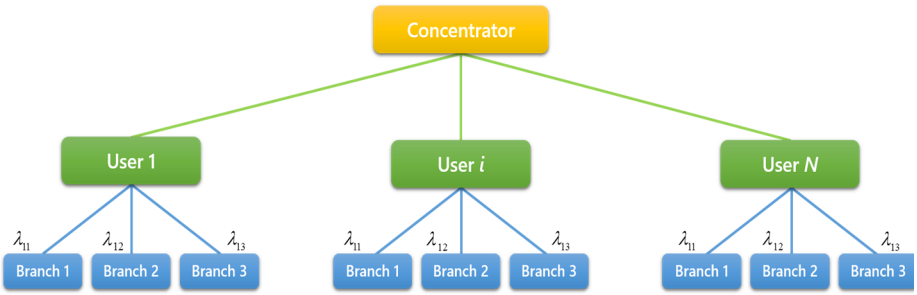

Figure 2.22 – Prioritization of circuit branches

$$\Psi(\bar{\sigma}, t) \geq 0 \tag{2.42}$$

Additional constraints may be determined assigning a priority to each circuit branch: naming λ_{ij} the priority level of the *ij-th* branch, it can be imposed that, while managing the load disconnecting or re-connecting branches, this is done according to the order defined by the set priorities, as represented in Figure 2.22. Therefore, the constraint may be formalized as

$$\sigma_{ij} \leq \sigma_{lk} \quad if \quad \lambda_{ij} \leq \lambda_{lk} \tag{2.43}$$

Naturally, it might be the case that two different branches have the same priority level: in this case, the adopted policy is to disconnect first the loads that are absorbing more power. In a similar manner, while powering back up the loads, in case of equal priority precedence is given to the ones which were absorbing less power prior to the disconnection. This strategy allows to serve the largest possible number of loads, rather than supplying fewer loads but with higher absorptions. A block diagram representation is provided in Figure 2.23. This policy may obviously be easily changed, to adopt the load management system to the specific context of application.

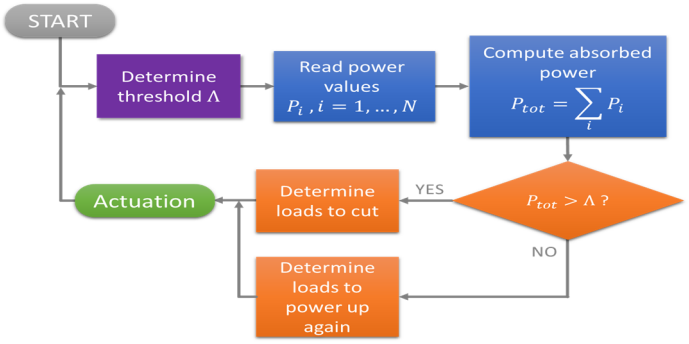

Figure 2.23 – Block scheme of the load management algorithm

An additional note regards how to set the priorities: they are user-defined and can be static or the user can set a rule according to which the same branch assumes a different priority level over time. For example, a rule can be set so as to keep the priority level of the branch feeding the air conditioning system high during the period of the day the user is in the building, and lower it otherwise.

Finally, the system may easily include the availability of locally produced electricity. Its effect can be seen as a positive contribution to the power threshold level or, equally, as a lowering of the power demand the grid has to supply. In this case, the cost function introduced in Equation (2.41) becomes:

$$\begin{aligned}\Psi(\bar{\sigma},t) &= \Lambda - P_{TOT}(t) = \\ &= \Lambda - \sum_{i=1}^{N}\sum_{j=1}^{M}\sigma_{ij}P_{ij}(t) + \sum_{h=1}^{N_{gen}}P_h(t)\end{aligned} \tag{2.44}$$

with N_{gen} the number of local power sources.

2.3.5.2 Selecting the threshold

The power threshold Λ is determined dynamically according to the cost of energy. Setting a minimum level of power that must necessarily be supplied, Λ is determined as:

$$\Lambda = \max[\Lambda(C(t)), \Lambda_{\min}] \tag{2.45}$$

where $C(t)$ represents the cost of electricity provided by the GME (Italian Electricity Market Operator).

Table 2.2 – Prices of electricity

CLASS	DESCRIPTION	PRICE €/MWh
F1	Peak	93.23
F2	Mid-level	88.97
F3	Off-peak	65.47

For the prototype system the threshold has been calculated considering a tariff plan with different prices of electricity for peak, mid-level and off-peak hours. The average prices for December 2011 are reported as an example in Table 2.2.

The user or the energy manager can set a power threshold setting a limit for the cost of electricity considering as reference the class F2. Then, the system adjusts the so determined power level according to the prices of energy, raising it during off-peak hours and lowering during peak hours, by weighting the power level with the price of energy in the current class versus the reference one.

2.3.6 Metrological characterization

2.3.6.1 Issues related to the characterization of smart meters

The presence of non-linear and time-variant loads in the network causes the distortion of voltages and currents. The main problems related to these disturbances stem from the flow of non-active energy caused not only by non-sinusoidal currents and voltages but also by the energy dissipated in the neutral path due to the zero-sequence current components that has economic significance. These flows consume energy and someone has to pay for it, so the utility companies are vitally concerned with energy loss in the network because generators cover this loss, and the distributing company has to pay for it at the high-voltage revenue metering points. In a certain way, they should make the polluting customers pay adequate penalty; otherwise, these costs are charged on all the actors of the energy market. Penalties are applied for absorptions with a low-power factor that are verified through reactive-energy metering.

This gives great importance to both active and non-active energy metering in non-sinusoidal conditions. The IEC standard [1.18] for characterization of the accuracy of static active meters takes as reference sinusoidal conditions, and some power-quality phenomena are only accounted as influence quantities that change the accuracy of meters. IEC standard for characterization of the accuracy of static reactive meters applies for sinusoidal currents and voltages containing the fundamental frequency only [1.19]; no reference is made to what should be measured in situations with harmonic distortion.

In this way, commercial instruments, built according to the IEC approach, are designed and tested mainly for sinusoidal waveforms, and, at most, additional tests are performed in specific non-sinusoidal conditions but accounting for larger accuracy tolerance. Moreover, since there is no clear reference as to which algorithm should be used for digital metering, different manufacturers adopt different implementations, which are equivalent in sinusoidal conditions, but provide very different results when utilized with distorted current and voltage waveforms.

In order to fully define the product *energy* in generation, transmission, and distribution stages and to economically regulate how energy is sold by electrical utilities and bought by final users, proper metering in non-sinusoidal conditions is required.

Starting from all these considerations, from a metrological point of view, the verification of energy meters becomes a strong need but, at the same time, a very complex task. In fact, a full analysis of all influence parameters that leads to non-sinusoidal conditions, and all their combinations requires a huge number of tests.

Here, results of the characterization of the implemented smart meter in static and dynamic conditions are presented; to provide test signal for non-sinusoidal conditions, sinusoidal waveforms were artificially distorted.

In order to prove the reliability of the implemented instrument, a thorough characterization, in static and dynamic conditions, has been performed. To this aim, the following instruments, shown in Figure 2.23, were used:

- Function Generator Yokogawa FG320 (Features: Dual channel output, frequencies range 1 µHz to 15 MHz, Amplitude range ± 10V, AC Amplitude accuracy ±(0.8% of setting + 14 mV), DC output accuracy ±(0.3% of setting + 20 mV)
- PXI 1042 chassis with a PXI-DAQ 6123 (Features: 16-Bit, 500 kHz/ch, Simultaneous Sampling)
- Pacific Power Source 3120 AMX (Features: Maximum Power: 12 kVA; ii) Frequency Range: 20 Hz to 50 kHz; iii) Line Regulation: 0.027 mV; iv) Load Regulation: 0.00135 mV; v) THD: 0.1%; vi) Voltage Ripple and Noise: -70 dB).

2.3.6.2 Static characterization

For static characterization, only the behavior of the A/D conversion systems of the microcontroller are taken into account. The tests are executed according to the set-up reported in Figure 2.24. The adopted function generator has two independent output channels that can be separately configured with proper values of amplitude and phase.

These signals are acquired at the same time by the two A/D channels of the microcontroller and by the A/D channels a PXI-DAQ 6123, adopted as reference. Through a software developed in Labview environment, it is possible to monitor and store continuously the values supplied by the generator and to obtain expected measurement results. These values are then compared with those provided by the smart meter. In the first set of tests a dc voltage is generated at

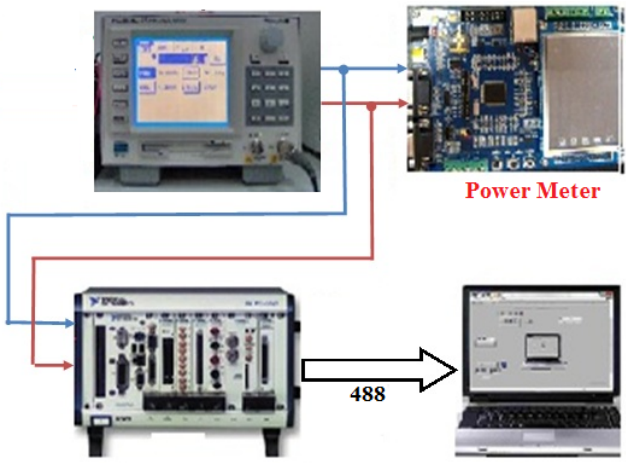

Figure 2.24 – Experimental set-up for static characterization

different levels, with steps of 10 % of full scale range. Each test is repeated ten times. A systematic deviation is found for each input level with a value that is within the range 0.1 - 0.8 %. Starting from the obtained results it is possible to evaluate, recurring to the least squares method, gain and offset correction parameters for each input channel. After the compensation the mean error is lower than 0.05 % and the standard deviation is lower than 0.03 %.

2.3.6.3 Dynamic characterization

For dynamic characterization, the signals provided by the function generator are amplified by the power amplifier, the Pacific Source 3120 AMX, and the PXI measurement system is again adopted as reference value; a simplified scheme of the testing station is reported in Figure 2.25. The test sets are chosen according to considerations reported in [2.26],[2.28]. The tests were performed in sinusoidal and non-sinusoidal conditions. In sinusoidal conditions the effects of frequency deviation and phase angle variation on active and reactive power were evaluated.

The sinusoidal tests have been performed varying input parameters around rated values: frequency (50 Hz ±15%), input voltage amplitude (50% to 100 %), input current amplitude (0% to 100 %), finally the phase displacement between $-\pi/4$ to $\pi/2$.

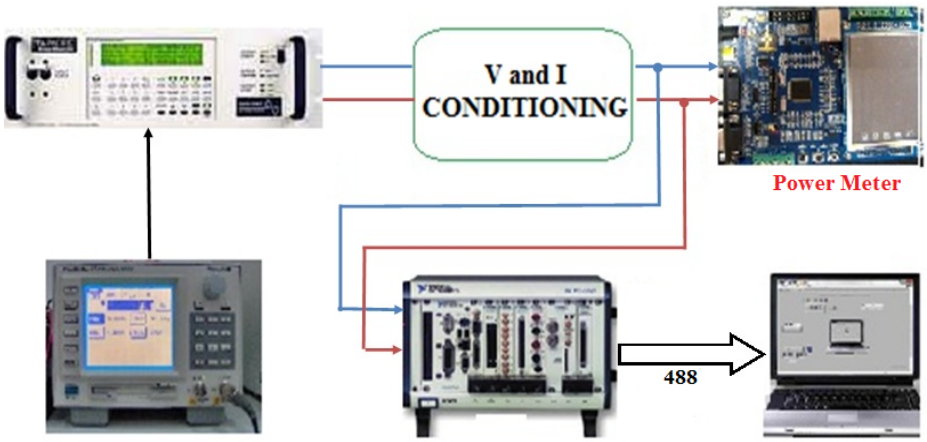

Figure 2.25 – Experimental set-up for dynamic characterization

In Figure 2.26 and Figure 2.27 the percentage relative uncertainties for active and non-active powers in sinusoidal conditions are reported.

The relative uncertainty is in both cases less than 0.2%, with highest values for fundamental frequency lower than 47 Hz and phase angles close to 90 degrees for active power and close to 0 degrees for non-active power.

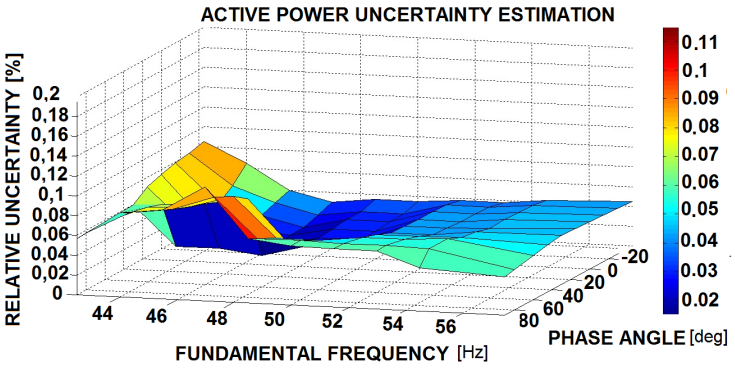

Figure 2.26 – Active Power Uncertainty Estimation vs phase angle and fundamental frequency

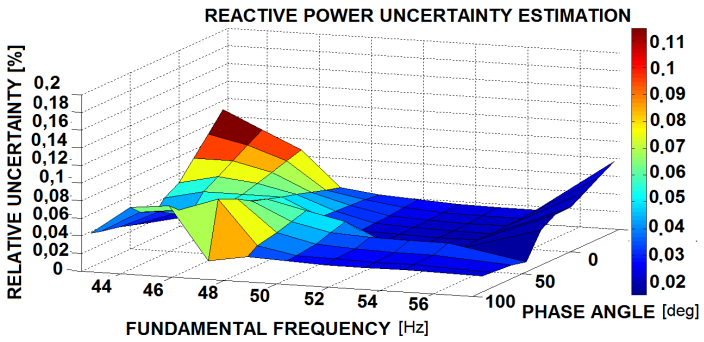

Figure 2.27 – Reactive Power Uncertainty Estimation vs phase angle and fundamental frequency

In non-sinusoidal conditions, the effects of the fundamental phase angle and the harmonic order variation on active and non-active power are evaluated. For the non-sinusoidal tests, according to [1.20], a fixed THD of 8% is adopted. For each tests five harmonic components spanning between 3rd and 39th harmonic order are superimposed to the

fundamental tone, with fixed THD. The testing procedures is better detailed in [1.21],[2.26-2.29].

In the Figure 2.28 and Figure 2.29 the percentage relative uncertainties for active and non-active power in non-sinusoidal conditions are reported. The values are compatible with the results in the sinusoidal case, with uncertainties lower than 0.2%. Naturally, the test conditions were slightly different and lack variation of fundamental frequency (the main source of uncertainty), therefore the meter seems to perform better than in sinusoidal conditions. Frequency variations have not been considered since intermodulation products would have brought to superimposed low frequency components, leading to not easily distinguishable uncertainty causes, with more difficult interpretation of the results.

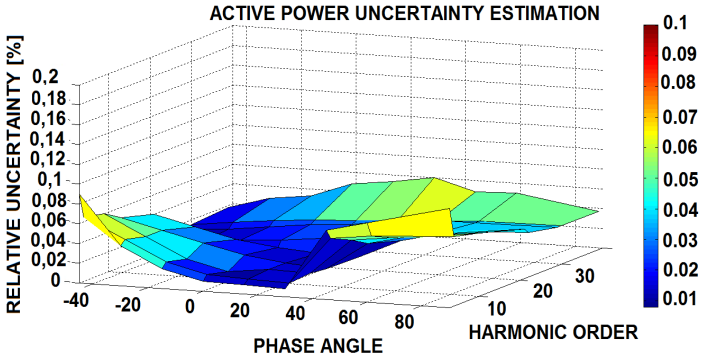

Figure 2.28 – Active Power Uncertainty Estimation vs harmonic order and phase angle

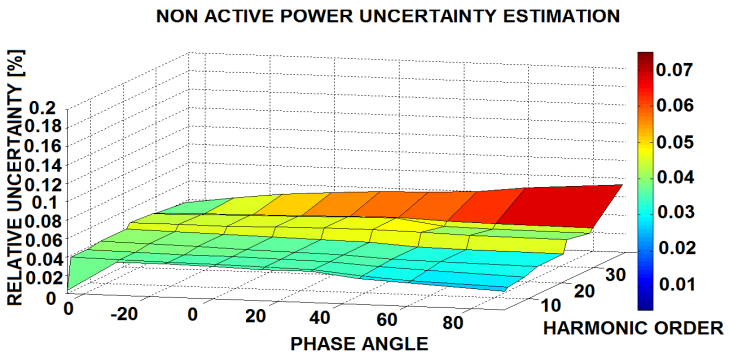

Figure 2.29 – Non Active Power Uncertainty Estimation vs harmonic order and fundamental frequency

Table 2.3 – Summary results of dynamic characterization

Quantity	Uncertainty (sin. test)	Uncertainty (non-sin. test)	Units
Voltage (r.m.s.)	0.03	0.04	[%]
Current (r.m.s.)	0.03	0.04	[%]
Frequency	0.67	0.67	[mHz]
Active Power	0.043	0.061	[%]
Apparent Power	0.13	0.15	[%]
PF (conventional)	0.002	0.002	[p.u.]
Non Active Power	0.6	0.62	[%]
Voltage THD	---	0.072	[%]
Current THD	---	0.07	[%]

The summary results for the meter dynamic characterization in both sinusoidal and non-sinusoidal cases are reported in Table 2.3.

Once characterized, the system has been tested according to current standards. In particular, the test signals were determined according to the following standards:

- The Measuring Instrument Directive (MID) [2.30], which establishes the requirements that the meters, devices, and systems must satisfy when placed on the market and/or putt into use for reasons of public interests, public health, public safety, public order, protection of the environment, protection of consumers, duty and tax levying and fair trading. It demands to the harmonized standards (technical specification adopted by CEN, CENELEC or ETSI prepared in accordance with the General Guidelines agreed between the Commission and the European standards organizations) a detailed explanation of the values and the test cases for the influence quantities, the disturbances and so on.
- The draft document (OIML R-46) of the Organization International de Métrologie Légale on Active Electrical Energy Meters [2.31], which gives an easily-adoptable set of

requirements and tests to meet the needs of the MID to the regulatory bodies.

Both the MID and the OIML R-46 documents have the same approach to the test of the energy meters and also the imposed test signals are substantially the same. Considering these standards, the following test cases are considered for the experimental characterization of the realized smart meter.

1. Sinusoidal signals with no influence quantities (Figure 2.30a).
2. Harmonics in voltage and current circuits (Figure 2.31a) with: fundamental frequency current: I1=11.5 A; fundamental frequency voltage: V1=230 V; fundamental frequency power factor: 1; content of 5th harmonic current: I5=40% of I1; content of 5th harmonic voltage: V5=10% of V1; 5th harmonic power factor: 1.
3. DC and even harmonics in the a.c. current circuit. The tests were performed considering a sinusoidal voltage and the current waveform, with a maximum value of 25 A, as shown in Figure 2.32a.
4. Odd harmonics in the a.c. current circuit. The tests were performed considering a sinusoidal voltage and the current waveform, with a maximum value of 5 A, as shown in Figure 2.33a).
5. Sub-harmonics in the a.c. current circuit. The tests were performed considering a sinusoidal voltage and the current waveform, with a maximum value of 5 A, as shown in Figure 2.34a).

The considered test waveforms have been generated via the function generator and amplified by the Pacific Source 3120 AMX. Then the values measured with the prototype meter have been compared to the ones measured by the D-class Yokogawa WT3000 watt-meter used as reference.

The maximum possible error shifts for each test case for the different meter classes considered in the OIML R-46 are reported in Table 2.4.

Table 2.4 – Maximum possible error shifts for considered test signals

Test case	Disturbance	Max possible error shift [%] per meter class			
		A	B	C	D
1	Sinusoidal signals	±2.0	±1.0	±0.5	±0.2
2	Harmonic component in the current and voltage circuits	±3.0	±1.8	±1.0	---
3	DC and even harmonic in the a.c. current circuit	±8.0	±4.0	±2.0	---
4	Odd harmonic in the a.c. current circuit	±8.0	±4.0	±2.0	---
5	Sub-harmonic in the a.c. current circuit	±8.0	±4.0	±2.0	---

For each test case, Figures 2.30 to 2.34 show the obtained results in terms of comparison between the electrical energy parameters measured by the proposed ARM-based smart meter and that measured by the WT 3000 reference instrument. In particular, the comparison was made respect to the root mean square of both voltage (Vrms) and current (Irms), active power (P), apparent power (S), and non-active power (Q). For all the considered test cases, the values measured by the ARM-based smart meter for Vrms, Irms are within 0.2% and P is within the 0.6 % range with respect to the measurements provided by the reference instrument. A greater difference was revealed in the measurement of non-active power. Nonetheless, these error shifts allow to classify the meter as a class C instrument as per OIML R-46.

The summary results for all test cases are reported in Table 2.5.

Table 2.5 – Summary results for tests according to OIML R-46 recommendations

Quantity	Max error [%]				
	Test case 1	*Test case 2*	*Test case 3*	*Test case 4*	*Test case 5*
Voltage (r.m.s.)	0.02	0.24	0.04	0.14	0.07
Current (r.m.s.)	0.02	0.08	0.02	0.41	0.18
Active Power	0.18	0.02	0.02	0.55	0.29
Apparent Power	0.06	0.14	0.02	0.46	0.88
Non Active Power	0.08	2.81	1.06	2.06	2.04

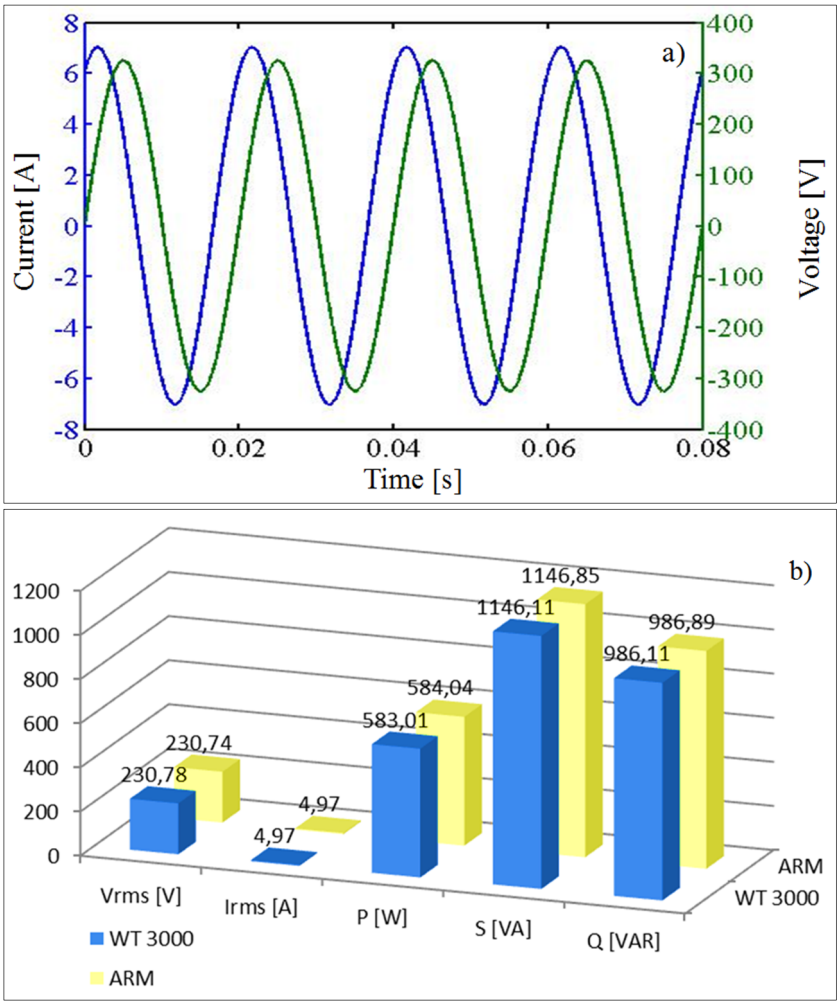

Figure 2.30 – Sinusoidal signals with no influence quantities: a) The considered voltage and current test signals and b) the corresponding obtained results

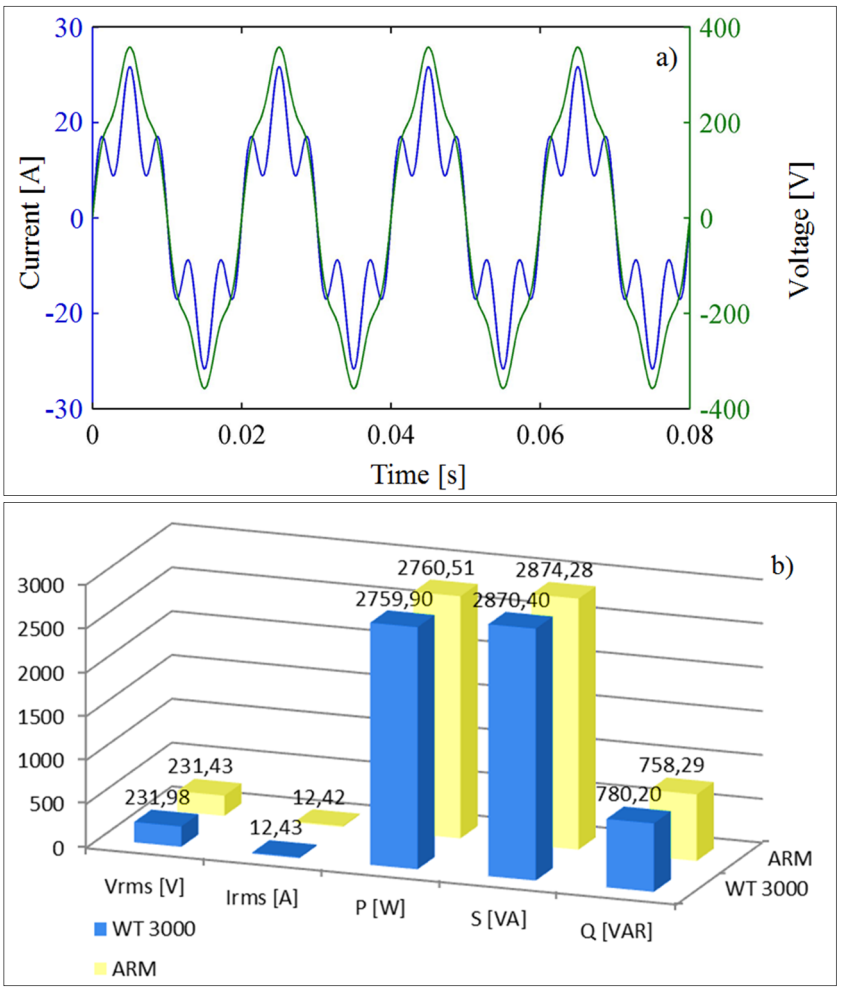

Figure 2.31 – Harmonics in voltage and current circuits: a) The considered voltage and current test signals and b) the corresponding obtained results

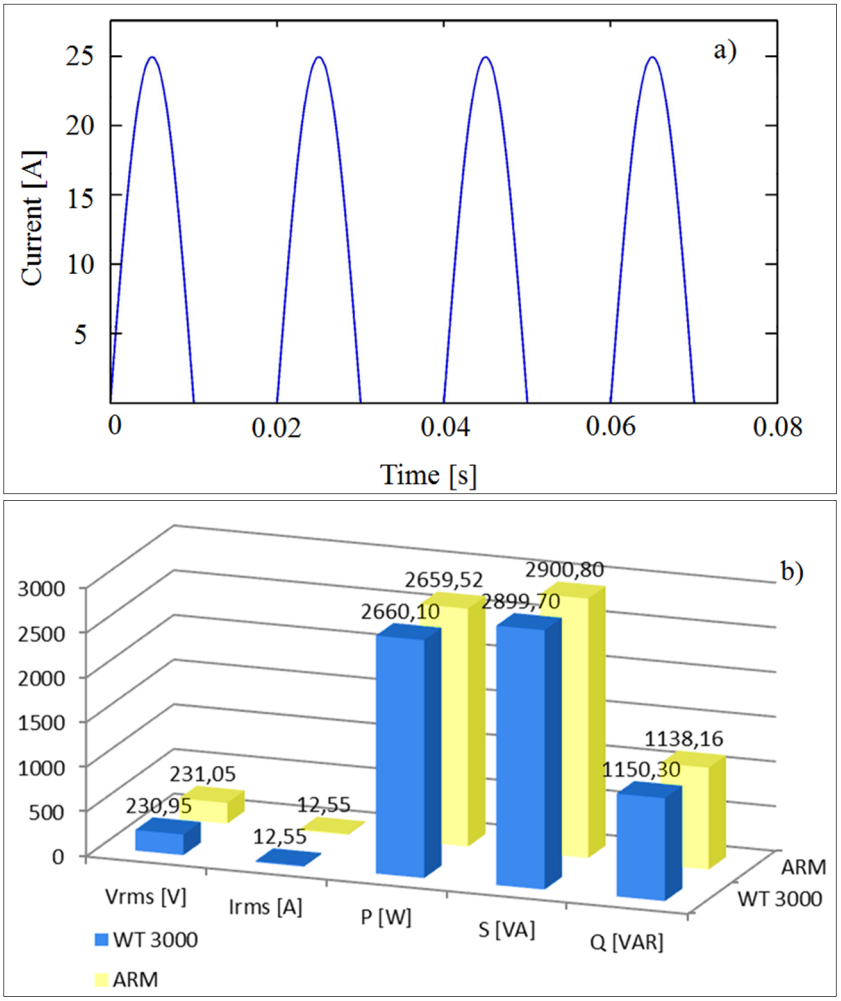

Figure 2.32 – DC and even harmonic in the a.c. current circuit: a) The considered current test signals and b) the corresponding obtained results

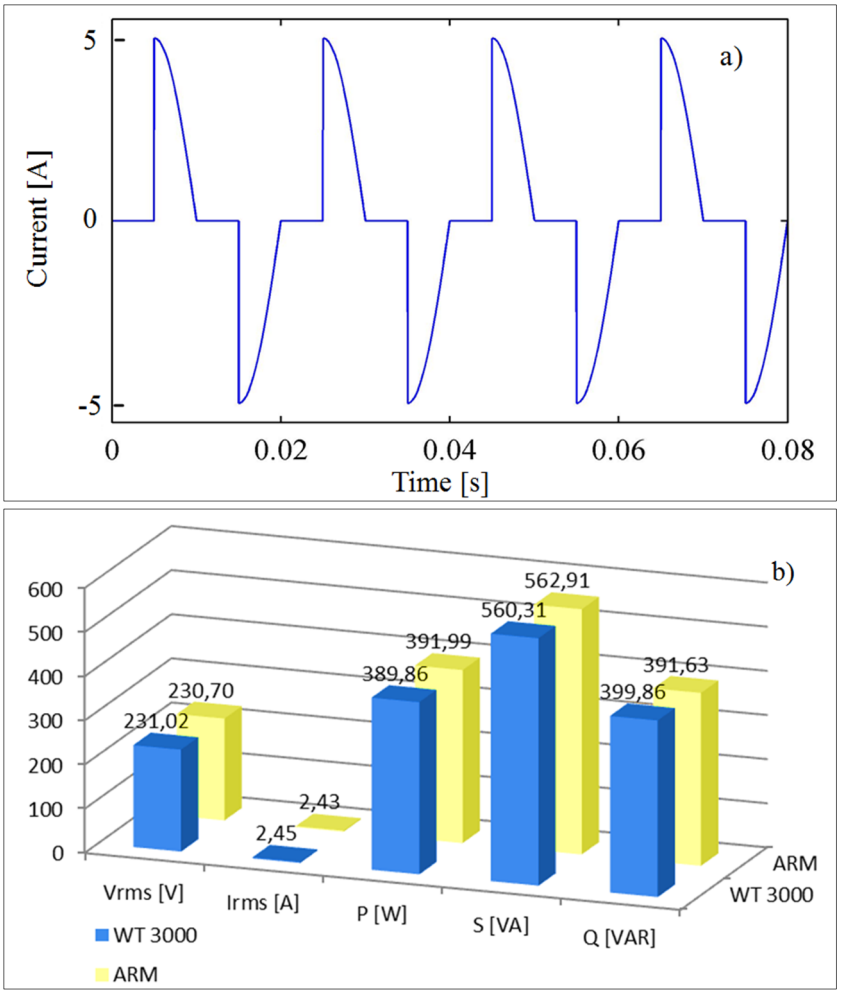

Figure 2.33 – Odd harmonic in the a.c. current circuit: a) The considered current test signals and b) the corresponding obtained results

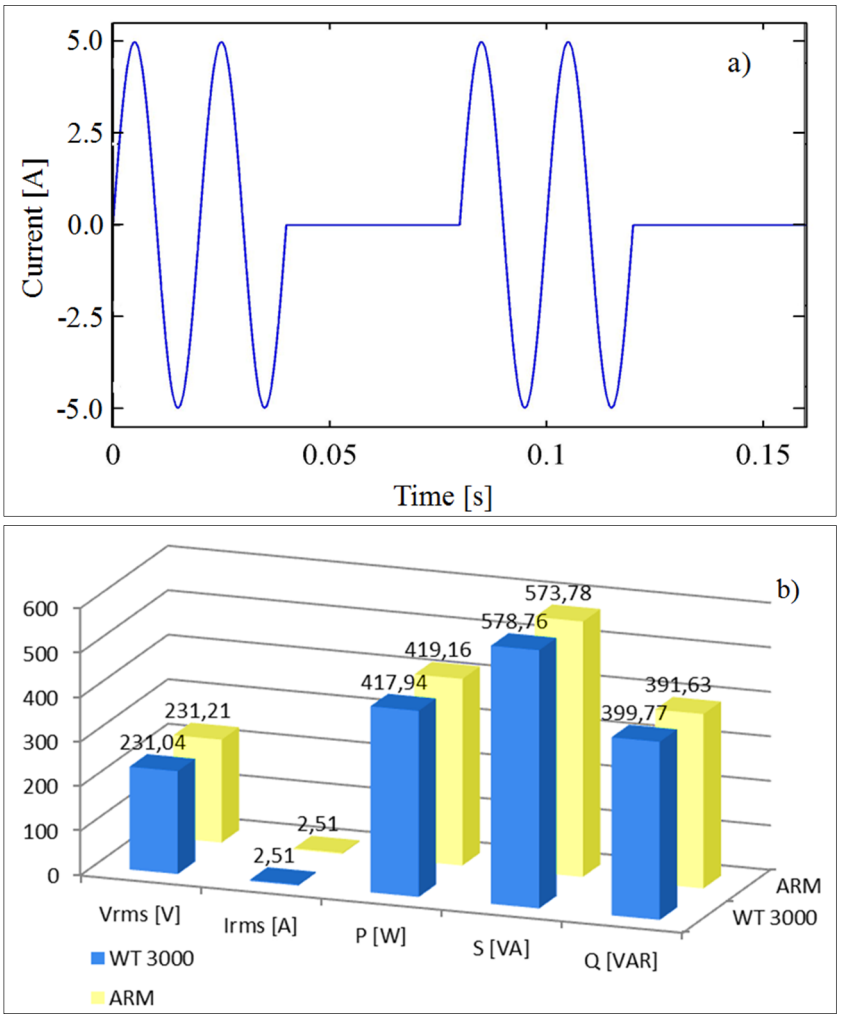

Figure 2.34 – Sub-harmonics in the a.c. current circuit: a) The considered current test signals and b) the corresponding obtained results

2.3.7 Case study for load management strategy

To test the load management algorithm we set up a test case and simulated it in the MATLAB environment. Considering the case of ten different users, from their individual consumptions a total power demand profile can be obtained. Figure 2.35 shows the load curves, together with the graph of the threshold defined for the system. As it can be seen, the algorithm successfully manage to contain power absorption below the threshold level. In this case, the load management algorithm allows for energy savings of around 80 kWh, with respect to the original demand.

Naturally the threshold may be modified for higher or lower electricity (and therefore cost) savings, as underlined in the following two examples.

In the first case (Figure 2.36) the amount of electricity saved with respect to the original demand reaches 170 kWh, doubling the savings at the expense of the number of loads served. The second case (Figure 2.37) exhibits a higher threshold, therefore less loads are curtailed and the electricity savings are in the order of 9 kWh.

We remind once more that, in this case, the choice of the threshold falls upon the user, which can decide the costs he wants to incur in for

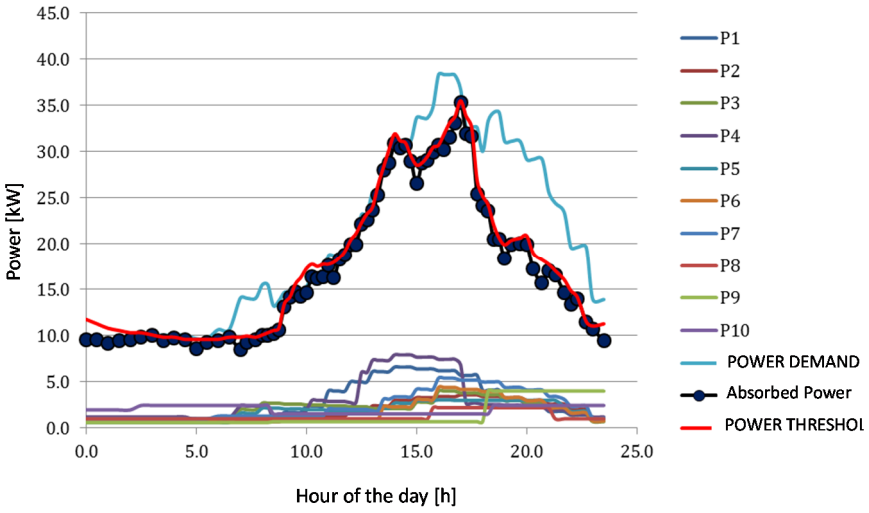

Figure 2.35 – Simulation example of the load management algorithm

electricity and rest assured not to go beyond that. This strategy, however simple, has allowed to prove the physical feasibility and functionality of the prototype AMI architecture. Naturally, for a full realization of a Demand Response program, the threshold may be determined through a negotiation between users and the market. Moreover, the availability of reserve capacity to the grid system operator may be warranted by opportunely modifying the threshold. In any case, once determined the value of Λ, proper action will be undertaken to reduce the absorbed power below this amount.

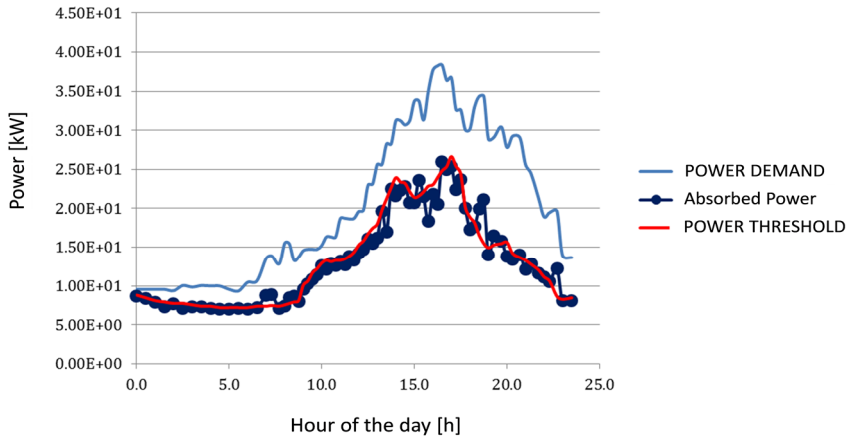

Figure 2.36 – Lowering the threshold determines more frequent load curtailments and higher savings

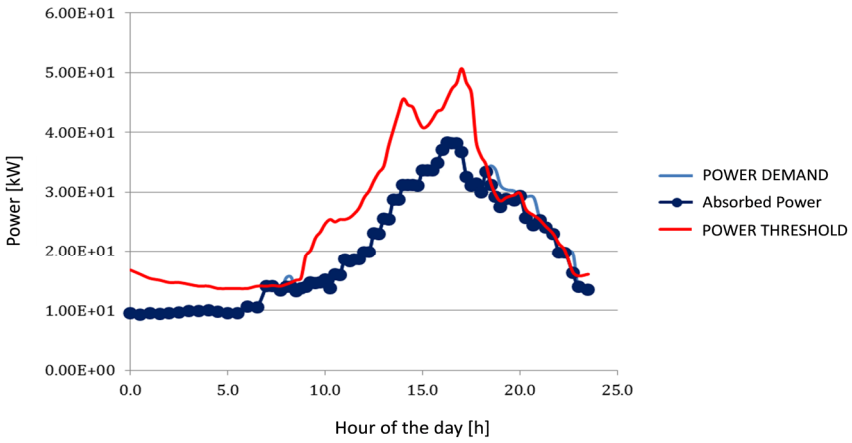

Figure 2.37 – Raising the threshold determines less frequent load curtailments and lower savings

The algorithm is implemented on the MU, which after finding the optimal solution, sends the commands to the smart meter that realizes the load curtailments through its actuators. The algorithm, implemented on the prototype system, constitutes part of the research project "Measurement and Control Systems and Devices for Application of Demand Side Management Programs (Sistemi e dispositivi di telemisura ed attuazione per applicazioni tecniche di demand side management alle piccole utenze)" and has been showcased during the final project verification [2.19].

2.4 Conclusions

In this Chapter, an implementation of a low-cost real-time smart meter has been described. Based on an ARM M3 microcontroller architecture, it employs an innovative wideband combined voltage and current transducer and makes use of advanced measurement algorithms that allow for accurate bidirectional power measurement in non-sinusoidal conditions and power quality evaluation. In fact, the thorough metrological characterization reported in the Chapter shows uncertainty bounded within 0.6% for active power and 0.04% for voltage and current. In addition, for type approval purposes, the performances of the meter have been evaluated according to the standard procedures recommended in the OIML R-46, allowing for classification of the meter in class C: as a mean of comparison, most commercial metering solutions available on the market exhibit worse performances, being classified as class B instruments.

The developed meter is designed to interface with gas and heat meters, thus acting as a central hub for all energy consumptions in residential or commercial environments.

The proposed device could not deliver the benefits commonly associated to smart metering if not included into a broader metering, communication and command infrastructure. Therefore, we propose an AMI implementation. The meter acquires the measurement and send the data to a management unit, which acts as an interface to the system operators and energy market, and implements a web-server with a user-friendly interface that customers can use to remotely monitor all their energy consumptions.

In addition, the management unit implements a load management strategy that, making use of the actuators present on the meter, manages load curtailments in response to energy price signals, therefore attaining the deployment of DR programs. The system was designed to favor user participation, allowing for prioritization of the loads and setting of a price-sensitive triggering condition for the load curtailments. Case studies have proven the effectiveness of the system in reducing demand peaks, while at the same time serving the largest possible number of loads compatibly with the defined triggering condition.

Chapter 3

Energy Storage for the power grid: measurement techniques for battery health estimation

The ability to store electricity is one of the key issues for the Smart Grid. Through usage of Energy Storage Systems (ESSs), load curves can be re-shaped, reducing demand peaks and avoiding the usage of expensive peaking generators. Renewable sources are by their nature variable and not easily predictable: in this case ESSs may work as electricity buffers, decoupling production and usage times. Different technologies may be adopted to store electricity: among these, batteries constitute one of the most promising. In fact, compared to other storage technologies, batteries are characterized by response times in the order of milliseconds, which makes them extremely useful in cases where load or production curves change rapidly.

An effective integration of battery storage into the power grid requires being able to include batteries into resource planning and account them for in operations. Thus, not only reliability of the technology is an essential requirement, but grid planners and operators need to assess the state of the battery system, if and how much it can be relied upon, and to make forecasts regarding its remaining useful life, so to be able to plan maintenance or substitution. Information regarding the state of the batteries, and how much they are decaying under current use, may empower grid operators to develop management policies that tend to limit battery degradation.

In this Chapter, we introduce our proposals for measurement techniques regarding two key aspects in battery characterization and monitoring: the estimation of the health of a battery and the estimation of the values of the parameters of its equivalent circuit model. In both cases, one of the main goals has been obtaining fast and lightweight

methods, implementable on a low-cost microcontroller device to be embedded on the battery system. Moreover, a system-level degradation model is introduced.

3.1 Electrochemical cell operations

A rechargeable battery is composed of one or more electrochemical cells that convert stored chemical energy into electrical energy during a discharge process or convert electrical energy into chemical energy during a charge process. An electrochemical cell is a chemical device for generating or storing electric energy. It consists of a positive electrode and a negative electrode, separated by electrolyte.

The electrolyte is capable of conducting ions between the two electrodes, but is itself an electronic insulator. The positive and negative electrodes are immersed in the electrolyte and the reacting substances usually are stored within the electrodes, sometimes also in the electrolyte. The chemical reactions associated with the energy conversion take place at the two electrodes [3.1-3.3]. During discharge (Figure 3.1b), the negative electrode contains the substance that is oxidized (i.e. releases electrons), while the positive electrode contains the oxidizing substance that is reduced (i.e. accepts electrons). Those electrons pass through the external load, thereby doing useful work. When the battery is charged, this reaction is reversed and a corresponding amount of energy from an external source has to be supplied to the cell (Figure 3.1a).

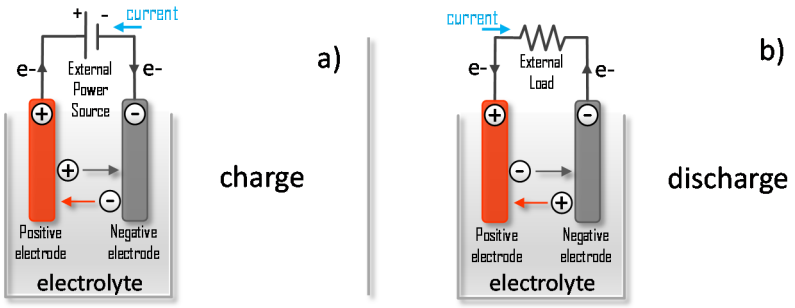

Figure 3.1 – Battery operation during charge (a) and discharge (b)

The current in the battery arises from the transfer of electrons from one electrode to the other. When there is no current flow through a cell, the difference between the potentials of the positive and negative electrodes gives an Open-Circuit Voltage (OCV, E0) of the cell. When current flows, however, mass transport is required to bring the reacting substances to the electrode surface or carry them away. As a result, the voltage under current flow is different from the OCV and the difference comprises (i) an overvoltage at the electrodes caused by electrochemical reactions and concentration deviations on account of transport phenomena and (ii) ohmic voltage drops caused by the electronic as well as the ionic current flows in the conducting parts including the electrolyte, current-collectors and active masses.

The sum of both, called polarization, is responsible for a decreased cell voltage (V_{dis}) during discharge and an increased cell voltage (V_{ch}) on charge as shown below:

$$V_{batt} = \begin{cases} V_{dis} & when \quad i < 0 \\ V_{ch} & when \quad i > 0 \end{cases} \tag{3.1}$$

with

$$V_{dis} = E_0 - V_{op+} - V_{op-} - iR \tag{3.2}$$

$$V_{ch} = E_0 + V_{op+} + V_{op-} + iR \tag{3.3}$$

where V_{op+} and V_{op-} are the over-voltages at the positive and negative electrodes, respectively, and R stands for the polarization resistance. Due to the polarization effects, the battery voltage under current flow may differ substantially from the OCV depending on the state-of-charge of the battery. These two polarization terms are important components for battery model development.

Other important factors affecting battery performance and models include: battery capacity (c_0), State of Charge (SoC), rate of charge and discharge, temperature, and age.

The battery capacity represents the maximum amount of energy that can be extracted from the battery under certain conditions, and it is determined by the mass of active material contained in the battery. The SoC is defined as the fraction of the full capacity that is available for further discharge. Usually it can be referred also as its reciprocal, the

Depth of Discharge (DoD). The OCV of a battery is normally a function of the SoC due to the polarization impact, which is a factor that must be considered in battery modeling. The charging/discharging rates affect the rated battery capacity. According to the Peukert's equation, if the battery is being discharged very quickly, then the amount of energy that can be extracted from the battery is reduced. As we will detail better in the next section, the age and history of a battery have impacts on the capacity of a battery. Even when following manufacturers' DoD specifications, the battery capacity only stays at the rated capacity for a limited number of charge/discharge cycles. If the battery has been taken below its maximum DoD during its usage, battery capacity may be prematurely reduced. The temperature of a battery also affects the energy that can be extracted from the battery. At higher temperatures, the battery capacity is usually higher than that at lower temperatures. But, intentionally elevating battery temperature is not an effective method to increase battery capacity as this also decreases battery lifetime.

3.2 Batteries for grid storage

Power systems are challenging to operate since supply and demand must be precisely balanced at all times. Power demand constantly fluctuates: even if generally following predictable patterns, it is impossible to forecast exactly. Therefore, the power systems have to be flexible. Currently, such flexibility is warranted for by generation resources: system operators adjust generator outputs in response to varying demand. Energy is stored in the form of primary energy sources (i.e., coal, gas, water).

Electricity storage, instead, always involves some sort of conversion – which depends on the specific storage technology – incurring in conversion losses. Nevertheless, many storage technologies have been developed in recent decades that rely on mechanical, electrochemical, thermal, electrical or chemical energy [3.4-3.6]. They differ in energy density, power rating, frequency of charge and discharge, efficiency, response time and must be chosen according to the specific application. In general, pumped hydro storage

(PHS) and compressed air energy storage (CAES) are the most diffused for bulk storage applications.

PHS uses the gravitational potential energy of two water reservoirs: water is pumped from the lower reservoir to the upper one at the expense of electricity during off-peak periods, and the downstream flow is used to produce electricity again, by means of turbines, when needed. CAES works by using electricity to compress air into a cavern or a tank, and releasing the air to drive a turbine, that converts energy back to electricity. Both technologies face site availability issues.

Batteries are a major component of the storage landscape and can serve a wide range of applications with diverse power and energy requirements. They differ according to their electrodes and electrolyte chemistries. Up to now, durability, costs and safety concerns have limited the commercial development. However, the extensive experience for portable applications is fueling the research and development, with positive outlook for production costs decrease and performance improvements.

3.2.1 Advantages and main applications

Batteries present some undoubtedly advantages over other storage technologies. First of all, they are characterized by high efficiencies, even though the specific values depend on the adopted chemistry. Moreover, they have high power and energy densities (respectively the amount of power and energy that is possible to store in the battery for unity of capacity, indicated in [W/l] and [Wh/l]). This characteristics, coupled with response times lower than the second, makes them ideal to follow fast variation in loads and sources. In this regard, they represent a much better solution for *load balancing* and for compensating the variability of renewable resources than conventional generators (for example, the gas-powered ones) and other storage technologies [3.5-3.7]. In fact, although they are characterized by lower power density than supercapacitors and flywheels, batteries still have power densities higher than PHS and CAES. Moreover, their low self-discharge allows not only for their functionality as temporary buffers, but also for effectively realizing load and sources shifting.

Another application example is represented by regulation services, characterized by fast variations.

Battery technologies developed for mobile applications and not specifically for grid storage are composed by several electrochemical cells connected in parallel and series: this gives the flexibility of realizing arbitrary battery sizes.

3.2.2 Main issues

At the moment, the main issue regarding battery usage as storage system for the power grid is represented by high costs compared to other storage technologies. However, favored also by the increasing diffusion of battery powered devices and Battery Vehicles, production costs of mainstream battery technologies are decreasing, and the development of new technologies specifically targeted to grid applications will bring the costs down in the near –term to under 250 $/kWh, with longer-term goals of about 150 $/kWh according forecasts by U.S. Department of Energy and Sandia National Laboratories [3.5-3.6].

The other great barrier to a greater diffusion of batteries in grid storage applications is the limited cycle life that, combined with high costs and low tolerance of some battery technologies for deep cycles, makes them currently not attractive for bulk storage applications.

Finally, batteries require more careful management during their operations. In fact, some battery technologies such as *NaS* and *liquid-metal* require high operating temperatures; on the other hand, Li-ion batteries need advanced battery management systems to prevent overcharging, overheating and consequent thermal runaway.

3.2.3 Battery technologies for grid support

Different types of batteries are currently employed for grid support services. They are characterized by different chemistries, different operating conditions, and are adopted for different applications.

The most mature technologies are represented by *lead-acid* and *sodium-sulfur* (NaS) batteries. Lead-acid batteries represent a reliable and low-cost solution, with a good battery life. Their primary

application is in load leveling and grid stabilization. Their drawback is represented by their sensibility to deep cycles, which limits the usable battery capacity, as well as their limited energy density. In addition, the cycle life is lower than other battery technologies. NaS batteries have higher energy density and can maintain long discharges (four to eight hours), which makes them suitable for load leveling, renewable sources integration and price arbitrage. However, they are operated at high temperatures (between 250° and 300° C) entailing safety issues and preventing suitability to small-scale applications.

Other relevant technologies, originally developed for mobile applications but that have found their applicability also in grid storage are represented by *nickel–metal hydride* (Ni-MH) and *lithium-ion* (Li-ion) batteries. Ni-MH batteries are mainly of interest since they are used in some battery vehicles, which can be used for grid support services in a vehicle-to-grid framework. Li-ion batteries are among the most robust technologies. They have very high energy and power densities, good efficiency and short response times. On the other hand, even though production costs are forecasted to decrease consistently over next years, Li-ion batteries are still expensive. Moreover, they are sensible to overheating, entailing to safety concerns and more sophisticated battery management systems. Li-ion batteries do not tolerate well deep cycles and are best suited for relatively short discharges (under two hours): these characteristics make them fit for services such as frequency regulation [3.2], [3.4-3.9].

Innovative technologies, such as *flow batteries* and *liquid-metal batteries* are still in demonstration phase, but have shown great potential for grid applications. *Flow batteries* rely on two separately stored electrolytes to decouple their power and energy capacities [3.10-3.11]. Compared to other battery technologies, they exhibit longer lifetimes, even under deep cycles. On the other hand, they are more complex than conventional batteries and have lower energy density. *Liquid-metal* batteries are of simple construction and rely on inexpensive materials [3.12-3.13]. Differently than conventional batteries, which use at least one solid material (that can limit conductivity and increase the risk of failure, with consequent impacts on battery life), they are composed of two layers of metal and a salt, which works as electrolyte. *Liquid-metal* batteries exhibit little capacity loss over time. The high operating temperatures required to keep the

metals in a liquid state make them more suitable for large-scale grid storage.

A summary of the different technologies and the related advantages and drawbacks is reported in Table 3.1.

Table 3.1 – Comparison of battery technologies for grid storage

Technology	*Main application*	*Advantages*	*Drawbacks*	*Cycle life [cycles]*
Lead- acid	-Load leveling -Grid stabilization	-Low cost -Good battery life	-Limited depth of discharge -Low energy density	100-2000
NaS	-Load leveling -Congestion relief -Renewable source integration	-High energy density -Fast response -Long discharge cycles -Long life	- High operating temperatures -Safety issues	2500-4500
Li-ion	-Power quality -Frequency regulation	-High energy density -High charge/discharge efficiency -Good cycle life -Fast response	-High production cost -Intolerance to deep discharges -Sensitivity to overtemperature	1000-10000
Flow batteries	-Peak shaving -Time shifting -Ramping -Frequency regulation -Power quality	-Very long life -Scalable -Very long cycle life	-Cost -Complicated design -Lower energy density	12000-14000
Liquid metal	-Load leveling -Peak shaving	-Simple realization -Inexpensive -Low capacity loss over time	-High operating temperatures	---

3.3 Battery models

Batteries are complex systems, and depending on the level of the detail required, they can be represented by several models.

3.3.1 Electrochemical models

Electrochemical models give a very detailed insight in the electrochemical processes that take place in the cell.

There exist several models that recur to physical laws and specific cell parameters to describe battery operation starting from the chemical reactions that happen in the cell [3.14-3.19]. Generally, these models involve coupled PDEs, therefore their solution results too computationally intensive to be implemented on devices embeddable on batteries and suitable for online monitoring purposes. Moreover, they depend on very specific parameters characteristic of the individual cell: such parameters not only vary among different battery types, but

Table 3.2 – Equations for the electrochemical model for Li-ion battery in [3.14]

Conservation of lithium in the solid phase $\frac{\partial c_s}{\partial t} = \frac{D_s}{r^2}\frac{\partial}{\partial r}\left(r^2 \frac{\partial c_s}{\partial r}\right)$	Where: - c_s *solid-phase lithium concentration* - c_e *electrolyte-phase lithium concentration* - ϕ_s *solid-phase potential* - ϕ_e *electrolyte-phase potential* - D_s *diffusion coefficient of Li/Li$^+$ in the solid phase* - D_e *diffusion coefficient of Li/Li$^+$ in the electrolyte phase* - ε_e *electrolyte volume fraction* - σ *electrode electronic conductivity* - κ *electrolyte ionic conductivity* - κ_D *electrolyte diffusional conductivity* - j^{Li} *reaction rate* - a_s *solid/electrolyte interfacial area per unit volume* - F *the Faraday constant* - R *the universal gas constant* - T *absolute temperature* - U *Open Circuit Voltage (OCV)*
Conservation of lithium in the electrolyte phase $\frac{\partial(\varepsilon_e c_e)}{\partial t} = \frac{\partial}{\partial x}\left(D_e \frac{\partial}{\partial r} c_e\right) + \frac{1 - t_+^0}{F} j^{Li}$	
Conservation of charge in the solid phase $\frac{\partial}{\partial x}\left(\sigma \frac{\partial}{\partial x}\phi_s\right) - j^{Li} = 0$	
Conservation of charge in the electrolyte phase $\frac{\partial}{\partial x}\left(\kappa \frac{\partial}{\partial x}\phi_e\right) + \frac{\partial}{\partial x}\left(\kappa_D \frac{\partial \ln(c_e)}{\partial x}\right) + j^{Li} = 0$	
Butler-Volmer equation $j^{Li} = a_s i_o \left\{\exp\left[\frac{\alpha_a F}{RT}\eta\right] - \exp\left[-\frac{\alpha_c F}{RT}\eta\right]\right\}$	
Overpotential η defined by $\eta = \phi_s - \phi_e - U$	

also depend on the shape of the batteries, on the specific production lot, on the environment where the battery is being used (i.e. some of them depend on temperature). However, having sufficient computational power and knowledge of the intervening parameters, such models have a high degree of accuracy. An example of electrochemical model is summarized in Table 3.2.

For system-level representation, the deep insight on the electrochemical processes may not be needed, and simpler and faster models can be used, such as equivalent circuit models and mathematical models.

3.3.2 Mathematical models

Mathematical models describe the battery at a higher level of abstraction than both the electrochemical and equivalent circuit ones [3.20-3.21]. In such models, there is not the representation of the system as a whole, nor the insight of the specific physical and chemical processes taking place in the battery: they look at the battery through analytical relations that model its external behavior. Therefore, they can make use of few equations and focus only on the battery properties of interest.

Mathematical models arise from the Peukert's law or the Shepherd equation, with additional terms empirically determined to improve the accuracy.

3.3.3 Equivalent circuit models

The equivalent circuit models resort to an analogy to electrical components, such as resistors and capacitors, to describe the V-I behavior of the cell. Two of the basic equivalent circuits are the simplified Randles cell and the Randles cell, which are reported in Figure 3.2-3.3 [3.22-3.24].

Depending on the degree of accuracy desired, it is possible to build a higher-order model starting from the Randles cell: in this case, the

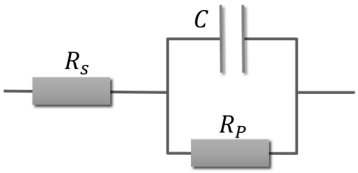

Figure 3.2 – Simplified Randles cell

The Simplified Randles cell is one of most common cell models. It includes a solution resistance, a double layer capacitor and a charge transfer (or polarization resistance). The double layer capacitance is in parallel with the charge transfer resistance. In addition to being a useful model in its own right, the Simplified Randles Cell is the starting point for other more complex models.

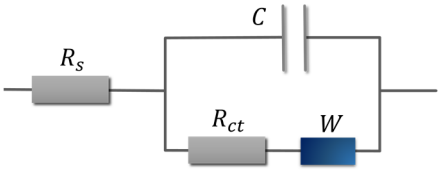

Figure 3.3 – Randles cell

The equivalent circuit was initially proposed by Randles for modeling of interfacial electrochemical reactions in presence of semi-infinite linear diffusion of electro-active particles to flat electrodes. In this model, the impedance of a faradaic reaction consists of an active charge transfer resistance R_{ct} and a specific electrochemical element of diffusion W, which is also called Warburg element ($Z_W = A_W/(j\omega)^{0.5}$, where A_W is Warburg coefficient).

higher attainable accuracy has to be balanced against the ease of implementation.

Equivalent circuit models are particularly suitable when the battery has to be studied as part of an electric circuit. However, it must be highlighted that the parameter of the equivalent circuit tend to change with the operational conditions of the cell and with aging. In particular, considering the simplified Randles cell, resistors and capacity values depend on temperature, current and state of charge (SoC); moreover, with the battery wearing off resistors values tend to increase, while the capacitance decreases. Therefore recent studies make use of Randles cell (or the simplified version of it), updating the value of the parameters basing on the operational conditions of the cell. There are two approaches that can be followed here: the first one, very efficient especially in the case of onboard battery management systems, is to resort to Look-Up Tables that result from a previous characterization of the battery and state the values of the parameters corresponding to the parameters of influence [3.25]; another method is to derive a function able to express the variation of the resistors and capacitors in the model with the parameter of influence. Generally the considered parameter of interest are SoC, temperature and possibly current.

3.4 Proposed techniques

Two are the main aspects to consider that have a direct impact on how a battery can be used and accounted for: the state of charge (SoC) and the health of a battery, here referred to as state of health (SoH). The SoC represents the energy stored in the battery as a percentage over the maximum storable quantity. The SoH, instead, is assumed as a measure of "how healthy" the battery is and expresses the available fraction of maximum battery capacity, with values ranging in the interval [0,1].

As well known from literature, the electrochemical reactions that take place inside the cells of a battery tend to shorten its life [3.26]. Therefore, the SoH, initially having value 1, decreases with subsequent use. In this work, we focus on battery health assessment. In particular, we focus on the *cycle life*, which attains the number of cycles of charge/discharge that a battery is able to sustain: this value is strongly dependent on usage and on environmental and operational parameters. It directly affects planning, given such information may be used in prognostics tools to make forecasts on the remaining useful life of a battery. Moreover, a decay faster than expected may be indicative of anomalous system operation. Finally, the system may adopt information regarding battery health and implement strategies that tend to preserve battery life as much as possible.

We developed two different measurement techniques for estimating the health of a battery and a method for the estimation of the parameters of the equivalent circuit model assumed for the battery. The description of these techniques is reported in the following paragraphs. These techniques are intended for online monitoring of batteries, therefore need to be implemented in measurement devices embedded don the batteries themselves.

In addition, we propose also a system-level model that allows for taking into consideration battery degradation while managing the allocation of services to the grid. This model and the developed online monitoring techniques can be used together to determine allocation of service provision taking into account battery degradation.

The described techniques are better detailed in [3.27 -3.29].

3.4.1 Parameter estimation

3.4.1.1 State of the art

Currently the state of art for measuring the value of the parameters characteristic of an electrochemical process is the Electrochemical Impedance Spectroscopy (EIS) [3.24],[3.30]. It can be successfully applied to batteries: to this end the cell is represented through an equivalent electric circuit [3.22-3.23]. The method essentially consists of a perturbative characterization in which a small AC potential is applied to the electrochemical system and, from the nonlinear current response, is possible to determine the spectrum of equivalent impedance characteristic of the process. Using such information is possible to infer the values of the process parameters. Of course, it represent a small signal characterization with consequent linearization of the system around the working point. Therefore is important, to the end of executing the measurements correctly, that the system is in steady state. For this reason executing an EIS characterization is a long process, especially considered that for each point a stimulus at a particular frequency must be provided and the corresponding current measured. Moreover, it is also computationally heavy, thus not suitable for on-board battery monitoring. On this regard, executing one measure at a time it is difficult to guarantee that the battery is in steady state.

There exist a number of online estimation methods in literature; mainly they can be divided into two categories: model based and non-model based. In the first case, it is assumed a fixed model for the cell, and the variability of the parameters is intended as the perturbation of the model values. In this field, Kalman filters and recursive system parameter estimation techniques have been found to be successfully applicable [3.31-3.33]. To the second category belong techniques such as RVM or neural network, which basically look at the battery as a system whose laws and relations are not known, but create such laws themselves learning along with system usage [3.34].

3.4.1.2 Implemented estimation technique

Our work focuses on a measurement method to perform battery parameter identification that is fast and can be implemented on a low-cost microcontroller to realize online battery monitoring. Representing the battery with a simplified Randles cell, a parametric estimation algorithm is applied. As in the EIS, the cell is perturbed with a stimulus signal, which in this case is a multisine current waveform, composed by the superposition of multiple sinusoidal waveforms. From the voltage response of the cell the parameters of the model, which describe the state of the cell, can be extracted.

Starting out with the measured voltage and current values, given the battery model, a model for the identification of the parameters must be chosen. There exist several models for the identification of parameters; the one that has the best performances as system simulator is the Output Error (OE) model [3.35]: however, it is not linear with respect to the model characteristic parameters. That means that an iterative optimization method should be used to calculate model parameters. This makes the OE model less attractive for an online battery monitoring embedded device. Another identification model, which allow a closed form calculation of the parameters, is the AutoRegressive eXogenus (ARX) [3.35].

These two identification models are the ones implemented in the proposed method. For both models the stimulus electric current pattern is composed of a sum of sinusoidal waveforms, opportunely separated in frequency and with different phases. From the knowledge of the input and the response the spectrum of the transfer function, that in this case corresponds to the impedance, is obtained.

A least square algorithm is implemented to identify the values of the coefficients characteristic of the transfer function $\{a_0, \dots, a_{nf+nb}\}$ that best fit the measured spectrum. Such coefficients are directly related to the values of the electrical components of the equivalent circuit. Additional detail on the measurement method may be found in [3.36].

3.4.1.3 Output Error (OE) model

If the *k-th* sample of the stimulus is represented by *x, c* represents the

undisturbed output and the system output includes error *e* and is represented by *y*, the relation between them may be expressed as:

$$y(k) = c(k) + e(k) \tag{3.4}$$

with

$$\begin{aligned} c(k) + a_0 c(k-1) + \ldots + a_{nf-1} c(k-nf) = \\ = a_{nf}\, x(k-nk) + \ldots + a_{nf+nb}\, x(k-nk-nb) \end{aligned} \tag{3.5}$$

The system is described by the equation

$$y(k) = G(z)\; x(k-nk) + H(z)\; e(k) \tag{3.6}$$

where in the OE model $H(z) = 1$ is the error transfer function and $G(z)$ is the input transfer function, given by:

$$G(z) = \frac{a_{nf} + \ldots + a_{nf+nb} z^{-nb}}{1 + a_0 z^{-1} + \ldots + a_{nf-1} z^{-nf}} \tag{3.7}$$

The optimization is carried out minimizing the one-step prediction error. Being non linear in the parameter of $G(z)$ an iterative method is required.

For a simplified Randles cell, the transfer function is:

$$G(z) = \frac{a_1 + a_2 z^{-1}}{1 + a_0 z^{-1}} \tag{3.8}$$

Considering the output vector of the identification function $\{a_0, a_1, a_2\}$, the values of the parameters are given by:

$$R_S = \frac{(a_1 - a_2)}{(1 - a_0)} \quad R_P = 2\frac{[a_2 - a_0 a_1]}{(1 - a_0^2)} \quad C = \frac{T(1-a_0)^2}{4[a_2 - a_0 a_1]} \tag{3.9}$$

with *T* the sampling period.

3.4.1.4 AutoRegressive eXogenous (ARX) model

The ARX model describes a relation between the input, error and output and most of the single input single output relationship is represented by this linear equation, which is given by

$$A(z)\, y(k) = B(z)\, x(k) + e(k) \tag{3.10}$$

where

$$A(z) = 1 + a_0 z^{-1} + a_1 z^{-2} + \ldots + a_{nf-1} z^{-nf} \tag{3.11}$$

$$B(z) = a_{nf} + a_{nf+1} z^{-1} + \ldots + a_{nf+nb} z^{-nb} \tag{3.12}$$

x is the command signal, y is the output, e is the white noise. The error transfer function is $H(z) = 1/A(z)$ and the input transfer function is given by:

$$G(z) = \frac{B(z)}{A(z)} = \frac{a_{nf} + a_{nf+1}z^{-1} + \ldots + a_{nf+nb}z^{-nb}}{1 + a_0 z^{-1} + a_1 z^{-2} + \ldots + a_{nf-1}z^{-nf}} \tag{3.13}$$

Given linearity of Equation (3.10), it is possible to estimate the parameters in closed form calculation.

The form the $G(z)$ assumes is the same as in Equation (3.8), and the determination of the parameters makes use of the same Equations as in (3.9): the only difference with respect to the OE case relies in the optimization procedure and on the way the output of such procedure are presented.

3.4.2 State of Health (SoH) estimation

In this work, we adopt an analytical description: starting from the analysis of capacity decay curves and using also operational and environmental parameters, a measure of the SoH of a Li-ion battery is obtained. The same topic has been faced in literature by several authors who resorted to the most diverse techniques [3.34],[3.37-3.41]. Most of them describe the behavior of batteries making use of a system model: mainly they focus on lifetime predictions, analyzing how discharge conditions influence the SoC and how long a specified load can be powered by a battery with a defined SoC. However, some of them include the modelling of battery capacity fade, therefore allowing for estimations of the SoH.

Modelling the physical and chemical processes that lead to capacity fade may allow to achieve very good accuracy, but at the same time would determine a high computational load. We propose methods based on fuzzy logic and on a neural network instead: they allow to have a less resource hungry software, therefore being able to implement it into low power and low cost devices.

In fact, the techniques introduced here are thought for being implemented on a microcontroller on-board the battery. The proposed SoH index is a measure of the health of the monitored battery. It corresponds to the normalized value of the battery residue capacity. The

index ranges from 1 to 0, with 1 being a battery at the full charge capacity taken at the beginning of its life, and 0 for a battery at the end of its life. The monitoring system is destined to be implemented on a microcontroller embeddable on the battery itself, therefore ensuring the functionality of the system even if the battery is moved since the microcontroller retains the history of the battery.

3.4.2.1 Factors influencing battery health

As reported previously, continuous cycling degrades battery capacity. Moreover, several environmental and operational factors can speed up or slow down such aging process. Some of the most influential ones are reported here.

The temperature has a big impact on battery operation and therefore on its life: a high temperature lowers the internal resistance and speeds up the chemical reactions, while a low temperature slows them down and increases the resistance. The optimal temperature range depends on the actual chemistry of a specific battery, however common to all is a considerable shortening of the useful life when outside that range. In Figure 3.4 is shown the impact temperature has on Li-ion battery life [3.42].

As for the current flowing into/out of the battery, experimental tests on commercial Li-ion batteries have shown that high current rates accelerate the capacity fading, as depicted in Figure 3.5 [3.43]. In the graph, the labels C/1, C/2, C/3 and C/5 indicate constant current discharge cycles: C/1 means a constant current that discharges the

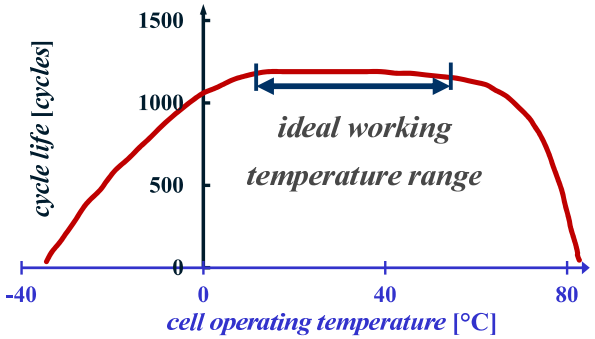

Figure 3.4 – Battery degradation with temperature

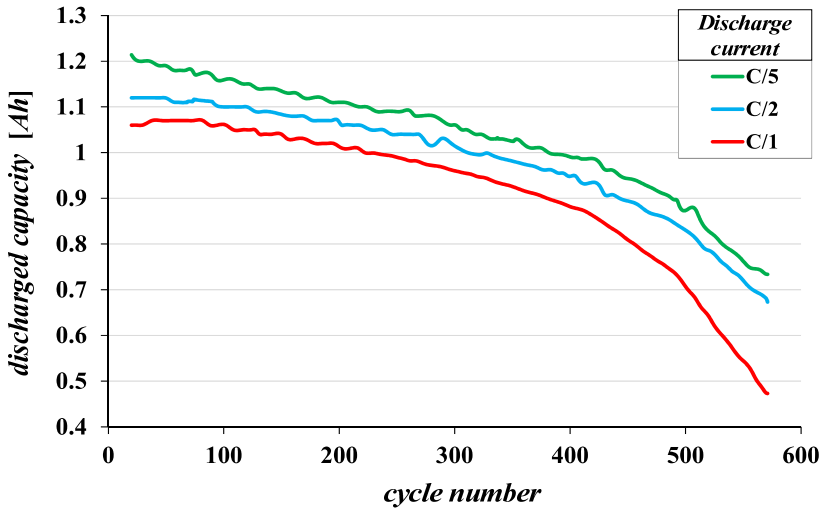

Figure 3.5 – Capacity degradation at different current rates

battery completely in 1 hour, C/2 in two hours, C/3 and C/5 a discharge that takes 3 and 5 hours respectively.

Deeply tied to battery cycle life is the Depth of Discharge (DoD). It represents how much a battery is depleted at each cycle and is usually indicated as a percentage of full capacity of the battery. At a given temperature and discharge rate, the amount of active chemicals transformed with each charge/discharge cycle will be proportional to the DoD. Many cell chemistries do not tolerate deep cycles (cycles

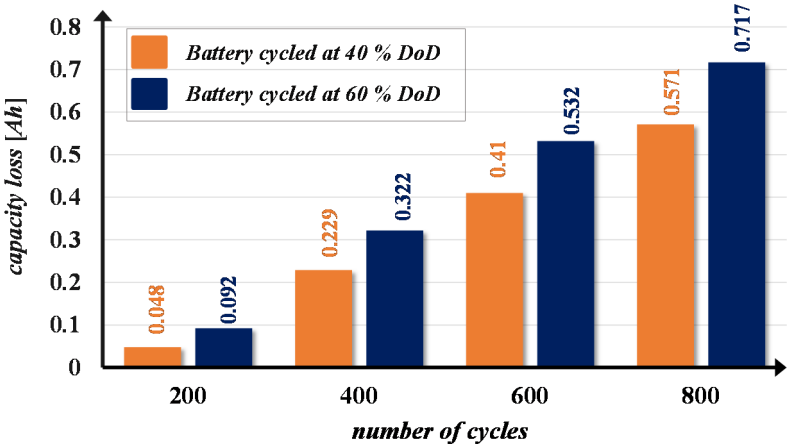

Figure 3.6 – Capacity loss at different cycle number with different DoD

performed at high DoD): the number of cycles yielded by a battery goes up exponentially the shallower the DoD. As reported in Figure 3.6, it is immediately clear the impact that the DoD has on battery aging: in the specific case an increase of DoD of 20% in battery cycling can produce a decrease of 25% in cycle life [3.44].

3.4.2.2 Measurement technique based on fuzzy logic

The aging of a battery is mainly related to operational temperature, DoD and charge/discharge current, as described in the previous paragraph. As a consequence, these variables are continuously monitored in the proposed approach.

The aging of a battery is related to all the previously illustrated factors, which then need to be considered together. In addition to these, other two input variables are considered: the number of cycles the battery has already been through and the values resulting from the two previous runs of the algorithm. Since the software is embeddable in a microcontroller that may reside directly on the battery, the initial value for this variable is assumed as 1 (practically, the software starts the monitoring with the first battery cycle). The resulting index is then assumed to be a function of these inputs, and is computed at every battery cycle.

The system assumes that data regarding the characterization of batteries of the same type of the one that is currently being monitored is available. In practice that means that an early laboratory characterization is carried out for batteries belonging to the same family. In all the following analysis, the data in [3.45] has been taken as reference.

Considering the curve of capacity decay with the proceeding of charge/discharge cycles, under well-defined values of temperature, current and DoD, a double exponential fitting curve for all the batteries of the same family is introduced. The generic fitting curve for Li-ion batteries belonging to the NASA data set is in the form:

$$y_{fit} = a_0 + a_1 e^{-\left(\frac{n}{\alpha_1}\right)^{\beta_1}} + a_2 e^{-\left(\frac{n}{\alpha_2}\right)^{\beta_2}} \tag{3.14}$$

where x represents the number of cycles and y is the normalized value of battery capacity. The computed index is assumed to follow the decay

of battery capacity since such data retains the information regarding the health of the monitored battery.

The fitting function reported in Equation (3.14) depends on seven different parameters: to decrease the number of parameters to be determined, we recur to a local approximation, which depends on only two parameters. Such curve can be effectively computed online, as an iterative interpolation: recurring to a simple exponential function in the form

$$y_{fit} = ae^{-\beta x} \tag{3.15}$$

it is possible to compute a local approximation of the fitting function using the two previous values of the fitting curve and thus predicting the following value. In particular, if $y_{fit}(k-1)$ and $y_{fit}(k)$ are two values of the function to be approximated, with k index of the individual sample, it is possible to compute the exponential function in the form expressed in Equation (3.15) using the following equations:

$$\Delta x(k) = [x(k) - x(k-1)] \tag{3.16}$$

$$y'_{fit} = [y_{fit}(k) - y_{fit}(k-1)] / \Delta x(k) \tag{3.17}$$

$$\beta(k) = -\left[\frac{y'_{fit}(k)}{y_{fit}(k)}\right] \tag{3.18}$$

$$a(k) = \frac{[y_{fit}(k-1) - y_{fit}(k)]}{e^{-\beta(k)x(k-1)}\left[1 - e^{-\beta(k)\Delta x(k)}\right]} \tag{3.19}$$

Using the so determined local function, it is possible to approximate the value of $y_{fit}(k+1)$ with the output of the curve in Equation (3.15) computed at $x(k+1)$.

In case the value of the index is computed using only Equations (3.15)-(3.19), the algorithm would not take into account the previously described external factors which impact battery life. Therefore, the final value of the parameters $a_F(k)$ and $\beta_F(k)$ are computed modifying the values obtained from the local approximation with the corrective coefficients $a_D(k)$ and $\beta_D(k)$, determined with the fuzzy algorithm: such coefficients are needed to consider the effects of temperature, current and DoD. The fuzzy algorithm is divided into three blocks, each one accounting for a different factor of influence and each one requiring as inputs the outputs of the previous block (in the case of the first block, such inputs are set at 1). Such a choice, as opposed to computing the

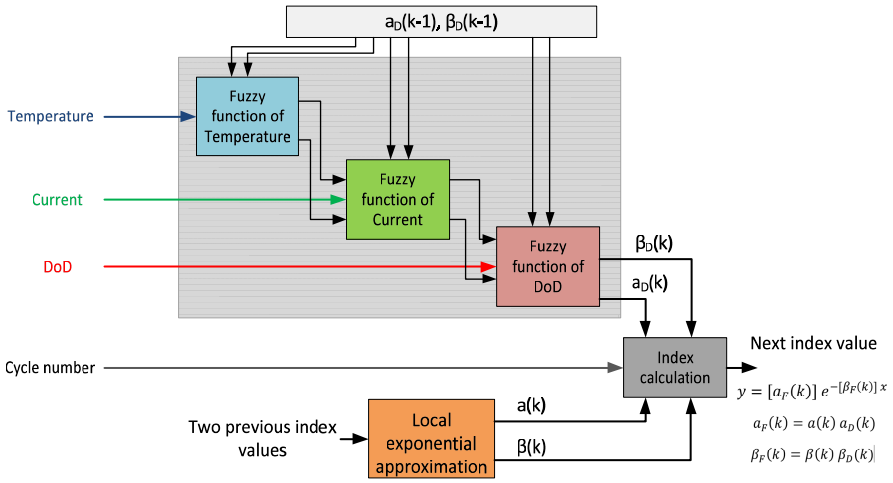

Figure 3.7 – Fuzzy logic controller block diagram

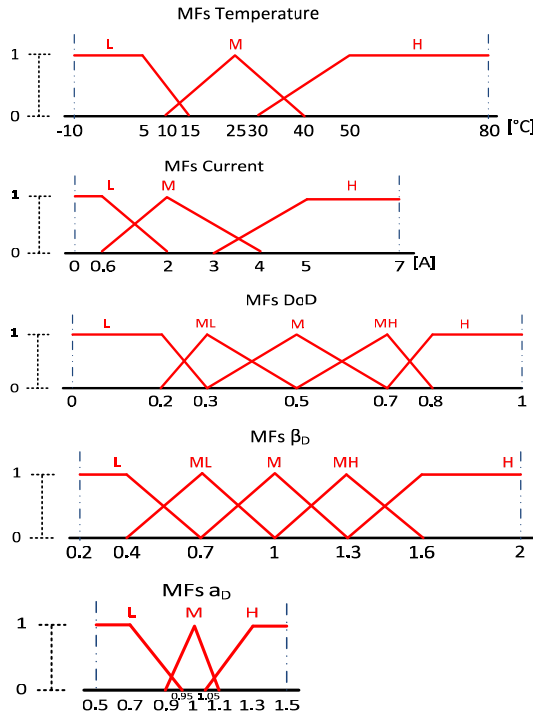

Figure 3.8 – Membership functions of input and output variables

values of the coefficient taking into account all the influencing factors at the same time, allows for an easier modeling and tuning up of the algorithm. Once the values of the local exponential approximation and the respective corrective coefficients have been determined, the value of the index is then computed. The block diagram of the process for computing the index is reported in Figure 3.7. In Figure 3.8 are reported the membership functions used. The membership functions are built around the

battery characteristics and the testing condition adopted in the used dataset.

Current and temperature are assumed to be sampled each second, and the value used as input is the average over the charge/discharge cycle. Each cycle is isolated basing on the inversion of current sign: only when this condition is reached the index is actually computed. Thresholds are considered for instantaneous values that are by themselves harmful for battery life.

The final goal is to implement the proposed algorithm on a microcontroller-based system powered by a STM32F407 ARM Cortex M4 microcontroller, which provides a good balance between computational capability and cost.

3.4.2.3 Measurement technique based on neural network

The second approach to the computation of the index is based on a neural network. The network uses a Nonlinear Autoregressive with eXogenous inputs model, with external inputs and a feedback connection considering as input also the output of the previous step (1 step delay). The considered external inputs are the present and previous step values of DoD, current, temperature and cycle number. In the same manner adopted in the case of the fuzzy algorithm, current and temperature are the average values over the charge/discharge cycle. All the inputs are provided to the network using normalized values. The equation defining the model is:

$$y(k) = f\left(y(k-1), \boldsymbol{x}(k), \boldsymbol{x}(k-1)\right) \tag{3.20}$$

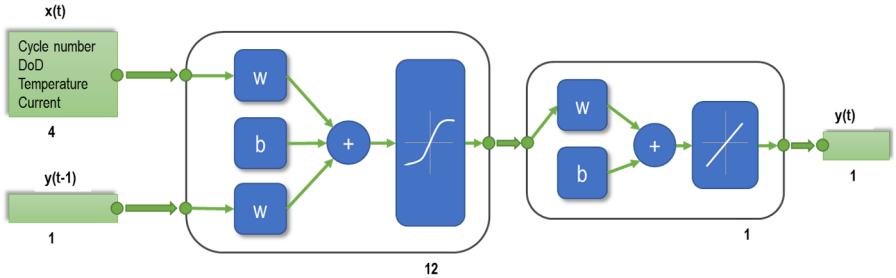

Figure 3.9 – Neural network scheme

The network is composed of one hidden layer and an output layer: the first makes use of a sigmoidal activation function, while the output layer is linear. Training of the network is carried out using Levenberg-Marquardt back-propagation. Network scheme is reported in Figure 3.9. In this case, the output of the network represents directly the value of the index, and no exponential fitting has been considered.

3.4.3 Battery degradation model for system level analysis

The techniques described in paragraphs 3.4.1 and 3.4.2 are destined to be implemented on devices embedded on the batteries. On the other hand, from a system point of view, to effectively integrate battery storage into the power grid, a complete but reasonably simple battery degradation model is needed.

To this end, we could assume the capacity decay curves provided by battery manufacturers as reference: they describe the capacity decay (and therefore the state of health decline) with respect to the number of cycles the battery has been subjected to. In fact, battery characterization involve accelerated aging tests, generally composed of sequences of full charge/full discharge, at specified current and temperature.

However, it must be considered that when the battery is used for grid support, the provision of services to the power grid rarely involves full cycles. Therefore, the battery degradation model must be able to describe state of health decline even under such circumstances.

Given that the decrease in battery health is related to the electrochemical reactions that happen inside each cell, and the amount of reactions depends on the amount of energy the battery provides or is charged with, we propose to use *energy throughput* as the independent variable in the decline of the state of health.

With battery test conditions known, we can relate cycles to energy throughput. In the following, the SoC will be referred to as χ, while the SoH metric is referred to as ξ. Indicating with c_0 and V_{nom} battery original capacity and nominal voltage respectively, the energy throughput at each complete cycle (for the same temperature and current adopted in the characterization phase) is:

$$\Delta E = 2V_{nom}c_0\xi \tag{3.21}$$

The term $c_0\ \xi$ represents the actual full capacity (expressed in [Ah]) and the term $V_{nom}\ c_0\ \xi$ is accounted for two times since we have to consider both charge and discharge. The cumulative energy throughput for n cycles is expressed as:

$$\Delta E_{TOT}(n) = \sum_{i=1}^{n} 2V_{nom}\, c_0\, \xi(i) \tag{3.22}$$

Moving from the number of cycles to the energy throughput, we are able to evaluate the impact on state of health of an arbitrary amount of energy transformed by the cell. We explicitly note that, in doing so, the ability to identify a single cycle is lost: in fact, the relation expressed in Equations (3.21)-(3.22) is one-way, and originates by the knowledge of the detailed conditions the original data were obtained in. Even though the notion of *cycle* is lost, for our purposes of considering the degradation of a battery, the only relevant information is the amount of energy throughput: the electrochemical reactions that determine the capacity decay depend on the amount of energy converted in the cell, independently of being caused by a discharge or charge phase.

Once the degradation is expressed as a function of energy throughput, in the implementation of the model for a system-level representation we obtain simpler decay curves by computing a piecewise linear approximation of the decay curve as a function of the energy throughput. Thus, a decay coefficient may be obtained for each section. The number of sections considered for each curve is three. In our case, such characterization is carried out on three curves with different DoD: specifically, the values considered for the DoD are 55%, 75% and 85%. Since the DoD is the opposite of the SoC, the procedure just described allows us to have a decay coefficient for each couple (χ, ξ): in fact, each curve gives us three coefficients, one for each interval of values of the SoH; in addition, for each SoH interval, we have the coefficient referred to three different DoD, thus SoC, conditions (see Figure 3.10).

Given a specified amount of energy ΔE provided to, or extracted from, the battery, the variation in SoH for the k-th battery is expressed as:

$$\Delta\xi_k(\xi_k, \chi_k, T_k, i_k) = w(T_k, i_k)\, \alpha(\chi_k, \xi_k)\, \Delta E_k \tag{3.23}$$

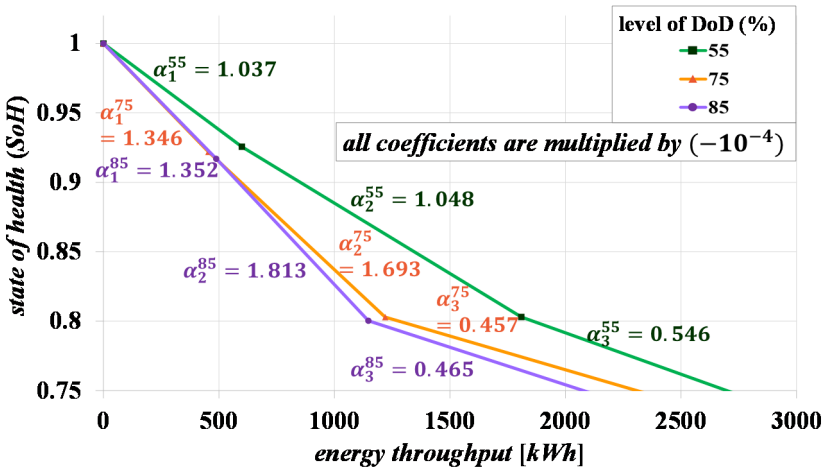

Figure 3.10 – Piecewise approximation of SoH and decay coefficients for a single cell

The different coefficients have been organized as a look-up table, accessed with the function $\alpha(\chi, \xi)$. The curves from which the coefficients have been extracted were measured under specific testing conditions: the ambient temperature T was maintained constant at 25° C and the discharge of the batteries was performed at a fixed current rate I_n of 4 A. Therefore, in Equation (3.23), we included the function $w(T, i)$, which acts as a weight and takes into account the effect on battery SoH of the variations of temperature and current with respect to the testing conditions the experimental curves were obtained in.

The weighting function is reported in Equation (3.24)

$$w(T_k, i_k) = \gamma_T (T_k - 25)^2 + \gamma_C \left(\frac{i_k}{I_n} \right)^{0.05} \tag{3.24}$$

where γ_T and γ_C are coefficients to adjust the impact on the SoH of the temperature and current weighting terms. The current term is modeled similarly to the expression of Peukert's law, so that a higher current will have a bigger impact, with a current equal to I_n weighting as 1.

3.5 Experimental results

In this paragraph are reported and commented the experimental results for the SoH estimation and equivalent circuit parameter estimation measurement techniques introduced in paragraph 3.4.

3.5.1 Parameter estimation

The simulations tests have been carried out considering the cell represented by the equivalent circuit model, with characteristic parameters value deducted by existent works in literature. Two different cases are considered, with both a Ni-MH and Li-ion battery examined. MATLAB and Simulink programming platforms are used for the simulations. The current stimulus is composed of a sum of sine waveform at different frequencies and phases, so to excite all the frequencies of interest in the spectrum of the battery impedance transfer function. In Figures 3.11-3.12 is reported an example of proposed technique for Ni-MH case.

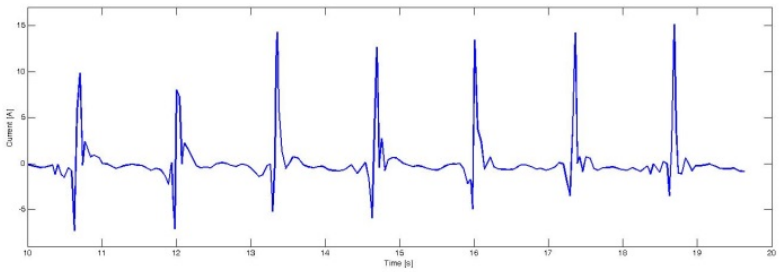

Figure 3.11 – Current stimulus

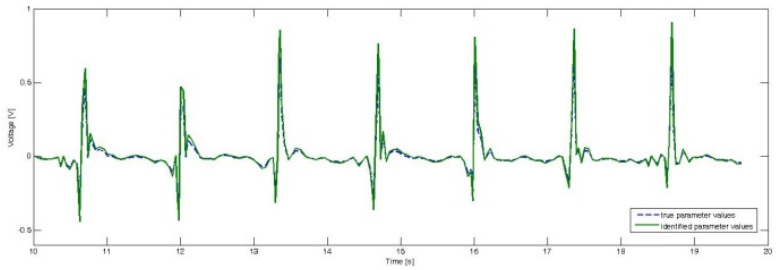

Figure 3.12 – Voltage response with real and identified parameter values

The identification method has been tested against measurement noise: white noise has been added both on the stimulus and on the output of the battery model, to simulate measurement errors on both acquired channels.

3.5.1.1 Tests for Ni-MH batteries

Simulations have been conducted on the model of Ni-MH battery using the following as value of characteristic parameters: Rs= 1 mΩ, Rp= 0.6378 Ω, C= 43.68 F. In Tables 3.3-3.4 are reported the results for noise amplitude up to 5%. The white noise has been added to each sample with amplitude calculated as a percentage (up to 5%) of the corresponding sample value. As evidenced by the numerical results, starting with the same battery model, an identification realized through an OE model is more effective than with the ARX model. This behavior, however, is to be expected given the different nature (iterative compared to closed-form) of the optimization method. The identification using the ARX model is, on the other hand, much faster and therefore suitable for implementation on microcontroller.

Moreover, for low noise figures, the results are comparable with the ones provided by OE method.

Table 3.3 – Simulation results for Ni-MH battery with OE system model

OUTPUT ERROR MODEL						
Parameter\Noise	**0 %**	**0.2%**	**0.5%**	**1%**	**2%**	**5%**
Rs [mΩ]	1.000	1.000	0.999	0.999	0.999	0.997
Rs_error [%]	*6.8e-4*	*0.025*	*-0.099*	*-0.043*	*-0.072*	*-0.26*
Rp [Ω]	0.648	0.638	0.637	0.637	0.637	0.638
Rp_error [%]	*-1.1e-6*	*-0.003*	*-0.014*	*-0.032*	*-0.077*	*0.039*
C [F]	43.68	43.67	43.67	43.68	43.67	43.66
C_error [%]	*2.1e-6*	*-0.006*	*-0.023*	*0.019*	*-0.026*	*-0.033*

Table 3.4 – Simulation results for Ni-MH battery with ARX system model

ARX MODEL						
Parameter\Noise	**0 %**	**0.2%**	**0.5%**	**1%**	**2%**	**5%**
Rs [mΩ]	1.000	0.999	0.998	0.999	0.981	0.883
Rs_error [%]	*6.8e-4*	*-0.030*	*-0.23*	*-0.089*	*-1.9*	*-12*
Rp [Ω]	0.638	0.631	0.595	0.498	0.301	0.084
Rp_error [%]	*-1.1e-6*	*-1.1*	*-6.7*	*-22*	*-53*	*-87*
C [F]	43.68	43.67	43.64	43.50	43.22	40.93
C_error [%]	*2.1e-6*	*-0.009*	*-0.089*	*-0.40*	*-1.03*	*-6.3*

3.5.1.2 Tests for Li-ion batteries

Simulation tests have been conducted on the model of Li-ion battery using the following as value of characteristic parameters: Rs= 24.22 mΩ, Rp= 7.36 mΩ, C= 458.1 F. In Tables 3.5-3.6 are reported the results for noise amplitude up to 5%. As it can be seen, the results are characterized by a much greater error than in the previous case, for both the OE and ARX identification method. It is to be noted that the identification method was tuned on Ni-MH batteries: therefore the results emphasize the differences that exists between different battery technologies and underline the importance of particularizing an online identification method on the specific technology.

Table 3.5 – Simulation results for Li-ion battery with OE system model

OUTPUT ERROR MODEL						
Parameter\Noise	**0 %**	**0.2%**	**0.5%**	**1%**	**2%**	**5%**
Rs [mΩ]	24.220	24.221	24.217	16.631	13.776	10.064
Rs_error [%]	*2e-7*	*0.007*	*-0.011*	*-31*	*-43*	*-58*
Rp [mΩ]	7.359	7.358	7.363	7.691	1.054	1.423
Rp_error [%]	*-7e-7*	*-0.032*	*0.041*	*4.5*	*43*	*93*
C [F]	458.10	458.47	457.77	0.022	0.021	0.028
C_error [%]	*1.5e-6*	*0.081*	*-0.071*	*-99*	*-99*	*-99*

Table 3.6 – Simulation results for Li-ion battery with ARX system model

ARX MODEL						
Parameter\Noise	**0 %**	**0.2%**	**0.5%**	**1%**	**2%**	**5%**
Rs [mΩ]	24.220	24.180	23.986	23.275	20.840	12.518
Rs_error [%]	*2e-7*	*-0.16*	*-0.96*	*-3.9*	*-14*	*-48*
Rp [mΩ]	7.360	0.359	0.380	1.063	3.492	11.777
Rp_error [%]	*-7e-7*	*-95*	*-95*	*-85*	*-52*	*60*
C [F]	458.10	281.89	47.237	4.678	0.482	0.0774
C_error [%]	*1.4e-6*	*-38*	*-89*	*-98*	*-99.*	*-99*

3.5.1.3 Execution times for microcontroller implementation

The parameter identification algorithm was implemented on ARM microcontroller. In particular the ARX system model was considered,

Table 3.7 – Execution time of algorithm on different microcontrollers and different number of samples

Exec time (ms)	64 samples	128 samples	256 samples
ARM – M3	18.76	36.36	63.57
ARM – M4	5.5	10.3	18.98

given its being less resource hungry. The execution time of the ARX model is reported in the following. The calculation of the unknown parameters, with least squares method, depends directly on the multiplication of pseudo-inverse of a matrix by the output vector. The matrix was composed using samples from input and output signals. To evaluate the execution time, the authors took the data from the Matlab Simulink model and considered the implementation on the microcontroller only related to its calculation capabilities.

With this data the matrix was created and after some steps a pseudo-inverse was calculated. Two different sets of data was considered, 64 and 128 samples. The Table 3.7 reports the execution time for two different microcontrollers. The data are for ARM Cortex M3 (STM32F103RB) and ARM Cortex M4 (STM32F407VG) microcontroller with a CPU system clock of 8 MHz.

The microcontrollers are low cost, embeddable on the battery, and have sufficient processing power to execute the tasks at hand. Indeed, the results are very good in spite of the both microcontrollers not running at the maximum system clock frequency.

3.5.2 State of Health estimation

Tests have been conducted considering the battery data in [3.45]. The measurements are referred to Tenergy 18650 2200mAh Li-ion batteries. They have been continuously charged and discharged until the capacity has dropped by 20% or 30% depending on the specific battery lot. The discharge took place at different current rates for the different battery lots, while the charge followed a constant current/constant voltage pattern (1.5 A CC – 4.2 V CV until current dropped to 20 mA). The charge and discharge cycles were executed using a bipolar power supply under known operational and

environmental conditions. Working with resampled data, the capacity values are assumed to be sampled every cycle. The batteries considered in the results presented here are the B29-B36 and B49-B56. In particular the batteries have been operated at different temperatures, discharge currents and depths of discharge so to take into account experimental results in all the operational and environmental conditions.

3.5.2.1 Experimental results for fuzzy logic based state of health estimation

First of all there is the need to evaluate the exponential fit, and verify that it can be representative for battery of the same family subjected to the same operational conditions. To this aim, batteries B49-B51 have been considered: they represent Li-ion batteries belonging to the same family and have been tested under the same conditions regarding temperature, current and discharge cycle. To determine a fit representative of the family, the capacity decay curve of each of them has been considered as reference, comparing the resulting fit with the real data from the other two batteries: the tests have shown similar errors for whatever of the three batteries acted as a reference. The results shown in the following regard the curves obtained with B51 as reference battery.

In Figure 3.13 the fitting curve is compared to the real battery data: as it can be seen, it allows to monitor the decay in battery capacity, and therefore health. The error tends to increase when the slope of the acquired data decreases: however it must be noted that such occurrence happens well after the threshold of 80% of original capacity, after which a battery is considered beyond its useful life.

Figure 3.14 shows the error, in percentages, in the cases of the curves for batteries B49, B50 and B51. As it can be seen, the error, expressed in percentage over the normalized experimental data, is contained below 10%. This is a measure of how well is possible to apply the fitting extracted from a battery to batteries of the same lot.

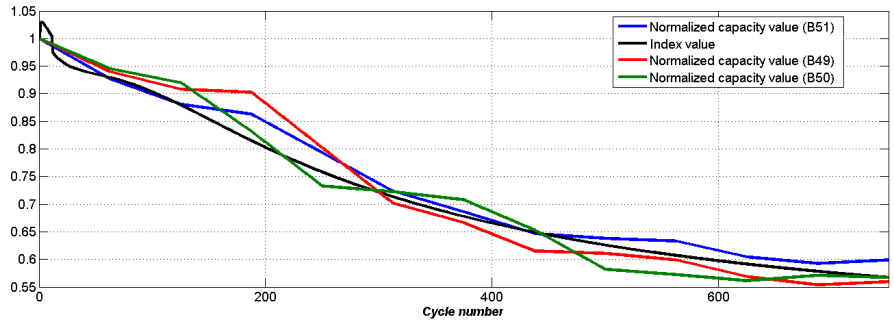

Figure 3.13 – Fitting curve compared to experimental data

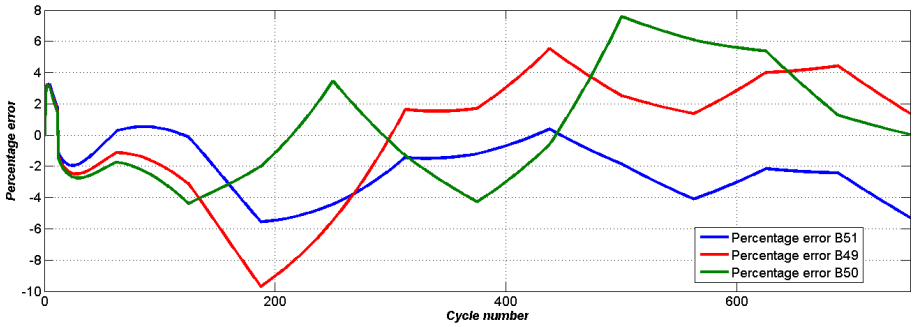

Figure 3.14 – Percentage error relative to experimental data

Once a fitting function for the family of batteries has been determined in standard testing conditions, the system is tested against variation of operational and environmental variables relying on fuzzy logic. For the fuzzy logic algorithm, a Mamdani-type inference method was used. The implemented rules are reported in Tables 3.8-3.13. As for the defuzzification, a *centroid* technique was applied.

Considering batteries belonging to the same temperature and current lot, but cycled with different DoD, the implemented fuzzy algorithm has been tested and compared to experimental data. From the literature [3.44] it is expected for the battery to deteriorate earlier if the DoD is increased. Therefore, an index representing the health of a battery should decrease faster in case of excessive DoD. At the same time, shallow cycles have the effect of prolonging battery life. Such expectation is met in the results provided by the proposed system.

Table 3.8 – Rules table of β_D for the temperature block

Temp.	$\beta_D(k-1)$ L	ML	M	MH	H
L	ML	M	MH	H	H
M	L	ML	M	MH	MH
H	ML	M	MH	H	H

Table 3.9 – Rules table of a_D for the temperature block

Temp.	$a_D(k-1)$ L	M	H
L	L	M	M
M	L	M	H
H	L	M	M

Table 3.10 – Rules table of β_D for the current block

Current	$\beta_D(k-1)$ L	ML	M	MH	H
L	L	L	ML	M	MH
M	L	ML	M	MH	H
H	ML	M	MH	H	H

Table 3.11 – Rules table of a_D for the current block

Current	$a_D(k-1)$ L	M	H
L	M	M	H
M	L	M	M
H	L	L	M

Table 3.12 – Rules table of β_D for the DoD block

DoD	$\beta_D(k-1)$ L	ML	M	MH	H
L	L	L	ML	M	MH
ML	L	L	M	MH	H
M	L	ML	M	MH	H
MH	ML	ML	M	H	H
H	ML	M	MH	H	H

Table 3.13 – Rules table of a_D for the DoD block

DoD	$a_D(k-1)$ L	M	H
L	M	H	H
ML	M	M	H
M	L	M	M
MH	L	M	M
H	L	L	M

As it can be seen from Figures 3.15-3.16, the fuzzy algorithm succeeds in determining index values that are compatible with the normalized capacity value determined with experimental measurements. Figure 3.16 evidences that the percentage error against true value is contained under 5%. Considering the high variability of the results determined by the operational conditions, and the qualitative nature of the SoH metric, the fuzzy algorithm manages in providing good performances, suitable for battery monitoring in grid applications.

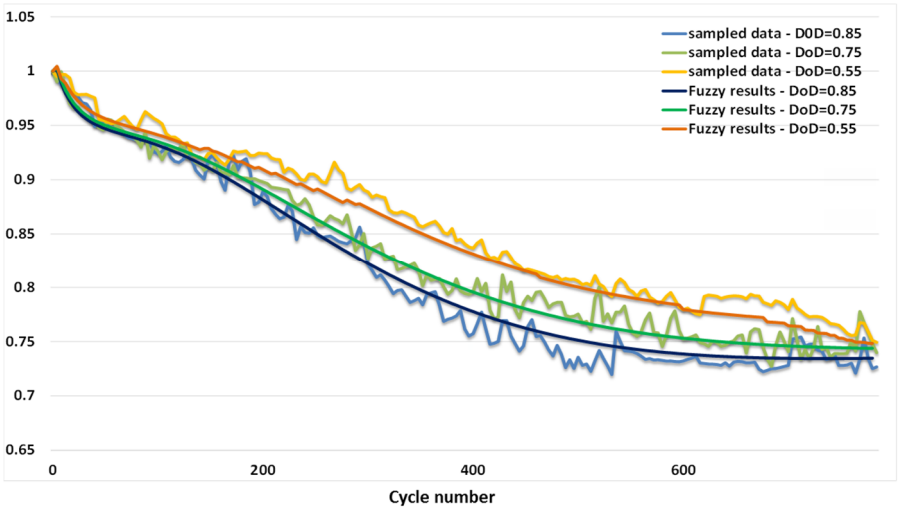

Figure 3.15 – Results of fuzzy logic algorithm compared to sampled data

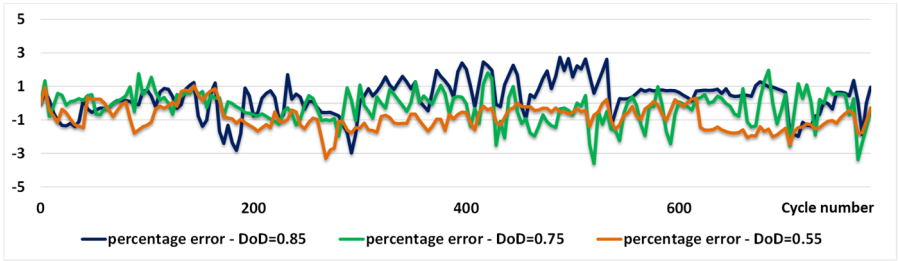

Figure 3.16 – Percentage error in results of fuzzy logic algorithm compared to sampled data

3.5.2.2 Experimental results for neural network based state of health estimation

Network training has been carried out using the experimental data in [3.45]: the availability of capacity curves for various currents, DoD and temperatures guarantees for the training set to be significant. Measurements of decay of battery capacity are extremely time consuming, requiring multiple years of tests. Therefore, to train the network, all the available capacity decay curves, for all the three DoD,

current and temperature values have been used: the training set constitutes a randomly extracted subset (70% of the available samples) of each of the curves.

The network requires temperature, DoD, current, cycle number and the output at the previous step as inputs. At the first step the previous input is assumed to be 1. The training has been conducted for networks with different numbers of neurons in the hidden layer; best results have been obtained with a 12-neurons layer architecture, which is the one used in the following tests.

A first test (see Figures 3.17-3.18) has concerned the use of the network for the same values of DoD characteristic of the sample data. This shows that the implemented network has good performance in fitting the correspondent experimental data: providing the network with a synthetic vector of parameters, which include DoD, temperature and

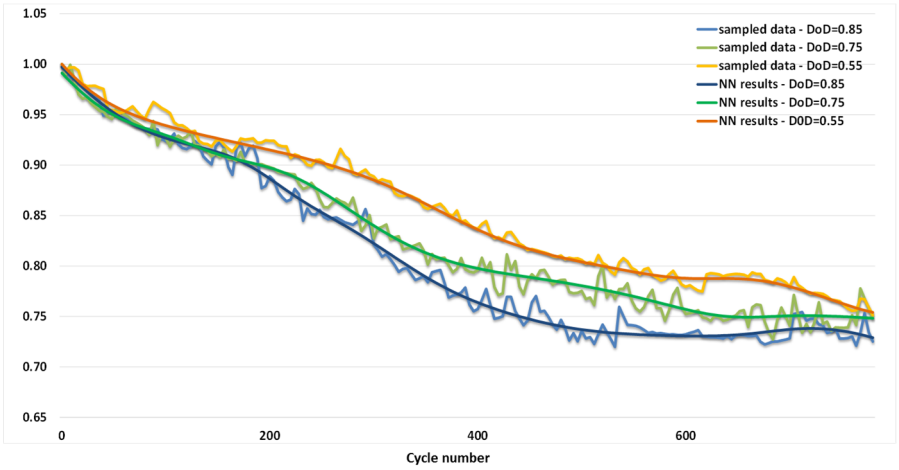

Figure 3.17 – Results provided by the neural network compared to sampled data

Figure 3.18 – Percentage error in results provided by neural network compared to sampled data

current, it is capable of approximating the true capacity values. In this case it must also be noted that the percentage error is relatively small: it is in fact less than 5%, therefore compatible with the results obtained with the fuzzy algorithm.

Different tests have been performed to verify the ability of the neural network to generalize the results. Since the network has been trained with a subset of experimental data with characteristic DoD of 0.55, 0.75 and 0.85, it has been tested the capability of handling estimations in case of different values of DoD, with fixed current and temperature.

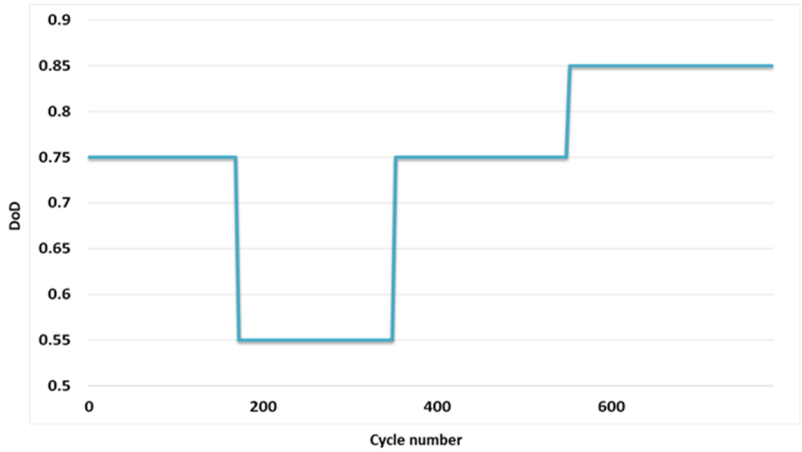

Figure 3.19 – Variable-DoD emulated curve

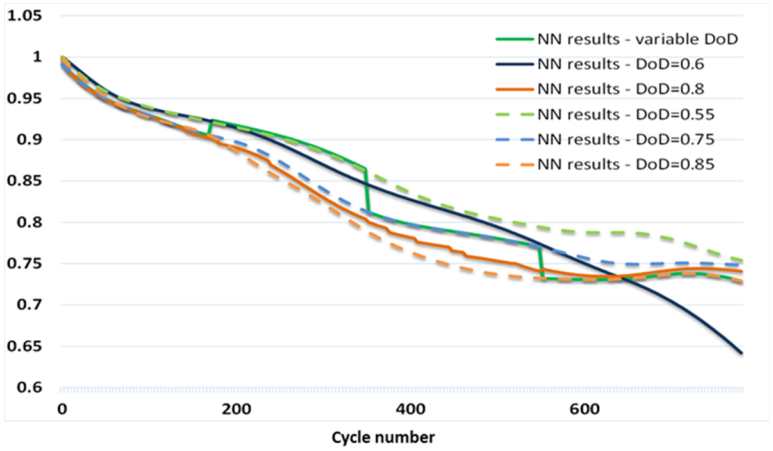

Figure 3.20 – Neural network results for different values of DoD

First of all, a curve with DoD variable among the values used during training has been emulated (Figure 3.19). The network managed to follow the variations of the input parameter. Moreover curves with fixed DoD, but different from the values used during the training phase, have been emulated and provided as input to the network. In this case, there is no experimental data available to confirm or reject as inadequate the performances of the system. However, since (as shown in Figure 3.17) the neural network provides a correct fitting of the experimental data, the curves determined at DoD equal to 0.55, 0.75 and 0.85 have been used as boundaries It is expected from theory that a decay curve with DoD of 0.6 exhibits, for the same cycle number, a capacity lower that the one for DoD equal to 0.55, but higher than the one for DoD equal to 0.75: since the computed index corresponds to the normalized capacity value, the index curve should be bounded among these curves. The same happens for the curve at DoD of 0.8, bounded by the curve at DoD values of 0.75 and 0.85. As shown in Figure 3.20, the neural network successfully manages to generalize the results, with experimental results are in complete accordance with the theory. In the case with DoD equal to 0.6, results provided by the network tend to be not contained between the bounding curves for high cycle numbers. However, such occurrence does not hinder the performances of the system, since happens for values of the index, and therefore battery capacity, corresponding to a battery already beyond its useful life. Similar results are obtained for temperature variations.

3.6 Conclusions

In this Chapter, we presented measurement techniques and models for estimation of battery degradation.

Once introduced the state of health metric, we proposed two techniques for its estimation. The first one used an exponential fitting for the capacity decay, and adopts a fuzzy logic algorithm to take into account variations in all environmental and operational factors that have an influence on battery degradation. The second technique resorts to a neural network to estimate the battery state of health. Tests conducted on experimental data show that both system exhibit good performances,

with errors contained under 5% of the correspondent experimental values for values of capacity of interest for grid applications. Larger errors are possible, but beyond the point a battery is considered at the end of its life. The results are encouraging and adequate for application to battery health monitoring in grid storage systems.

In addition, a technique to estimate the values of the parameters of the equivalent-circuit battery model has been described. The value of the parameters influences not only the electrical behavior, but can also be used to estimate battery health. The proposed technique adopts a perturbative characterization for parameters estimation. Analyzing the response of the battery to a current stimulus with two different system models – OE and ARX – the value of the parameters is obtained. Making use of a multisine stimulus, the proposed method is significantly faster than offline method such as EIS: even though not being as precise, the proposed technique is suitable for online monitoring purposes. Simulation results show errors less that 10% if optimized for the specific battery technology, with OE model performing better than ARX one. Being not resource hungry, the method can be implemented on a microcontroller embeddable in the battery.

Taking into account battery degradation while allocating the provision of grid services among the batteries requires a system-level battery degradation model. Therefore, in this Chapter a model that relates battery energy throughput to capacity decay, taking into account also the impact of depth of discharge, temperature and discharge current, was proposed.

Chapter 4

Battery Vehicles as Distributed Energy Resource: battery management in Vehicle-to-Grid based aggregations

In recent years, Battery Vehicles (BVs) have been the object of consistent research and business efforts. Technology improvements have led the cost for a BV to drop and the all-electric range of vehicles to increase: BVs now represent a viable alternative mean of transportation, offering to customers the opportunity to operate a vehicle with lower fuel costs and lower environmental impact. Costs of BVs are expected to decline by nearly 50% by the end of this decade and, combined with incentives provided by some U.S. state governments, the number of battery vehicles on the roads is destined to raise: market projections account BVs for a share of the car sales market comprised between 5% and 13% by 2020. As an example, California has a goal of having 1.5 million battery vehicles on its roads by 2025 [4.1-4.2].

While their diffusion may represent an additional, if not unbearable, burden for the power grid, if properly managed the electric vehicles may represent a resource to support the power grid. In fact, their batteries can be used as grid storage when the vehicles are parked and connected to the grid: this is the core idea behind the Vehicle-to-Grid (V2G) framework.

In this Chapter, a management strategy for aggregation of BVs is presented. Making use of the measurement techniques and the models described in Chapter 3, we consider the allocation of vehicles in the provision of services to the grid taking into account not only the state of charge (that represents the energy stored into each battery) but also the health of the batteries involved. In this way, is possible to prolong battery life, without altering the level of service to the grid the vehicles provide.

4.1 Battery Vehicles (BVs)

Economic and environmental reasons have led to identify in BVs a sustainable means of transportation: in fact, whether relying on clean energy sources, BVs bring overall improvements in terms of greenhouse gases and air pollutant emissions over Internal Combustion Engine Vehicles (ICEVs) [4.3-4.4].

With the name *BVs* are generally addressed different kind of vehicles: Hybrid Electric Vehicles (HEVs), Plug-in Hybrid Electric Vehicles (PHEVs) and All Electric Vehicles (AEVs). As stated before, battery cycle life depends also on the typical charge/discharge pattern a battery is subject to. The usage pattern for a battery in a BV is strongly dependent on the architecture of the vehicle. Therefore in the following paragraphs an introduction to the different types of electric vehicles is given.

Here we will focus on the last two categories, which are pluggable into the power grid and therefore of interest in the V2G context.

4.1.1 Hybrid Electric Vehicles (HEVs)

HEVs are vehicles that, in addition to the internal combustion engine (ICE), are provided also with an electrical motor and the related Energy Storage System (ESS), either super-capacitor or battery based. In the following the ESS will be assumed to be battery-based. In HEVs the ICE may be used in series with a generator to provide electricity to the electric motor, or in parallel to the motor, or in a hybrid configuration (see Figure 4.1). In any case, the battery cannot be charged from the grid, but using Electric Range Extenders (EREs) or the ICE itself. Independently of the configuration adopted, typically the onboard battery is small and used only as a support to the fuel-powered ICE. As a consequence the ESS should feature a battery capable of a high power output, whereas the energy capacity is not a so critical aspect [4.3], [4.5].

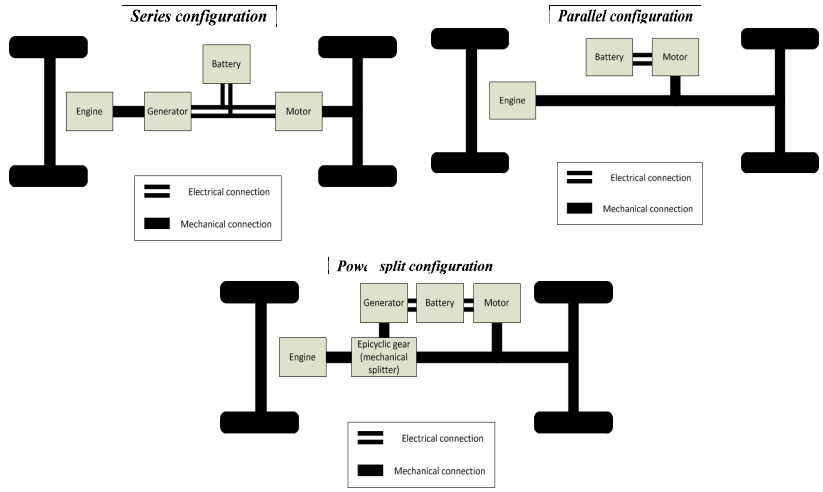

Figure 4.1 – Different propulsion system configurations for a HEV

4.1.2 All Electric Vehicles (AEVs)

In the AEVs the combustion engine is totally absent: the only propulsion system is the electrical motor and the only energy source is the battery (see Figure 4.2). More than the peak power, with AEVs it is important the amount of energy the storage system can hold, since it directly translates into driving range. Different choices can be made in

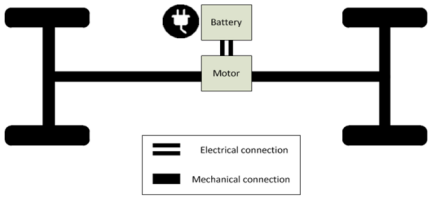

Figure 4.2 – AEV propulsion system configuration

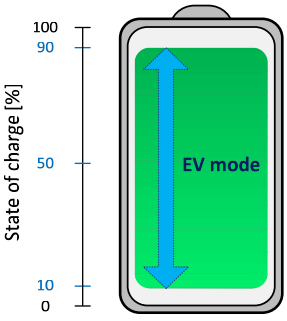

All Electric Vehicle

Figure 4.3 – Typical battery usage in All Electric Vehicles

the way the battery is managed. Generally, to prevent accelerated battery aging, the state of charge is kept between 90% and 10% of the total capacity. The operational mode then consist simply in a sequence of full charge/full depletion [4.3], [4.5]. The situation is depicted in Figure 4.3.

4.1.3 Plug-in Hybrid Electric Vehicles (PHEVs)

PHEVs are basically HEVs with the possibility of being directly connected to the power grid: other than only through the engine or using the energy recovered with EREs (as in HEVs), the battery can thus be charged also relying on the grid. This opens to a whole lot of different ways of using a vehicle: it can be run using the energy in the battery, waiting until it depletes to a predefined level before turning on the combustion engine (charge depletion mode); it can be run relying primarily on fuel, with the motor used only as a support (charge sustain mode); it can be run using only the electrical energy (all electrical mode) [4.3], [4.5]. This plethora of usage modes determines different operational modes for the battery, as represented in Figure 4.4. It is important to point out that is not possible to define a "typical discharging/charging path", since it depends on the operational mode, on the driving style of the owner, on electricity market related considerations, on the availability of fuel. Moreover a pattern may change from day to day.

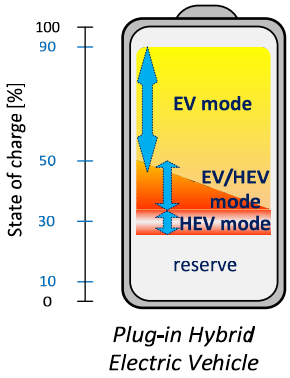

Figure 4.4 – Typical battery usage in Plug-in Hybrid Electric Vehicles

4.2 The Vehicle-to-Grid (V2G) framework

4.2.1 Basic idea

The BVs represent an additional load for the power grid, with their charge capable of having a significant impact on the distribution grid.

Thus, proper measures regarding vehicles and grid integration must be undertaken [4.1]. The first step in this regard are the so-called *smart charging* strategies: the BVs are to be charged during off-peak times, achieving two different types of advantages. The first and obvious one is that they would not contribute to raising the demand peak. However, their charge during off-peak periods leads to easier planning and better utilization of generation resources: in fact, BVs would give an important contribution especially in conditions when low demand would require to turn off some generation devices, with incurring high costs. In addition, smart charging can also lead to better utilization or renewable sources.

The vehicles would be used mainly for commuting, therefore spending most of the daily time connected to the grid and in an idle state: the vehicles have to be charged, but even so is reasonable to think that recharge would take only a portion of the time spent connected to the power grid. The availability of such a storage resource connected to the grid and underutilized has then sparked the idea of using it as energy resource, therefore not anymore only as passive devices but as active ones. Vehicles can be used to lower consumptions of a building and work as emergency power in case of outages: this represent the simplest integration scheme, which goes under the name of Vehicle-to-Building (V2B). Its extension is represented by the usage of BVs to provide services to the power grid: they can act as buffer for renewable sources, as emergency resource in case of outages, or provide the power grid with ancillary services, such as frequency up/down regulation. This concept goes under the name of Vehicle-to-Grid (V2G) [4.6-4.10]. In 2013, the project eV2g by University of Delaware and NRG energy proved the feasibility of the concept, with the first instance of EVs in a test fleet successfully bidding into the PJM regulation market [4.11-4.12]. Obviously, the provision of such services from BVs has not to hinder their primary functionality as vehicles.

4.2.2 The role of the aggregator and services provided to the grid

Any practical implementation of a V2G framework depends heavily on the effective functioning of an aggregator. In fact, the contribution

that the energy stored in each BV can provide to the grid is negligible in itself. Therefore, to be able to affect the power grid, the vehicles need to be grouped in sizable aggregations - from thousands to hundreds of thousands- that act as single entities, both as loads and as generation/storage devices.

Acting as a load, the aggregation of BVs represents the total capacity of the batteries: its significant size allows it to benefit from the buying power typical of a large commercial/industrial customer. The aggregator can then negotiate better prices and make purchases of energy, batteries or other services at rates lower than the ones accessible by the individual BV owner [4.6].

In the same manner, acting as a relevant-size Distributed Energy Resource (DER), the aggregation can supply both capacity and energy services to the power grid. The storage onboard the BVs may be of great use in fully exploiting renewable sources. One such service that these vehicles can provide is regulation. It is used to balance variations in load by correcting for short-term changes in electricity use that might affect the stability of the power system. Regulation helps match generation and load and adjusts generation output to maintain the desired frequency.

The aggregation of vehicles can provide both up and down regulation services, which are paid for the capacity it offers, independently of the actual provision of the energy service: in case the vehicles also provide energy to the grid, they receive additional payment. Also in this case the higher negotiating power empowers it to strike better deals, with some of the savings passed on to vehicles' owners.

The batteries employed in the BVs are particularly suited for provision of regulation services, given their fast response times. On the other hand, sizable aggregation may also provide energy to the grid. However, we must point out that they cannot be considered as an energy source to be stably integrated into the power grid. The whole concept of V2G revolves around the idea of find a use for BVs during their idle state without hindering their functionality as vehicles: constantly using them to provide relevant amounts of energy would resort in each battery being frequently utilized at around its full capacity, with limiting

consequences on both battery life and remaining state of charge at the end of the provision of services.

4.3 Our proposal: consideration of battery health in the V2G management scheme

4.3.1 Aggregator as owner of the batteries

As seen in paragraph 4.2.2, the aggregator is crucial to the realization of a V2G framework, acting as the interface between vehicles and the grid operator and representing a single entity, able to have an impact both on the power grid and on the market.

The aggregator is also in charge of selecting the BVs that need to provide energy to the grid, or that can be charged during each time interval: for our purposes, the considered minimal time interval is 5 minutes long. This choice allows a prompt response of the aggregation to requests to raise/lower capacity the DER provides to the grid, while at the same time allowing for better distributing the burden of providing services to the grid among the largest part of vehicles in the aggregation.

The business model we assume for the aggregator is as owner of the batteries. It is responsible for their acquisition and maintenance, and rents them out to the BV owners, applying discounted rates should they choose to participate in the provision of V2G services. Being in charge of allocating the provision of services among the vehicles of the aggregation, a management strategy that allows prolonging the maximization of the lifetime of the batteries, thus maximizing the value if its assets, is of interest for the aggregator.

4.3.2 Assumptions and requirements

In the following, we will focus on BVs used for daily commuting purposes. Recent studies have shown that the average commuting time is around 52 minutes, thus the vehicles are in idle state for around 22 hours per day. Our framework is based on the assumption that a commuting vehicle, once reached the destination, is connected to the grid [4.6]. We assume that the vehicles are parked into parking lots

during the day, when the aggregated fleet of vehicles provides ancillary services to the grid, and at home during the night. In particular, considering the average commuter reaching his workplace and leaving his vehicle in a parking lot during office hours, the period for the provision of services to the grid spans from the from 8am to 6pm. Since the fleet related to the same aggregator can be in non-contiguous parking lots, we assume each vehicle is univocally identified through SIM card technology tied to the individual battery.

Each vehicle embeds a metering device that can measure the SoC and compute the battery SoH, adopting the fuzzy algorithm described in Chapter 3. Therefore, upon connection to the charging station placed in the parking lot or at home, the vehicle identifies itself and communicates its SoC and SoH to the aggregator. In addition, some other relevant information is shared upon connection: this may be technology related, such as battery characteristics and safety range for the SoC to preserve battery life, or related to operational conditions, such as ambient temperature, or user-defined, such as desired time of departure and required SoC for that time.

4.3.3 Management scheme

The method we propose adopts a fundamental principle: since the decay of a battery capacity (and thus, of SoH) is higher, for the same energy throughput, when the battery already exhibits a low SoH, then prioritizing the vehicles whose battery has high SoH minimizes the total capacity, and therefore total lifetime, losses. To avoid an unequal exploitation of only the vehicles with healthier batteries and not to have too deep cycles, for every time interval a vehicle cannot be discharged more than once unless all the vehicles have been discharged at least one time, or no other vehicle can support grid services in that time interval. Figure 4.5 shows the block diagram relative to the proposed management strategy.

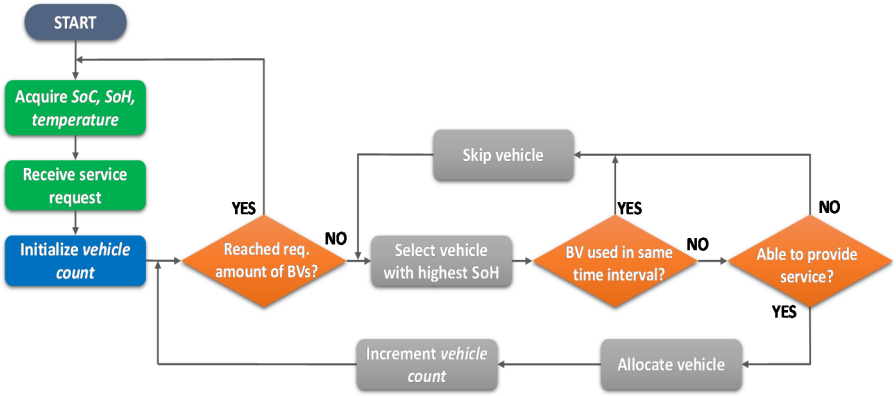

Figure 4.5 – Block diagram of the implemented strategy

4.4 V2G strategy evaluation: case study

4.4.1 Specifications of the system

In our simulations to test the strategy, we considered the battery of the vehicle composed of 600 Tenergy 18650 cells, arranged in 10 stripes of 60 cells. The battery parameters are obtaining by scaling the parameters of the single cell. The nominal voltage V_{nom}^{batt} is obtained multiplying the nominal voltage of the single cell for the number of cell in series that compose the battery. As for the battery nominal capacity c_0^{batt}, we obtain it multiplying the maximum energy storable into each cell for the total number of cells, and then dividing by the battery voltage.

The current in/out the battery during the provision of V2G services is considered having a fixed value of 10 A. Given that the length of each time interval (as previously stated, we consider 5-minutes long time intervals) and the nominal battery voltage are fixed, the amount of energy transferred in/out of each vehicle selected for the grid support services each time interval is a pre-determined constant value.

In designing the simulations, whose results are presented in in the paragraph 4.4.3, two randomly generated arrays containing SoC and

SoH of the vehicles of the managed fleet are considered as inputs for the management system, together with the ambient temperature. Without loss of generality, we assume that at the end of the 120 time intervals (twelve 5-min long time intervals for each of the ten hours from 8am to 6pm) the vehicles that provide services to the grid are recharged of the same amount of energy they were discharged. In this way, each vehicle at 6pm will have the same amount of energy it used to have upon connection to the grid.

An additional input is represented by the raise/lower capacity signal. Positive values represent the request to increase the capacity, therefore represent request for energy to be provided from the vehicles to the grid; negative values represent requests to lower capacity, therefore constitute energy flows used to charge back the vehicles instead. In the simulations the energy profile was obtained considering a zero-average arbitrary profile, scaled by the minimum number of vehicles to be involved in service provision each time interval (referred to as *base unit*). To avoid the chance of experiencing systematic effects, the array containing the energy request samples is randomly ordered at every run of the simulation. Figure 4.6 shows one energy profile referred to the case of a number N of vehicles equal to 11520, with a base unit of $N/40$ vehicles.

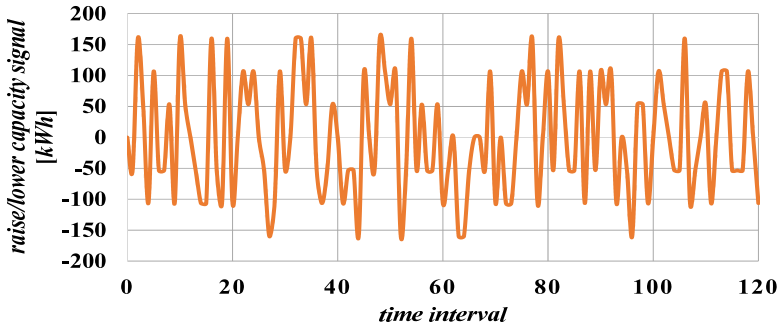

Figure 4.6 – Example of energy profile considered as input for the management system

4.4.2 Test configurations

We conducted simulations for two different cases. The first case is represented by the proposed strategy that assumes both the state of charge and state of health as state variables.

For the second case, a strategy where only the SoC is considered as relevant parameter in the management is examined. The allocation of vehicles depends on their order of arrival (from the implementation point of view, we consider that the array containing the SoC of the vehicles is populated according to their order of arrival) according to the principle *first arrived-first served*. For each vehicle selected, the SoC is compared with the energy request (towards or from the grid): only in case it is able to satisfy the request, the vehicle is actively allocated in provision of the service. We used this SoC based strategy as reference, against which compare the performance of our strategy.

The implemented strategies are simulated using MATLAB. The tests have been executed for different number of vehicles and for different base units. In addition, we generated the random SoC and SoH samples for the input vector using both a Gaussian distribution and a uniform one. Specifically, the Gaussian distribution considered for the SoH is centered at 0.9, with standard deviation equal to 0.033, so that the 99.7% of values still don't exceed 1 or be lower than 0.8; as for the uniform distribution, 0.8 and 1 have been considered as minimum and maximum values respectively.
As for the number of the vehicles considered in the simulations, and the relative base unit, different configuration have been tested and are reported in Table 4.1.

Table 4.1 – Specifications of the simulated configurations

Name	*Configuration*		
	number of vehicles (N)	***base unit***	**distribution**
28800-80g	N= 28800	N/80	Gaussian
28800-80u	N= 28800	N/80	Uniform
19200-80g	N= 19200	N/80	Gaussian
19200-80u	N= 19200	N/80	Uniform
19200-40g	N= 19200	N/40	Gaussian
19200-40u	N= 19200	N/40	Uniform
11520-80g	N= 11520	N/80	Gaussian
11520-80u	N= 11520	N/80	Uniform
11520-40g	N= 11520	N/40	Gaussian
11520-40u	N= 11520	N/40	Uniform
960-80g	N= 960	N/80	Gaussian
960-80u	N= 960	N/80	Uniform
480-80g	N= 480	N/80	Gaussian
480-80u	N= 480	N/80	Uniform

4.4.3 Test results

Figure 4.7 gives a picture of the impact on the SoH of the V2G-related continuous charge and discharge during 120 time intervals, which correspond to 10 hours of provision of services to the grid in response to a signal as the one showed in Figure 4.6. In particular, the results are obtained with the proposed management strategy, in the *11520-40g* configuration. As to be expected, the decrease in SoH is of limited value, given the relatively small energy throughput each battery sustains if allocated for service provision. In addition, the decrease in the SoH is mainly related to the batteries with a better initial state of health: in fact, our management strategy gives higher priority to them.

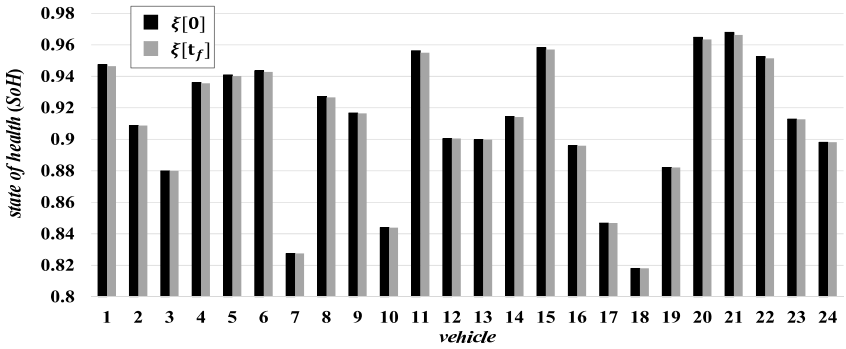

Figure 4.7 – Sample of computed SoH values for a subset of vehicles – simulation in configuration 11520-40g

For a more thorough characterization, we executed for each configuration a series of 100 simulation runs of the implemented strategy. Since the generation of the input values of SoC and SoH is random, the results regarding the variation of the SoH will be different. We considered the percentage variation of the results of our strategy compared to the reference case as a measure to evaluate the performance of the system. In particular, positive values indicate the increment of performance, represented by a slower battery aging, therefore longer battery life, compared to the reference case.

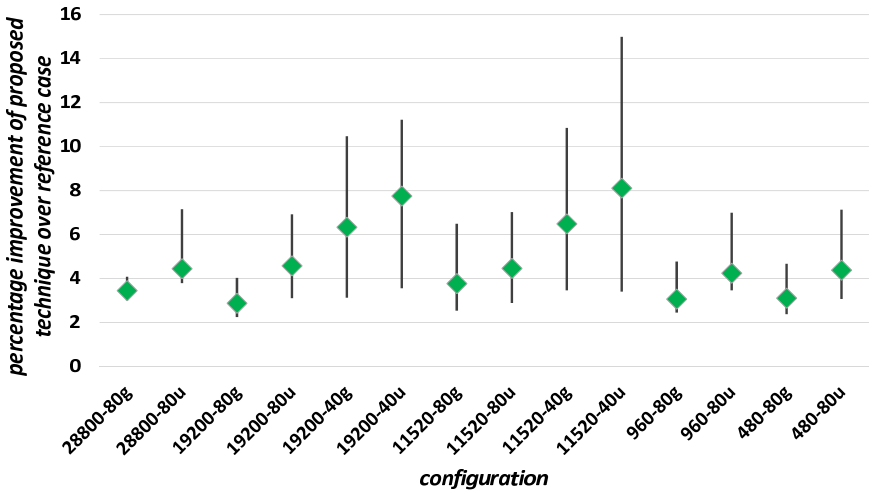

Figure 4.8 – Average percentage improvement and min-max interval as result of 100 simulation runs for each configuration

Representative test results are reported in Figure 4.8 and show average improvements between 3% and 8%. The improvement over the reference case tends to be higher when initial values are generated according to a uniform distribution. As highlighted also by the extended results relative to configurations 11520-40g and 11520-40u reported in Figures 4.9-4.10, our strategy is more effective if the initial SoH of the batteries is uniformly distributed. This phenomenon is directly determined by the fact that values close to the boundaries of the SoH input range are more frequently generated than in the Gaussian case. This accounts also for a generally higher dispersion of the results. In addition, the greatest benefits of our strategy occur with a higher *base unit*: also in this case the results are not unexpected, since raising the energy request, with the same number of vehicles in the fleet, means that the stress for the individual battery is higher, which is the condition where an advanced management strategy is more beneficial.

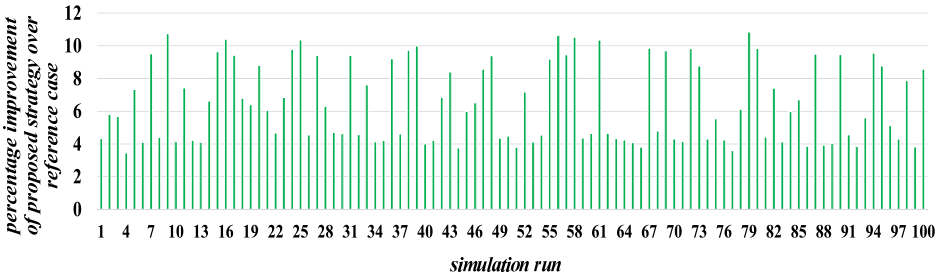

Figure 4.9 – Percentage performance improvement over reference case for 100 simulation runs - configuration 11520-40g

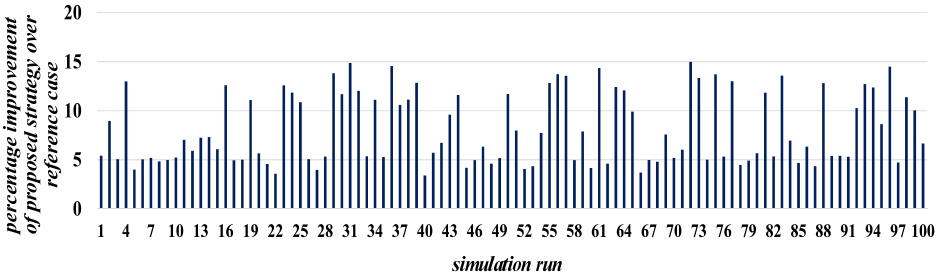

Figure 4.10 – Percentage performance improvement over reference case for 100 simulation runs - configuration 11520-40u

To explain the benefits of a strategy oriented to preserve the lifetime of batteries and of the results obtained with the proposed strategy, a practical example can be considered. If, by means of the V2G management strategy, we achieve a decrease in battery health slower by 5% compared to the case assumed as reference (where the SoC is the only relevant parameter used for the management), on average the batteries will have a lifetime longer by 5%. The USABC recommendations indicate at least three thousands EV cycles as a requirement for BV batteries. Considering a worst case scenario of two full charge/full discharge cycles per day (when the vehicle is used in a V2G framework), the battery will operate for 1500 days. Therefore, an increase of 5% in lifetime will determine 150 additional cycles, which means 75 additional days of operation.

4.5 Conclusions

In this Chapter, we presented an application of the battery measurement techniques and the system-level model introduced in Chapter 3 to the management of BV aggregations in ancillary service provision to the power grid. Assuming that the aggregator of the BV fleet – the service provider representing the interface between the aggregation of vehicles and the system operators and energy market – is responsible for the acquisition and maintenance of the batteries, it has it has overall responsibility for their management.

Therefore, we proposed an innovative management strategy that, taking into account not only the battery state of charge, but also the state of health, allows to maximize the sum of the lifetimes of all the batteries, therefore maximizing the value of aggregator's assets. Assuming the presence of a device embedded on the battery that is able to estimate the state of health, our system uses this information, together with the battery state of charge, to allocate the inbound or outbound energy transfers so that their impact on the health of batteries is reduced.

Testing conducted for different numbers of vehicles, different initial conditions and different levels of energy request evidences that the proposed strategy performs always better than the case in which only the state of charge is used for the management, assumed as reference case. Moreover, it must be considered that the additional cost for the

implementation of the proposed strategy might lie only on the microcontroller to be embedded on each battery. However, for the computation of the SoH, it can be used the same metering system already required for the measurement of the SoC.

Simulation results show that there is an increase in battery lifetime of the order of 3% to 8% compared to the reference case.

Conclusions

In this thesis work, we have proposed innovative measurement techniques and devices for monitoring and control applications to Demand Response Resources and battery storage technologies.
In a smart grid, which implements a pervasive system automation and favors active user participation and interaction, demand-side resources complement supply-side ones, ensuring not only system stability, but also a more efficient energy utilization. For their effective integration into the power grid a metering and communication network, allowing for real-time monitoring of the state of the grid and of the available resources, and suitable models and operational tools for grid management are needed.

To this aim, we developed a microcontroller based measurement device that implements a smart meter to be installed in customers' premises and that integrates with the developed metering infrastructure to provide timely and accurate measurements of all energy consumptions to system operators and to users themselves, and to implement demand response programs. In addition, we developed measurement techniques to monitor the health of batteries employed in grid service provision: suitable for online monitoring applications, the proposed techniques can be implemented on the same microcontroller device, to be embedded on the batteries themselves.

The implemented smart meter is based on an ARM M3 microcontroller and represents a low-cost solution (about 30 €/unit) for real-time bidirectional power and energy measurements. It adopts advanced algorithms for power measurements in non-sinusoidal conditions and power quality evaluation, exhibiting good measurement performances: in fact, extensive testing carried out according to the OIML R-46 recommendations has allowed to classify the device as a class C instrument (with maximum errors of 0.5% for sinusoidal conditions and 2% for distorted test signals), as opposed to the class B

of most commercial metering solutions. Interfacing with gas and heat meters, it acts as a central hub of all energy consumptions in residential or commercial environments. In addition, an advanced metering infrastructure prototype has been introduced. Measurement data are sent to a management unit, which acts as an interface to the system operators and the energy market, implementing a web-server with a user-friendly interface: thus, customers can remotely monitor all their energy consumptions. The presence of actuators on the meter, sided by a load management strategy implemented on the management unit, has allowed for the realization of load management policies in response to energy price signals, therefore attaining the deployment of demand response programs. The system allows for active user participation, with the selection of the triggering condition to activate automatic management, and by prioritizing the loads, allowing for demand peaks reduction with the least discomfort.

Energy storage systems play a fundamental role in a smart grid, allowing for decoupling electricity production and usage times. Among the several technologies employed for grid storage, batteries are of particular interest for their high efficiency, high energy density and fast response time. For their effective integration into grid planning and operations the degradation the batteries are subjected to while cycled must be taken into account.

We introduced two techniques for estimating battery state of health. Based on a fuzzy logic and on a neural network approach, they both represent lightweight measurement techniques that can be implemented on measurement devices embedded on the battery, thus realizing online monitoring. With errors within 5% of experimental data, the performances are adequate for battery degradation monitoring in grid applications.

In addition, a perturbative technique to estimate the values of the parameters of the equivalent-circuit battery model has been described. The value of the parameters influences not only the electrical behavior, but can also be used to estimate battery health. The proposed technique is faster than traditional offline techniques, such as electrochemical impedance spectroscopy, and can be implemented on measurement devices onboard the battery. Results show errors lower that 10% if the method is optimized for the specific battery technology.

While the developed techniques are useful for performing measurements on the batteries, to manage the allocation of services among the batteries acting as energy resource for the grid a system-level degradation model is required. To this aim, we developed a model that relates battery degradation to its energy throughput and to the conditions the battery is operated in. Resorting to the proposed model, is possible for service providers to take into account battery capacity decay while allocating them for service provision.

An application of the battery monitoring techniques and of the degradation model is represented by the management of fleets of battery vehicles in ancillary service provision to the power grid. In fact, they constitute not only a load, but also a distributed energy resource, that can be successfully employed to provide regulation services. We proposed a management strategy that allows the aggregator – the service provider that acts as the interface between the aggregation of vehicles and the system operators and energy market and that is responsible for management of the fleet – to allocate service provision so to maximize the sum of the lifetimes of all the batteries. Our strategy takes into account the state of health, as well as the state of charge, to allocate energy transfers to and from the batteries, so that their impact on life of batteries is reduced. Simulations conducted for different numbers of vehicles, different initial conditions and different levels of energy request evidence that the proposed strategy performs always better than the case in which only the state of charge is used for the management, assumed as reference case, with results showing an increase in battery lifetime of the order of 3% to 8%.

References

[1.1] X. Fang, S. Misra, G. Xue, D. Yang, “Smart Grid – The New and Improved Power Grid: A Survey”, *IEEE Communications Surveys & Tutorials*, vol.14, no.4, pp.944-980, 2012. doi: 10.1109/SURV.2011.101911.00087.

[1.2] A. S. Debs, “Modern Power Systems Control and Operation”, *Kluwer Academic Publishers*, 1988.

[1.3] H. Farhangi, "The path of the smart grid," *IEEE Power and Energy Magazine,* vol.8, no.1, pp.18-28, January-February 2010 doi: 10.1109/MPE.2009.934876.

[1.4] J. Ehanakaye, K. Liyanage, J. Wu, A. Yokoyama, N. Jenkins, “Smart Grid: Technology and Applications”, *Wiley*, 2012.

[1.5] European Commission, “European Smart Grid Technology Platform: vision and strategies for Europe’s electricity”, 2006. Available at: http://ec.europa.eu/research/energy/pdf/smartgrids_en.pdf.

[1.6] US Department of Energy (DOE), “Smart Grid System Report”, 2009. Available at: http://energy.gov/sites/prod/files/2009%20Smart%20Grid%20System%20Report.pdf.

[1.7] National Institute of Standards and Technology (NIST), “Technology, Measurement and Standards Challenges for the Smart Grid”, 2013. Available at: http://www.nist.gov/smartgrid/upload/Final-Version-22-Mar-2013-Smart-Grid-Workshop-Summary-Report.pdf.

[1.8] National Institute of Standards and Technology (NIST), “Framework and Roadmap for Smart Grid Interoperability Standards – Release 2.0”, 2012. Available at: http://www.nist.gov/smartgrid/upload/NIST_Framework_Release_2-0_corr.pdf.

[1.9] CEN/CENELEC/ETSI, “Final Report of the Joint Working Group on Standards for Smart Grids”, 2011. Available at: http://www.etsi.org/WebSite/document/Report_CENCLCETSI_Standards_Smart%20Grids.pdf.

[1.10] Ye Yan; Yi Qian; Sharif, H.; Tipper, D., "A Survey on Smart Grid Communication Infrastructures: Motivations, Requirements and Challenges", *IEEE Communications Surveys & Tutorials*, vol.15, no.1, pp.5,20, 2013. doi: 10.1109/SURV.2012.021312.00034.

[1.11] U.S. Department of Energy (DOE), “Benefits of Demand Response in Electricity Markets and Recommendations for Achieving Them. A report to the United States Congress Pursuant to Section 1252 of the Energy Policy Act of 2005” , 2006. Available at: http://energy.gov/sites/prod/files/oeprod/DocumentsandMedia/DOE_Benefits_of_Demand_Response_in_Electricity

_Markets_and_Recommendations_for_Achieving_Them_Report_to_Congress.pdf.

[1.12] M. H. Albadi, E.F. El-Saadany, "Demand Response in Electricity Markets: An Overview", *IEEE Power Engineering Society General Meeting 2007*, vol., no., pp.1,5, 24-28 June 2007. doi: 10.1109/PES.2007.385728.

[1.13] P. De Martini, "DR 2.0 A Future of Customer Response", 2013. Available at: http://www.demandresponsesmartgrid.org/Resources/Documents/FINAL_DR%202.0_13.07.08.pdf.

[1.14] P. Siano, "Demand response and smart grids - A survey", *Renewable and Sustainable Energy Reviews*, Volume 30, February 2014, Pages 461-478, ISSN 1364-0321, http://dx.doi.org/10.1016/j.rser.2013.10.022.

[1.15] A. Kowli, G. Gross, "Quantifying the variable effects of systems with demand response resources," Bulk Power System Dynamics and Control (iREP) - VIII (iREP), 2010 iREP Symposium , vol., no., pp.1,10, 2010. doi: 10.1109/IREP.2010.5563260

[1.16] IEEE Standard Definitions for the Measurement of Electric Power Quantities Under Sinusoidal, Nonsinusoidal, Balanced, or Unbalanced Conditions," IEEE Std 1459-2010 (Revision of IEEE Std 1459-2000) , vol., no., pp.1,50, March 19 2010. doi: 10.1109/IEEESTD.2010.5439063

[1.17] IEC EN 62052-11, "Electricity metering equipment (AC) - General requirements, tests and test conditions. Part 11: Metering equipment", 2003.

[1.18] IEC EN 62053-21, "Electricity metering equipment (a.c.) -Particular requirements. Part 21: Static meters for active energy (classes 1 and 2)", 2003.

[1.19] IEC EN 62053-23, "Electricity metering equipment (a.c.) -Particular requirements. Part 23: Static meters for reactive energy (classes 2 and 3)", 2003.

[1.20] IEC EN 50160, "Voltage characteristics of electricity supplied by public distribution systems", CENELEC ,1999.

[1.21] IEC 61000-4-30, "Electromagnetic compatibility (EMC). Part 4-30: Testing and measurement techniques – Power quality measurement methods", 2003.

[1.22] G. Budeanu, "Reactive and fictitious powers," publ. no. 2 of the Romanian National Institute, Bucharest, 1927.

[1.23] W. Shepherd, P. Zakikhani, "Suggested definition of reactive power for nonsinusoidal systems," Proc.Inst. Elec. Eng., vol. 119, pp. 1361-1362, Sept. 1972, and vol. 119, pp. 1361-1362, Sept 1972.

[1.24] D. Sharon, "Reactive power definition and power factor improvement in non-linear systems", *IEEE Trans. on Power Systems*, 120(6), 704-706, 1973.

[1.25] S. Fryze, "Active, reactive and apparent power in circuits with non sinusoidal voltage and current", Przegl. Elektrotech., 22, p.673-676, 1932, (in Polish).
[1.26] N. L. Kusters and W. J. M. Moore, “On the definition of reactive power under nonsinusoidal conditions,” *IEEE Trans. on Power Apparatus and Systems*, Vol. PAS-99, No. 5, pp 1845-1854, Sept/Oct 1980.
[1.27] C. H. Page, “Reactive power in nonsinusoidal situations,” *IEEE Trans. Inst. Meas*., vol. IM-29, pp. 420-423, Dec. 1980.
[1.28] L.S. Czarnecki, "Considerations on the reactive power in non-sinusoidal situations", IEEE *Trans. Inst. Meas*., vol. 34, 1985, p.399-404.
[1.29] Ferrero, G. Superti-Furga, "A new approach to the definition of power components in three-phase systems under nonsinusoidal conditions", *IEEE Trans. Inst. Meas*., vol.40, no.3, pp.568,577, 1991. doi: 10.1109/19.87021.

[2.1] Smart Regions project deliverable 2.1, “European Smart Metering: Landscape Report 2012 – update 2013”, 2013.
[2.2] V. Giordano et alii, “Smart Grids Projects in Europe: Lessons Learned and Current Developments”, European Joint Research Council report, 2013.
[2.3] Pike Research, ”Smart Grids in Europe”, Pike Research Cleantech Market Intelligence, available at: http://www.pikeresearch.com/research/smart-grids-in-europe, accessed February 2011.
[2.4] T. Ryberg, “Smart Metering in Europe – 9th Edition”, Berg Insight, 2012.
[2.5] OpenMeter Deliverable D1.1 (2010), Report on the Identification and Specification of Functional, Technical, Economical and General Requirements of Advanced Multi-Metering Infrastructure, Including Security Requirements, OPENMeter, Energy Project No 226369. Funded by EC. Available at: http://www.openmeter.com/files/deliverables/ Open%20Meter_D3%201_Architecture_v6_.pdf, accessed March 2011.
[2.6] OpenMeter Deliverable D3.1 (2010),”Design of the Overall System Architecture”, OPENmeter, Energy Project No 226369. Funded by EC. Available at: http://www.openmeter.com/files/deliverables/ Open%20Meter_D3%201_Architecture_v6_.pdf, accessed April 2011.
[2.7] N. Arcauz, A. Goñi, M. Adriansen, B. Roelofsen, T. Schaub, F. Tarruel, B.Schumacher, Open Meter Overview Of The Market For Smart Metering. Open metering deliverables public report 31/1/2012, http://www.openmeter.com
[2.8] B.A.U.M. Consult GmbH, “Smart Energy made in Germany Interim results of the E-Energy pilot projects towards the Internet of Energy”. Available at: http://www.e-energy.de/documents/E-Energy_Interim_results_Feb_ 2012.pdf, accessed June 2013.
[2.9] SmartWatts project. Available at: http://www.smartwatts.de/

[2.10] MeRegio project. Available at: http://www.meregio.de/
[2.11] Meter-ON project. Available at: www.meter-on.eu
[2.12] Federal Energy Regulatory Commission, “Assessment of Demand Response and Advanced Metering”, Staff report, December 2012.
[2.13] https://www.echelon.com/products/smart-meters/
[2.14] http://www.gedigitalenergy.com/smartmetering/catalog/p2mp.htm
[2.15] http://www.ti.com/solution/docs/appsolution.tsp?appId=407
[2.16] http://www.accent-soc.com/applications/smart_metering.php
[2.17] G. Di Leo, M. Landi, V. Paciello, A. Pietrosanto, “Smart metering for demand side management,” in 2012 IEEE International Instrumentation and Measurement Technology Conference Proceedings, pp. 1798–1803, 2012.
[2.18] D. Blume, J. Schlabbach, T. Stephanblome, “Spannungsqualität in elektrischen Netzen (Power Quality in Electrical Power Systems)”, *Vde Verlag GmbH*, 1999 (in German).
[2.19] University of Salerno et alii, “Measurement and Control Systems and Devices for Application of Demand Side Management Programs (Sistemi e dispositivi di telemisura ed attuazione per applicazioni tecniche di demand side management alle piccole utenze)”, *joint research project funded by the Italian Ministry of Industrial Development*, 2009-2012 (in Italian).
[2.20] University of Salerno et alii, “Multiutility Measurement System for Energy Monitoring (Sistema di misura polifunzionale per la determinazione dei consumi energetici)”, *joint research project funded by the Italian Ministry of Industrial Development*, 2010-2013, (in Italian).
[2.21] ST Microelectronics, “STM32F10X microcontroller Reference Manual”. Available at: http://www.st.com/web/en/resource/technical/document/reference_manual/CD00171190.pdf , accessed 2011.
[2.22] J. G. Proakis, D. G. Manolakis, “Digital Signal Processing: Principles, Algorithms, and Applications”, 3rd ed., *Prentice Hall International, Inc.*, pp. 480-481, 1996.
[2.23] C. Liguori, A. Paolillo, “IFFTC-Based Procedure for Hidden Tone Detection”, *IEEE Trans. Inst. Meas.*, 56(1), pp. 133-139, 2007.
[2.24] F. Moraes, A. Amory, N. Calazans, E. Bezerra, J. Petrini, “Using the CAN protocol and reconfigurable computing technology for web-based smart house automation”, *14th Symp. on Integrated Circuits and Systems Design*, 2001.
[2.25] ISO 11898-1:2003, “Road vehicles - Controller area network (CAN) - Part 1: Data link layer and physical signaling”.
[2.26] D. Gallo, C. Landi, N. Pasquino, N. Polese, "A New Methodological Approach to Quality Assurance of Energy Meters Under Nonsinusoidal Conditions", *IEEE Trans. Inst. Meas.*, vol.56, no.5, pp.1694-1702, 2007. doi: 10.1109/TIM.2007.903607.

[2.27] A. Delle Femine, D. Gallo, C. Landi, M. Luiso, "Advanced instrument for field calibration of electrical energy meters", *IEEE Trans. Inst. Meas.*, Vol. 58, No. 3, pp.618–625, 2009.
[2.28] IEC 61000-4-7, "Electromagnetic compatibility (EMC). Part 4-7: Testing and measurement techniques – General guide on harmonics and interharmonics measurements and instrumentation, for power supply systems and equipment connected thereto", 2002.
[2.29] D. Gallo, C. Landi, M. Landi, M. Luiso, "Smart Metering", chapter in "Computational Intelligence Applications in Smart Grids", *Imperial College Press*, 2014 (in press).
[2.30] EU, "The Measuring Instruments Directive (2004/22/EC)", 2004.
[2.31] OIML R-46, "Active Electrical Energy Meters. Part 1: Metrological and Technical Requirements. Part 2: Metrological controls and performance tests", 2010.

[3.1] H. A. Kiehne, "Battery Technology Handbook", 2nd edition, *Marcel Dekker, Inc.*, 2003.
[3.2] C. Daniel, J. O. Besenhard, Handbook of Battery Materials", 2nd edition, *Wiley-VCH Verlag & Co. KGaA*, 2011.
[3.3] D. Linden, T. B. Reddy, "Handbook of Batteries", 3rd ed.; *McGraw-Hill*, 2001.
[3.4] A. Vassallo et alii, "Leading the Energy Transition Factbook: Electricity Storage", SBC Energy Institute, 2013.
[3.5] U.S. Department of Energy (DOE), "Grid Energy Storage", report, 2013. Available at: http://energy.gov/sites/prod/files/2013/12/f5/Grid%20Energy%20Storage%20December%202013.pdf.
[3.6] A. A. Akhil et alii, "DOE/EPRI 2013 Electricity Storage Handbook in Collaboration with NRECA", Sandia National Laboratories, 2013.
[3.7] P. Denholm et alii, "The Value of Energy Storage for Grid Applications", National Renewable Energy Laboratory technical report, 2013.
[3.8] U. Bertelè, V. Chiesa, M. Delfanti, "Smart Grid Report – Storage systems and electric vehicles (Smart Grid Report – Sistemi di storage ed auto elettrica)", Energy&Strategy Group, Polytechnic University of Milan, 2013.
[3.9] A. Dinger et alii, "Batteries for Electric Cars: Challenges, Opportunities and the Outlook to 2020", Boston Consulting Group *Focus*, 2010.
[3.10] K. Bradbury, "Energy Storage Technology Review", 2010. Available at: http://people.duke.edu/~kjb17/tutorials/Energy_Storage_Technologies.pdf.
[3.11] H. Chen, T. N. Cong, W. Yang, C. Tan, Y. Li, and Y. Ding, "Progress in electrical energy storage system: A critical review," Progress in Natural Science, vol. 19, p. 291312, 2009.

[3.12] H. Kim et alii, “Liquid Metal Batteries: Past, Present, and Future”, *Chemical Reviews*, 113 (3), pp. 2075-2099, 2013.

[3.13] D. J. Bradwell, H. Kim, A. H. C. Sirk, D. R. Sadoway, “Magnesium-Antimony Liquid Metal Battery for Stationary Energy Storage”, Journal of the American Chemical Society, 134 (4), pp. 1895-1897, 2012.

[3.14] T. Fuller, M. Doyle, and J. Newman, “Simulation and optimization of the dual lithium ion insertion cell”, J. Electrochem. Soc., Vol. 141, pp. 1–10, 1994.

[3.15] T. Ohzuku, Y. Makimura, “Layered Lithium Insertion Material of LiCo1/3Ni1/3Mn1/3O2 for Lithium-Ion Batteries”, *Chemistry Letters*, Vol. 30 (2001) , No. 7 p.642. doi: 10.1246/cl.2001.642.1246/cl.2001.642.

[3.16] S. J. Moura, J. L. Stein, H. K. Fathy, “Battery-Health Conscious Power Management in Plug-In Hybrid Electric Vehicles via Electrochemical Modeling and Stochastic Control*”, IEEE Transactions on Control Systems Technology,* Vol. PP, issue 99.

[3.17] S. Bhide, T. Shim, “Novel Predictive Electric Li-ion Battery Model Incorporating Thermal and Rate Factor Effects”, *IEEE Transactions on vehicular technology*, Vol.60, No. 3, March 2011.

[3.18] A. Di Filippi, S. Stockar, S. Onori, M. Canova, Y. Guezennec, “Model-Based Life Estimation of Li-ion Batteries in PHEVs Using Large Scale Vehicle Simulations: An Introductory Study”, IEEE Vehicle Power and Propulsion Conference (VPPC), 2010.

[3.19] Xinfan Lin A.G. Stefanopoulou, H. E. Perez, J. B. Siegel, Yonghua Li, R. D. Anderson, "Quadruple adaptive observer of the core temperature in cylindrical Li-ion batteries and their health monitoring," American Control Conference (ACC), 2012 , vol., no., pp.578,583, 27-29 June 2012.

[3.20] O. Tremblay, L. Dessaint, "Experimental Validation of a Battery Dynamic Model for EV Applications", *World Electric Vehicle Journal,* Vol. 3, 2009.

[3.21] D. Gallo, C. Landi, M. Luiso, R. Morello, “Optimization of Experimental Model Parameter Identification for Energy Storage Systems”, Energies, Vol. 6, pp. 4572-4590, 2013. doi:10.3390/en6094572.

[3.22] L. Gao, S. Liu, and R. A. Dougal,“Dynamic lithium-ion battery model for system simulation,” *IEEE Trans.Compon. Packag. Technol*., vol. 25, no. 3, pp. 495–505, Sep. 2002.

[3.23] M. R. Jongerden and B. R. Haverkort, “Battery modeling”, Technical Report TR-CTIT-08-01, CTIT, University of Twente, 2008.

[3.24] Gamry Instruments, “Basics of Electrochemical Impedance Spectroscopy”, AN.

[3.25] T. Huria, M. Ceraolo, J. Gazzarri, R. Jackey , "High fidelity electrical model with thermal dependence for characterization and simulation of high power lithium battery cells," IEEE International Electric Vehicle Conference (IEVC), 2012, pp.1-8, 2012.

[3.26] Rutooj Deshpande, Mark Verbrugge, Yang-Tse Cheng, John Wang, Ping Liu, “Battery Cycle Life Prediction with Coupled Chemical Degradation and Fatigue Mechanics”, J. Electrochem. Soc. 2012 159(10): A1730-A1738; doi:10.1149/2.049210jes.

[3.27] M. Landi, G. Gross, “Measurement Techniques for Online Battery State of Health Estimation in Vehicle-to-Grid Applications”, *IEEE Trans. Inst. Meas.*, (in press).

[3.28] G. Gross, M. Landi, C. Liguori , V. Paciello, “Measurement technique for online EV battery state of life monitoring”, in 19th IMEKO TC-4 Symposium, 2013.

[3.29] G. Gross, M. Landi, “Measurement of a health index for Li-Ion batteries,” in Proc. of 2013 IEEE International Instrumentation and Measurement Technology Conference (I2MTC), 2013, pp. 177–182.

[3.30] A. Lasia, ”Electrochemical Impedance Spectroscopy and its Applications in Modern Aspects of Electrochemistry”, *Springer US*, 2002.

[3.31] G. L. Plett, “Extended Kalman filtering for battery management systems of LiPB-based HEV battery packs. Part 1. Background”, *Journal of Power Sources*, vol. 134, pp. 252-261, 2004.

[3.32] G. L. Plett, “Extended Kalman filtering for battery management systems of LiPB-based HEV battery packs. Part 2. Modeling and identification”, *Journal of Power Sources*, vol. 134, pp. 262-276, 2004.

[3.33] G. L. Plett, “Extended Kalman filtering for battery management systems of LiPB-based HEV battery packs. Part 3. State and parameter estimation”, *Journal of Power Sources*, vol. 134, pp. 277-292, 2004.

[3.34] B. Saha, K. Gobel, J. Christopersen, “Comparison of Prognostic Algorithms for Estimating Remaining Useful Life of Batteries”, *IEEE Transactions of the Institute of Measurement and Control*, Vol. 31 no. 3-4 293-308, 2009.

[3.35] L. Ljung, “System Identification: Theory for the User”, 2nd Edition, *Prentice Hall*, 1999.

[3.36] L. Ferrigno, C. Liguori, A. Pietrosanto, "Measurements for the characterization of passive components in non-sinusoidal conditions", *IEEE Trans. Inst. Meas.*, Vol.51, no.6, pp. 1252- 1258, 2002.

[3.37] D. Rakhmatov, “Battery voltage modeling for portable systems”, ACM Trans. Des. Autom. Electron. Syst. 14, 2, Article 29 (April 2009). doi:10.1145/1497561.1497572

[3.38] S. Sastry, O. Gimdogmus, T. T. Hartley, R. J. Veillette, “Coordinated discharge of a collection of batteries”, *Journal of Power Sources*, vol.166 pp. 284–296, 2007.

[3.39] B. Saha, K. Goebel, S. Poll, J. Christophersen, “Prognostics Methods for Battery Health Monitoring Using a Bayesian Framework”, *IEEE Trans. Inst. Meas.*, Vol. 58, No. 2, 2009.

[3.40] K. Goebel, B. Saha, A. Saxena, J. Celaya, J. Christophersen, "Prognostics in Battery Health Management," *IEEE Instrumentation & Measurement Magazine*, Vol.11, no.4, pp.33-40, August 2008, doi: 10.1109/MIM.2008.4579269.

[3.41] M. V. Micea, L. Ungurean, G. N. Cârstoiu, V. Groza, "Online State-of-Health Assessment for Battery Management Systems", IEEE Trans. on Instrumentation and Measurement, Vol. 60, No. 6, 2011.

[3.42] Kejun Qian, Chengke Zhou, Yue Yuan, Allan, M., "Temperature effect on electric vehicle battery cycle life in Vehicle-to-grid applications", CICED, 2010.

[3.43] M. Dubarry, B. Y. Liaw, "Identify capacity fading mechanism in a commercial LiFePO4 cell", *Journal of Power Sources,* vol. 194, pp 541–549, 2009.

[3.44] G. Ning, B. N. Popov, "Cycle Life Modeling of Lithium-Ion Batteries", *Journal of Electrochemical Society*, 151 (10), A1584-A1591, 2004.

[3.45] B. Saha and K. Goebel, "Battery Data Set", NASA Ames Prognostics Data Repository, 2007. Available at: http://ti.arc.nasa.gov/tech/dash/pcoe/ prognostic-data-repository/.

[4.1] CAISO, "California Vehicle-Grid Integration (VGI) Roadmap: Enabling Vehicle-Based Grid Services", Technical Report, 2013.

[4.2] Electric Power Research Institute, "Texas Plugs In: Houston and San Antonio Residents' Expectations of and Purchase Intentions for Plug-In Electric Vehicles", Technical Report, 2012.

[4.3] G. Pistoia, "Electric and hybrid vehicles – power sources, models, sustainability, infrastructure and the market", *Elsevier*, 2010.

[4.4] T. R. Hawkins, B. Singh, G. Majeau-Bettez, A. H. Strømman, "Comparative Environmental Life Cycle Assessment of Conventional and Electric Vehicles", *Journal of Industrial Ecology,* 2012. doi: 10.1111/j.1530-9290.2012.00532.x, 2012.

[4.5] U.S. Department of Energy (DOE), Alternative fuels data center, available at: http://www.afdc.energy.gov/vehicles/electric.html

[4.6] C. Guille, G. Gross, "A conceptual framework for the vehicle-to-grid (V2G) implementation," *Energy Policy*, Elsevier, vol. 37(11), pages 4379-4390, 2009.

[4.7] J. Tomić, W. Kempton, "Using fleets of electric-drive vehicles for grid support", *Journal of Power Sources*, Volume 168, Issue 2, pp. 459-468, 2007.

[4.8] C. Guille, G. Gross, "The integration of PHEV aggregations into a power system with wind resources," Bulk Power System Dynamics and Control (iREP) - VIII (iREP), 2010 iREP Symposium , pp.1-9, 2010.

[4.9] Sekyung Han; Soohee Han; Sezaki, K., "Development of an Optimal Vehicle-to-Grid Aggregator for Frequency Regulation", *IEEE Transaction on Smart Grid,* vol.1, no.1, pp.65-72, 2010.

[4.10] Sekyung Han, Soohee Han, K. Sezaki, "Estimation of Achievable Power Capacity From Plug-in Electric Vehicles for V2G Frequency Regulation: Case Studies for Market Participation", *IEEE Transactions on Smart Grid*, vol.2, no.4, pp.632,641, 2011.

[4.11] W. Kempton et alii, "A Test of Vehicle-to-Grid (V2G) for Energy Storage and Frequency Regulation in the PJM System", Technical report, 2013. Available at: http://www.udel.edu/V2G/resources/test-v2g-in-pjm-jan09.pdf.

[4.12] http://news.delaware.gov/2013/04/26/in-first-electric-vehicle-to-grid-technology-sells-power-to-pjm-power-grid/